PEM-West Trajectory Climatology and Photochemical Model Sensitivity Study Prepared Using Retrospective Meteorological Data

by

John T. Merrill
Center for Atmospheric Chemistry Studies
Graduate School of Oceanography
University of Rhode Island

and

Jose M. Rodriguez
AER, Inc.
Cambridge, MA

This report summarizes trajectory and photochemical model calculations based on retrospective meteorological data for the operations area of the NASA PEM-West Mission. The "trajectory climatology" discussed here is intended to provide guidance for flight planning and initial data interpretation during the field phase of the expedition by indicating the most probable path air parcels are likely to take to reach various points in the area. The photochemical model calculations which are discussed below indicate the sensitivity of the chemical environment to various initial chemical concentrations and to conditions along the trajectory. These results have been prepared for the use of the PEM-West Science Team. No citation should be made to these results in publications or presentations without the explicit permission of the authors. In the post-expedition analysis these calculations will be used to provide a climatological context for the meteorological conditions which are encountered in the field.

Part 1. Trajectory and Airflow Probability Analysis

John T. Merrill

Meteorological Data and Trajectory Analysis

The basic meteorological data used are the gridded isobaric fields of the NMC global analysis, prepared by the National Meteorological Center of the US National Weather Service. This consists of fields of wind components, geopotential heights and other data on constant pressure levels, eight of which lie within the troposphere. The analysis is produced twice per day, at the main synoptic times of 0000 and 1200 UTC (= Greenwich Mean Time). The values are based on observations and on short-term forecasts from earlier times. I use isentropic analysis techniques which I have developed over the years to interpolate the wind components from the standard assimilation levels to hypothetical surfaces of constant potential temperature (Merrill, 1989). The subsequent trajectory analysis assumes that air parcels will move along these surfaces, i.e., that the air motion is dry adiabatic.

We have prepared isentropic analyses (including the humidity and geopotential height values needed by the photochemical model) for the required days of the year for the years 1988-1990. Using these we have calculated trajectories for the period September 15 - October 15 for these years, at potential temperature values from 310 to 340 K, at intervals of 10 K; this covers the middle troposphere to the lower stratosphere. Multiple years are included in the analysis to include some of the expected interannual variability.

The trajectory climatology for the PEM-West mission consists of trajectories at several potential temperature levels. Each "ends" at a set of points which lie at integral multiples of 2.5° in latitude and longitude, along lines which broadly outline the planned flight tracks for the intensive missions; the locations are shown in Figure 1. The letters J, H and G on the map indicate that trajectories ending at that location are associated, in the trajectory archive data file, with the sites at Japan, Hong Kong and Guam, respectively.

An example of a set of trajectories for the area near Japan is shown in Figure 2. The lower panel shows the motion of air parcels back in time from locations over and near Japan; these trajectories all end at 0000 UTC on September 22, 1990. There are dots along the path at 0000 UTC each day. If the day of the month is an integral multiple of 5 the dot is replaced by a small circle, and kinks between dots are at the intermediate 1200 hour. The upper panel shows the corresponding vertical motion. The low-latitude trajectories lie near 500 hPa (~6 km above sea level) and exhibit downward motion as they approach Japan. The trajectory ending farthest southeast of Japan shows anticyclonic flow from the east. Examination of other examples shows that at higher latitudes the flow is faster (i.e., the dots are further apart), at higher

elevations, and exhibits less vertical motion. All of these characteristics are expected and are consistent with a simple understanding of the large-scale circulation in the area. Trajectories back in time from these same end points will be calculated during the field phase of the expedition using operational meteorological data.

Airflow Probability Analysis Based on Trajectories

Here we present the main results of the trajectory analysis. The statistical approach to summarizing the trajectory results used here has been developed for atmospheric chemistry analysis (Merrill, et al., 1989). In it an ensemble of trajectories is used, all ending at the same point. This superposition of trajectories from many days is designed to detect the main paths of transport along isentropic surfaces. Maps of the cumulative probability of trajectory passage are plotted. The probability is the ratio of the number of hours spent by trajectories in an area divided by the total hours for all trajectories in the ensemble. Probabilities determined in this way show a strong central tendency, specifically, the maximum probability is always at the common end point of the trajectories. To emphasize the long range airflow the raw sums used in the probability calculations are multiplied by a geometrical correction factor which removes the central bulls-eye. The results presented here have had this correction factor applied.

The trajectory probability maps are to be interpreted as follows. The area within the highest probability contour contains the most probable path for air which ultimately arrives at the designated end point. The width and conformation of the lower probability contours indicates the relative width of the most common transport path, i.e., its variability. Note that low probability values are not plotted. This is in part because the trajectories which pass there are unusual and may not present a statistically significant picture of the airflow. However, it is important to note that this does not mean such motion is unimportant. In fact, it is sometimes true that winds blowing from an uncommon direction can transport crucial substances to an area. Case studies are the appropriate means for studying such events, however, not the probabilistic approach used here.

Results for Japan

Figures 3 and 4 show the probability results for areas near Japan, for 320 and 330 K respectively. The 320 K potential temperature surface varies between approximate pressure levels of 600 to 300 hPa in this area, corresponding to heights of 4 - 9 km. The 330 K surface lies at somewhat higher elevations, approximately 5-10 km. The surfaces slope upward with increasing latitude, so the lower elevations are at the lower latitude side of the area in question. The six aircraft operations areas chosen for this discussion are indicated by the darkened circle on each panel of the figure.

At 320 K there is a split in the flow for sites 1 and 3. The flow directly from the west, from the interior of China, is rapid and nearly isobaric (i.e., neither rising nor falling, in general). The branch of the flow from the southwest, from areas south of the Tibetan plateau, is slower and ascending. (Neither the speed nor the vertical motion are shown on these plots; they are based on examination of other plots and the trajectories themselves.) At site 2 the flow from the west dominates, while at site 4 the flow from the southwest is most probable. At the lower latitude sites 5 and 6 there is a different mixture of flows: flow from the east (open ocean areas) is important at site 5 and dominant at site 6.

At 330 K some of the same features are apparent as at 320 K. However, the split in the flow at the higher latitude sites is not as important. This is in part because at these higher elevations the influence of the Tibetan mountain barrier is reduced. Thus at sites 1 and 3 there is much less of a gap between the westerly and southwesterly flows. Also, at sites 5 and 6 the westerly flow dominates over the easterly flow, consistent with the onshore flow being confined to lower and mid-tropospheric levels at this latitude.

Results for Hong Kong

Figure 5 shows probability fields for sites near Hong Kong, at 320 and 340 K. At the higher elevation (upper panels) the flow is from the west at site 2, and an admixture of easterly and westerly flow at site 1. Again, the flow from the west is very rapid compared to that from the east, particularly at the higher elevation of 340 K. At the lower elevations the easterly flow is more important at site 1, while the westerly branch is more important at site 2 (consistent with its higher latitude). The results for 330 K fall in between the results for 320 and 340 K.

Note that at site 1 there is a high probability of airflow from the direction of the Philippines. Sporadic volcanic activity continues at Mount Pinatubo, raising the possibility of encountering relatively fresh volcanic emissions on one or more flights from Hong Kong.

Results for Guam

The results for Guam are shown in Figures 6 and 7. At 320 K, Figure 6, the flow is from the east at all the latitudes studied. However, notice that the width of the area of high probability varies. The very narrow shape at site 3 is indicative of a steady flow from the east. At the other sites, particularly site 1, the greater latitudinal width of the pattern indicates that flow from north or south of east does occur as well. Flow from south of east could include interhemispheric transport (although no important instances of this were noted in this three-year September climatology). Flow from north of east can and does include cases where westerly winds from Asia move far enough offshore that the air circles an anticyclone and approaches Guam from east of north.

In Figure 7 at sites 2 and 4 the possibility of air from continental Asia is more apparent. Also, at site 1 there is a significant probability of flow directly from the west, again probably carrying a continental signature.

References

Merrill, J.T., M. Uematsu, and R. Bleck, 1989: Meteorological analysis of long-range transport to the Pacific Ocean. *J. Geophys. Res.*, **94**, 8584-8598.

Merrill, J.T., 1989: Atmospheric long-range transport to the Pacific Ocean. *Chemical Oceanography*, **10**, 15-50, J.P. Reily, Ed.

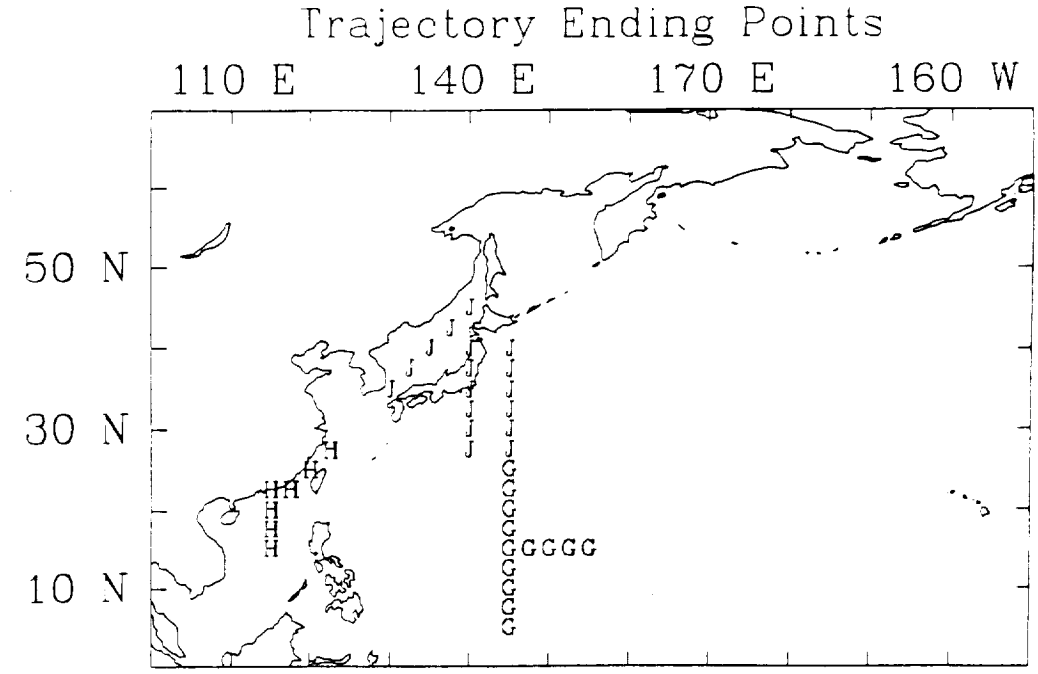

Figure 1

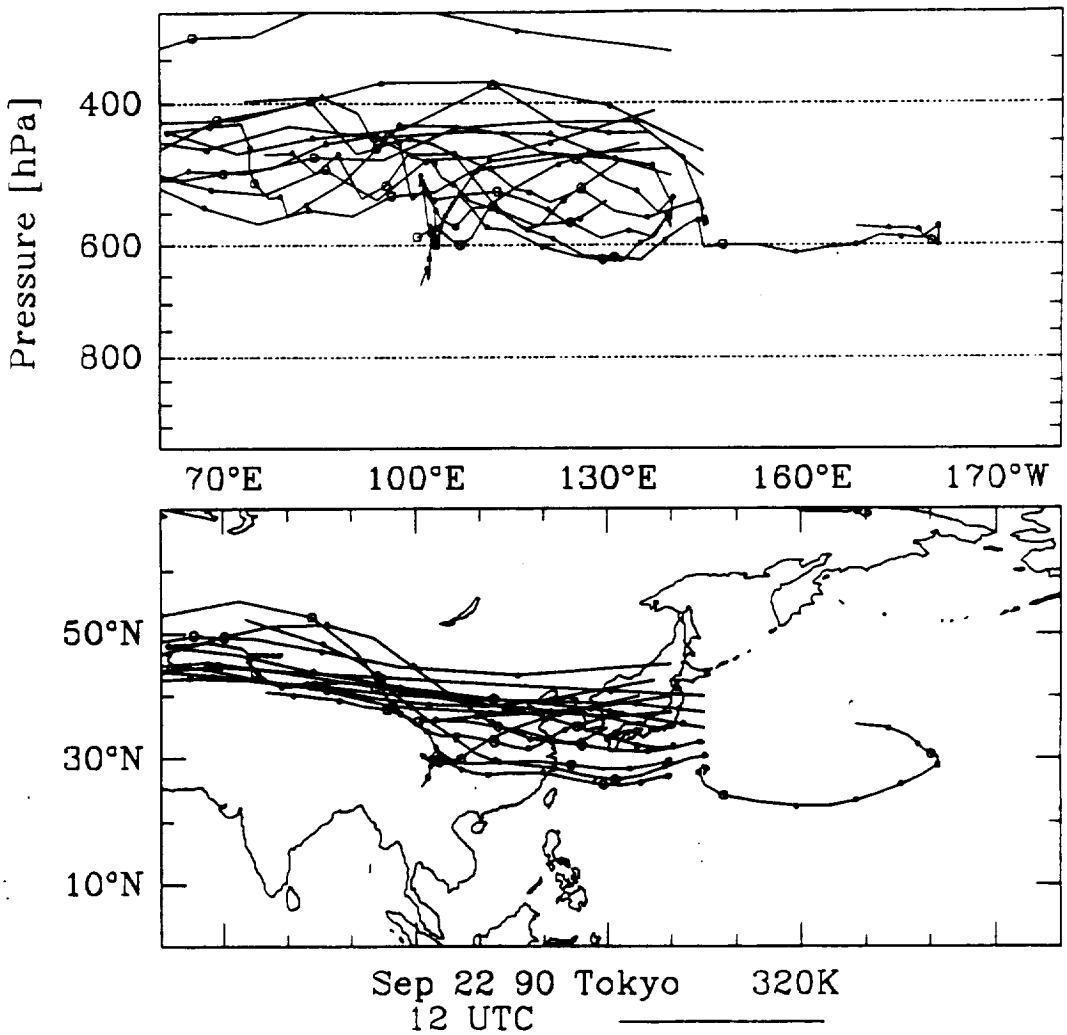

Figure 2

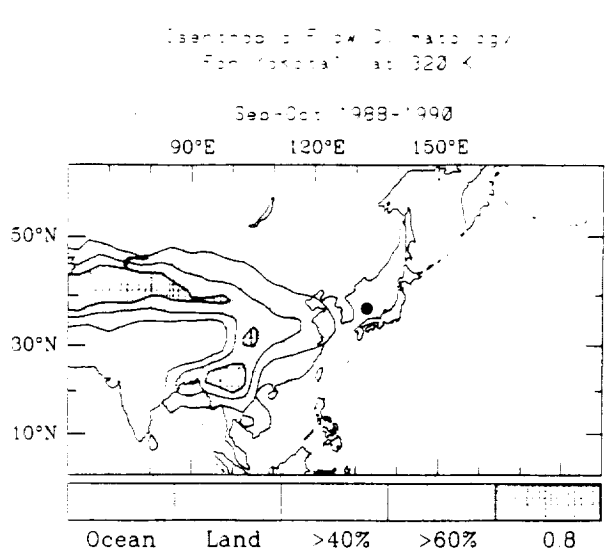

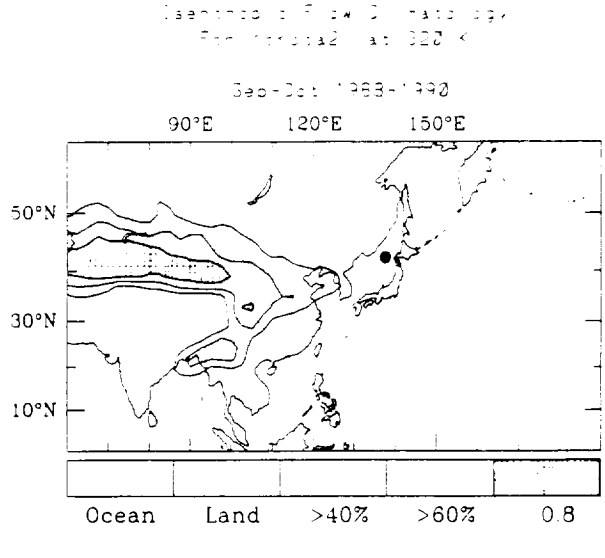

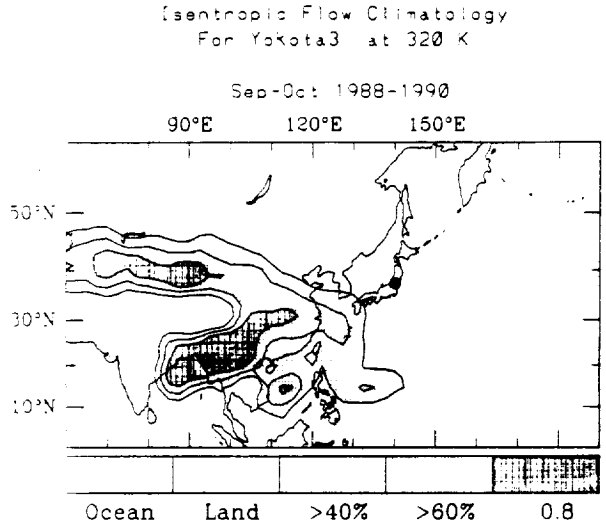

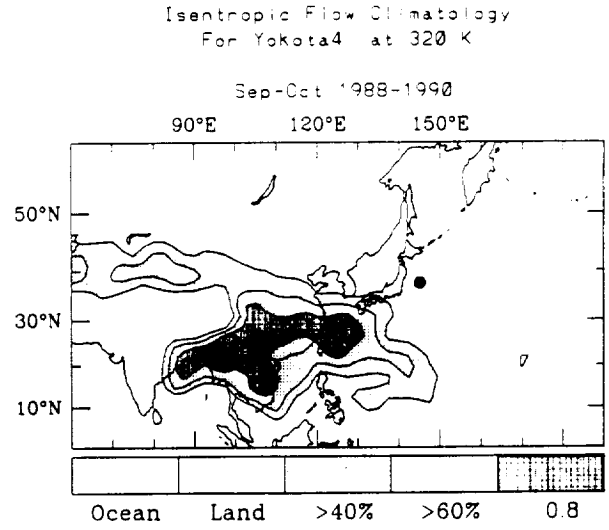

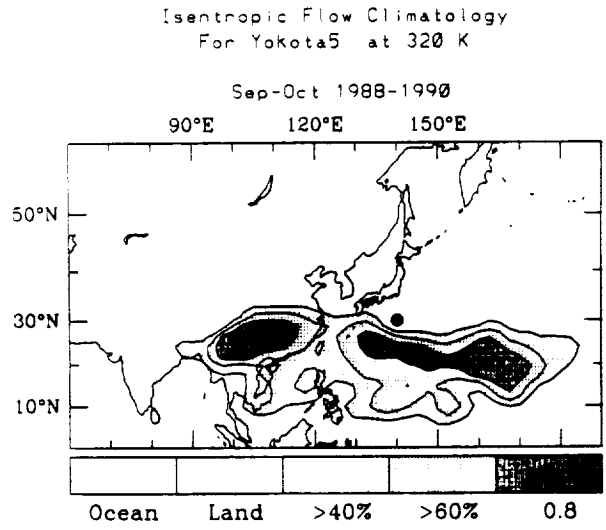

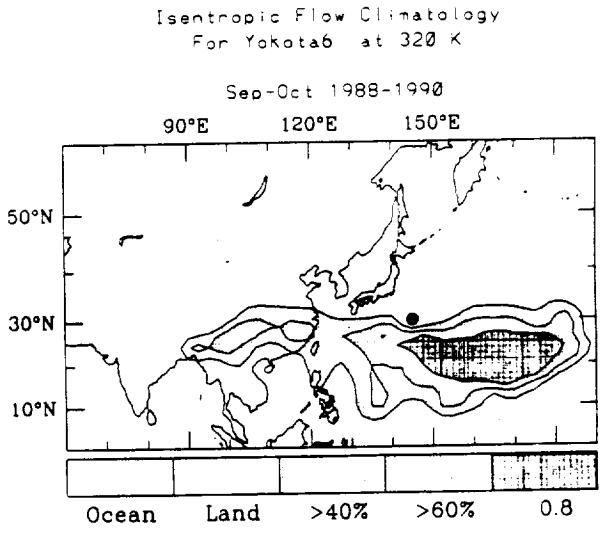

Figure 3

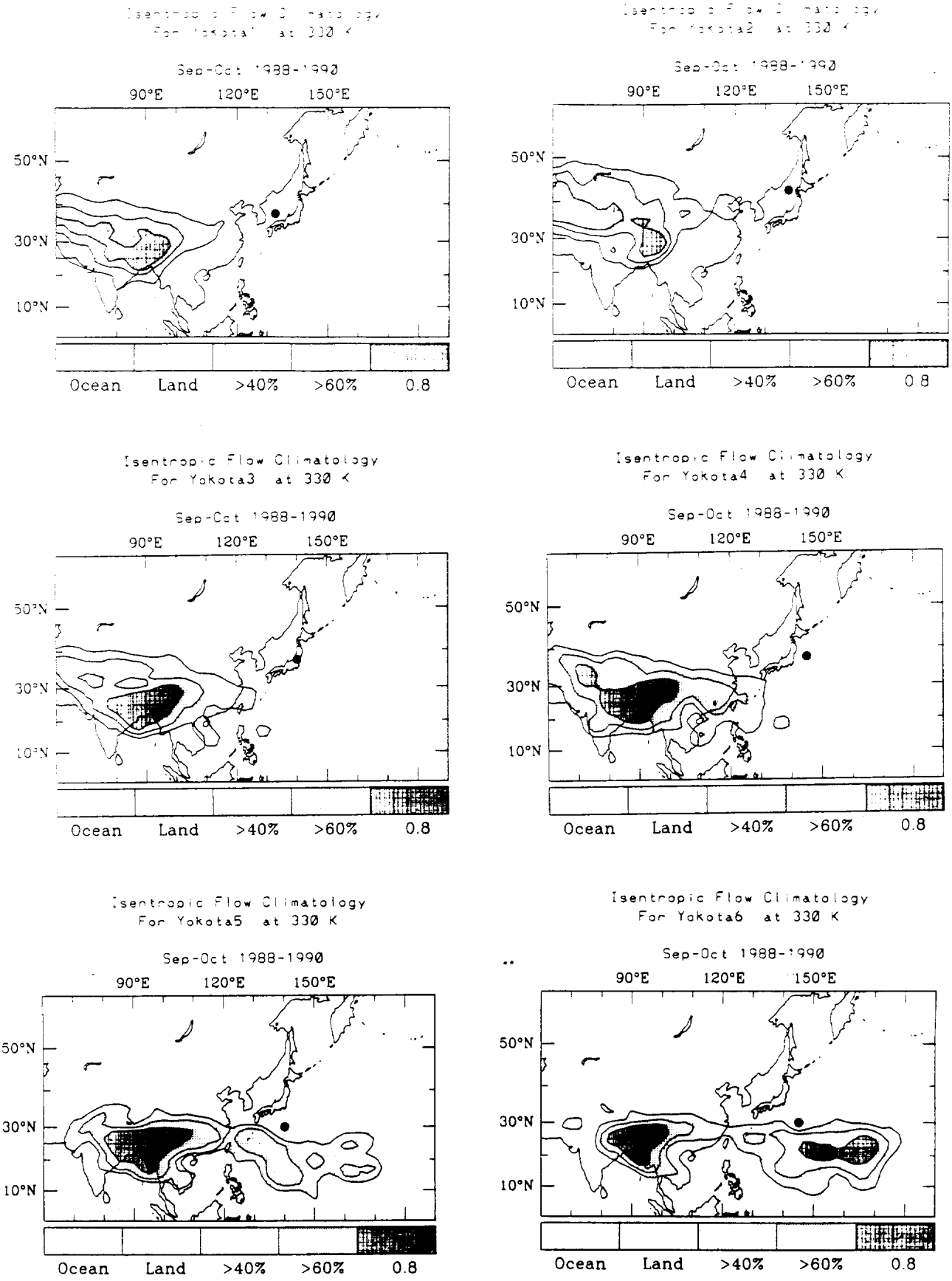

Figure 4

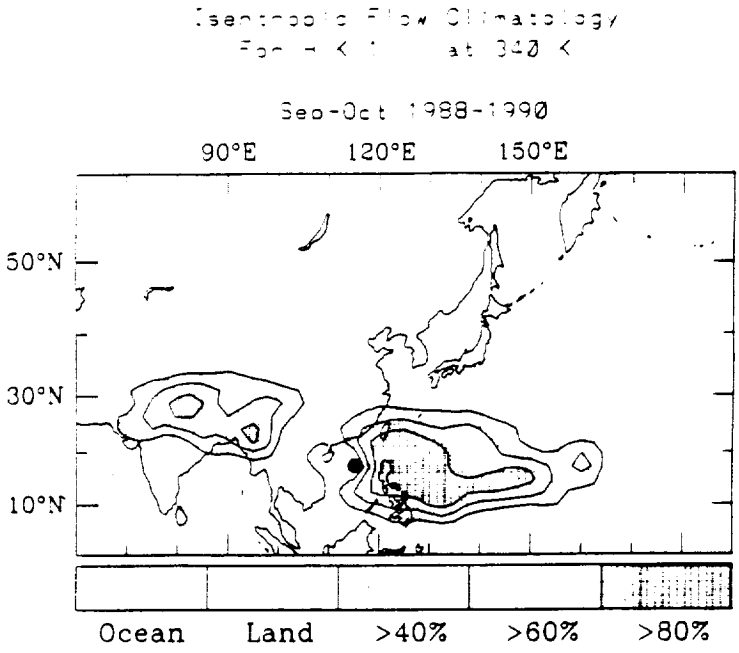

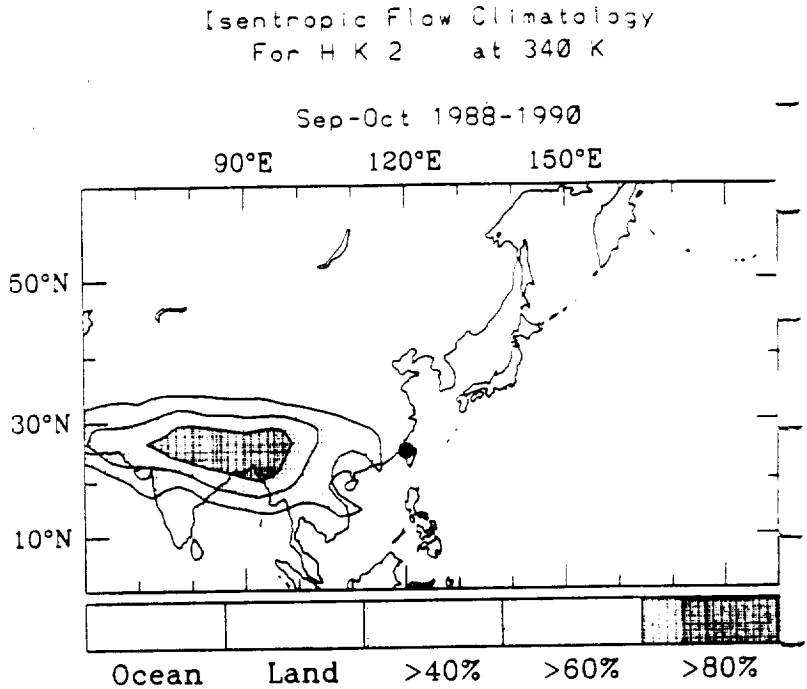

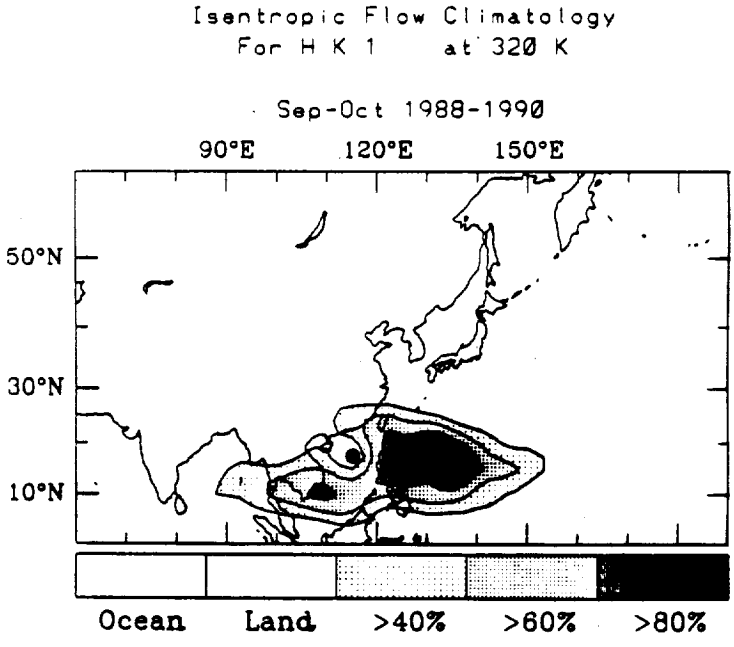

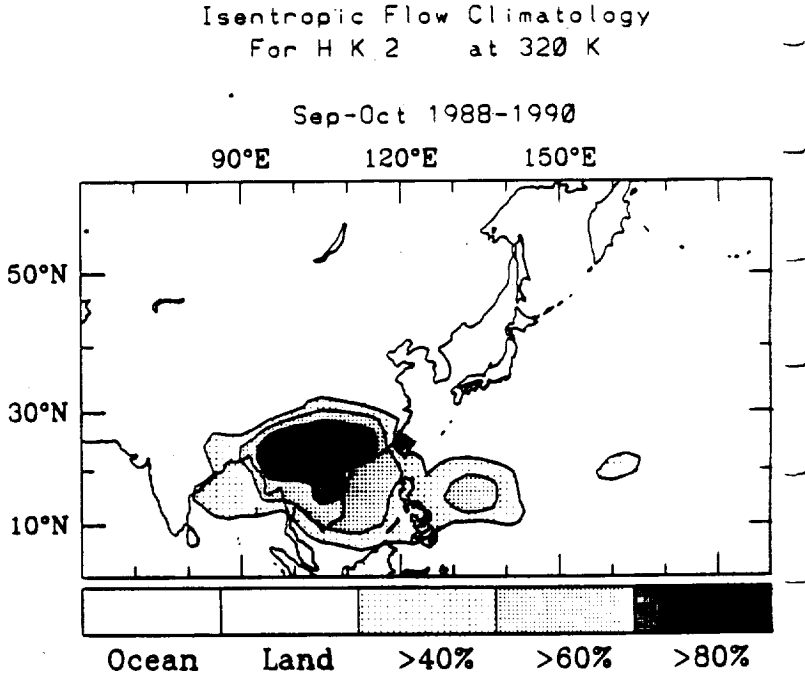

Figure 5

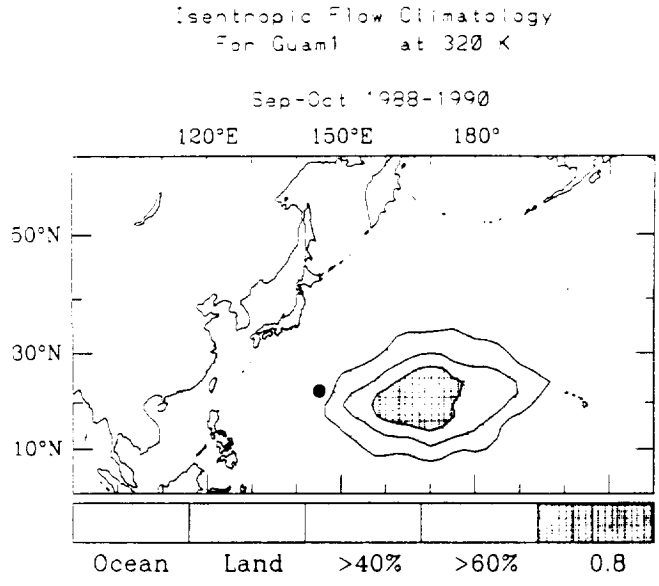

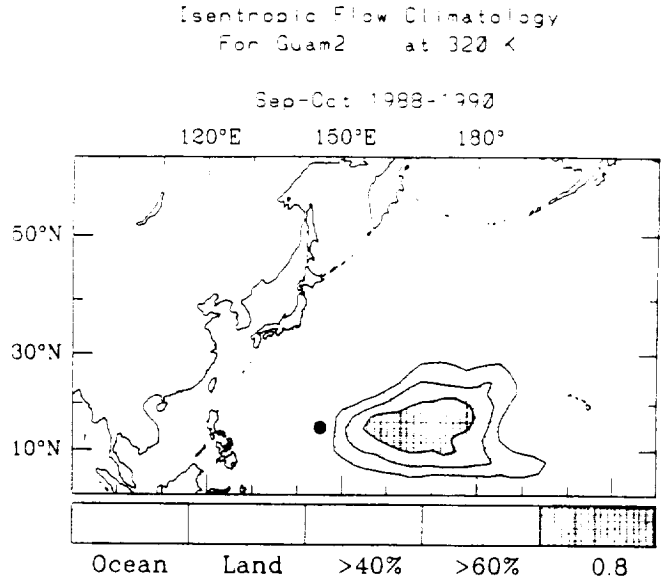

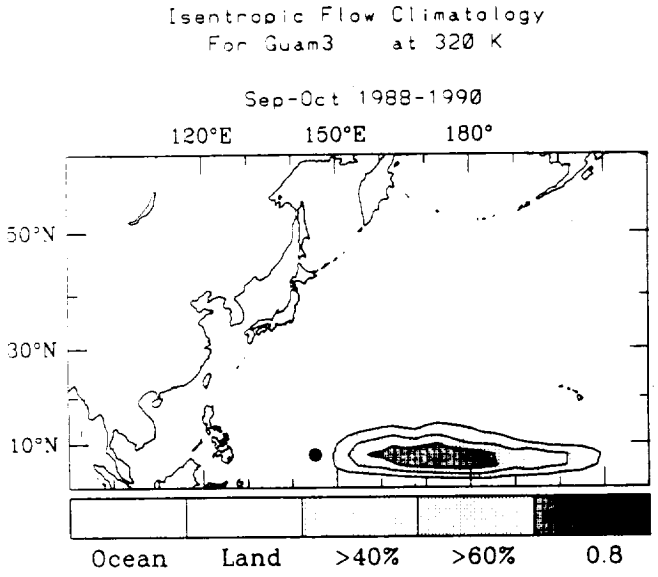

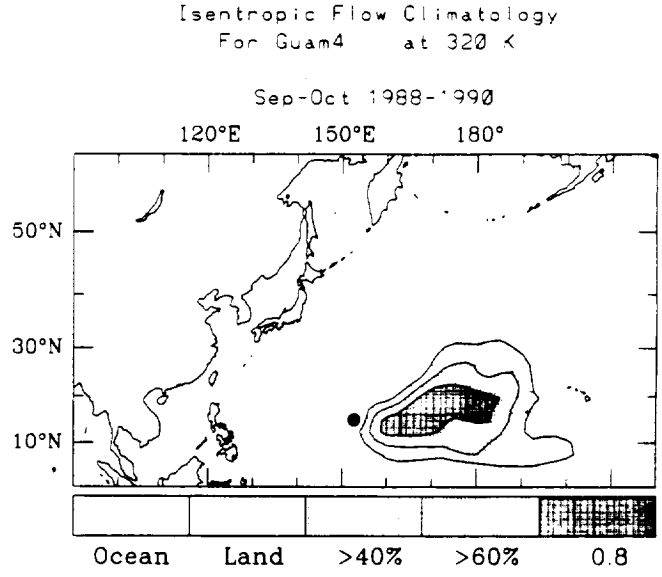

Figure 6

Part II: Photochemical Calculations

by José M. Rodriguez

1. Introduction

This section presents results of photochemical calculations of the time development of concentrations of different species along an air parcel. Because of uncertainties in initial conditions, radiation field, clouds, washout and other parameters, it is not our purpose to provide a "climatology" of expected concentrations for the Pacific West region. Our philosophy in these calculations is rather to illustrate the sensitivity of results to different input parameters for a given air parcel trajectory. This preliminary sensitivity analysis provides guidelines for the expected variability that uncertainties in the photochemistry introduce in the results. We stress that other processes, such as mixing, in-situ sources of NOx, or diabatic motion, are not included in a Lagrangian formulation and will introduce additional uncertainties in the calculations.

II. Description of calculations

The photochemical model solves the equation

$$dn_i/dt = P_i(t) - L_i(t)\, n_i(t) \qquad (1)$$

where n_i, P_i, and L_i denote the concentration (cm^{-3}), photochemical production ($cm^{-3}\ s^{-1}$) and loss frequency (s^{-1}) for species i, respectively. The time dependence of n_i, P_i, and L_i are determined by changes in the radiation field, temperature, pressure, and humidity along the air parcel.

The photochemical model includes complete chemistry for HOx, NOx, chlorine and bromine species, as well as complete oxidation of methane and ethane. Column densities of O_2 and O_3 above a given altitude are taken from the AER 2-D results, which are in good agreement with satellite observations. Photolysis rates are calculated including the effects of multiple scattering, and assuming an albedo of 0.3. Unless otherwise indicated, the calculations are for clear sky conditions.

III. Model Initialization

Solution of equation (1) requires specification of initial conditions for the calculated species. Two kinds of species can be identified:

a) Long-lived species: Photochemical time constants for these species are of order of days or longer. Their initial concentrations are thus not fully determined by the conditions at the starting point, and are treated as input to the model. Initial conditions for these species are taken from results of the AER 2-D model, unless otherwise specified. In particular, mixing ratios for CH_4, CO and C_2H_6 are taken to be 1.67 ppmv, 89 ppbv, and 1.6 ppbv respectively. These concentrations are consistent with observations of the above species.

Initial concentrations of HNO_3, PAN, NO_t ($NO + NO_2 + HO_2NO_2 + 2xN_2O_5 + NO_3 + ClNO_3$) and O_3 are specified as part of the sensitivity calculations, as described below.

b) Short-lived species: Photochemical time constants for these species (for example, OH, HO_2, NO, NO_2) are less than 1 day, and their concentrations are determined from the long-lived species, radiation field, temperature, and pressure at the initial point. We carry out a "spin up" run of several diurnal cycles at the initial location in order to calculate the photostationary state for the fast species at this location.

IV. Sensitivity calculations

Calculations are shown for the air parcel shown in Figure 1. This parcel represents a 6-day trajectory at a potential temperature of 320K, ending in the Tokyo area on September 23, 1990. Tick marks are given every 12 hours. The changes in water vapor, temperature, pressure and altitude along the trajectory are shown in Figure 2, as calculated by the URI analysis. In this and subsequent figures, day 6 corresponds to the end of the trajectory over the Tokyo area.

The calculations address sensitivity of the photochemical development to the following:

1) Sensitivity to initial conditions for NO_t
2) Sensitivity to initial conditions for HNO_3
3) Sensitivity to initial conditions for PAN
4) Sensitivity to initial conditions for O_3

5) Sensitivity to washout along the trajectory
6) Sensitivity to clouds.

The calculations assume an "average" set of conditions as follows:

NO_t from Spivakovsky et al. (1991)
HNO_3 from CITE-2 measurements (LeBal et al., 1990) over land.
PAN from CITE-2 measurements (Ridley et al., 1990) over land.
O_3 from the 2-D model near 6 km (34 ppbv)
No washout.
Clear sky.

For each of the sensitivity runs, the above are assumed except for the parameter whose impact is being tested. Sensitivity to NO_t, HNO_3, PAN, and O_3 adopt "high" and "low" initial values taken from the variability observed in the measurements. These values are summarized in Table 1. The washout run assumes a washout time constant of 3 days for HNO_3, H_2O_2, CH_2O, and aldehydes. The run testing sensitivity to clouds assumes clear sky, and 100% cloud coverage with optical thickness of 12, above and below air parcel. The effects of clouds on photolysis rates are calculated using the parameterization given by Chang et al. (1987).

V. Results

Results of our calculations are given in Figures 3 -8. These figures illustrate the sensitivity to NO_t (Figure 3), HNO_3 (Figure 4), PAN (Figure 5), O_3 (Figure 6), washout (Figure 7), and clouds (Figure 8). For each of the sensitivity runs, we present 16 panels corresponding to calculated NO, NO_2, NO_x ($NO + NO_2$), NO/NO_2, HNO_3, PAN, HNO_3/NO_x, PAN/NO_x, O_3, OH, HO_2, H_2O_2, NO_y($PAN + HNO_3 + NO_t$), NO_x/NO_y, PAN/NO_y, and HNO_3/NO_y. The choice of the above is intended to provide information pertaining expected oxidative state of atmosphere, concentration and partitioning of nitrogen species, and production of ozone.

Given the preliminary nature of the above calculations, no conclusions are given at this point. We would like to emphasize, however, these points:

a) The concentrations of NO_x after 6 days seem fairly independent of initial conditions; in the absence of other processes, such as mixing or production by lightning, these concentrations are then essentially determined by the photochemistry. However, we can expect mixing and in-situ sources to be important.

Measurements by PEM-West instruments should provide important insight on the magnitude of these corrections.

b) Ozone production and OH are most sensitive to the adopted NO_t and radiation field. Special effort should be devoted to constraining these parameters from PEM and other measurements.

c) Maximum calculated production of ozone is of order 1 ppbv/day. Production of ozone along the parcel trajectory seems to increase the initial ozone by at most 30%, and the calculated ozone is determined primarily by the adopted initial conditions.

d) A wide range of partitioning of the nitrogen species can be obtained based on the previous history of the air parcel.

VI. Other air parcels

We have also carried out calculations for the marine air parcel shown in Figure 9. The initial conditions for this air parcel have been modified to better reflect the expected marine environment (ie., lower NO_t, HNO_3, O_3). However, the sensitivity of the results to the uncertainties considered are similar to the ones presented in Figures 3-8. For the sake of brevity, we omit these results in this report, but are available upon request.

Table 1: Adopted Initial Conditions for Sensitivity Runs				
Initial Conditions	**NO_t (pptv)**	**HNO_3 (pptv)**	**PAN (pptv)**	**O_3 (ppbv)**
High	100	284	249	60
Average	50	218	149	34
Low	10	150	49	20

References

Chang, J.S., R.A. Brost, I.S.A. Isaksen, S. Madronich, P. Middleton, W.R. Stockwell, and C.J. Walcek (1987) A three-dimensional eulerian acid deposition model: physical concepts and formulation. *J. Geophys. Res.*, **92**, 14,681-14,700.

LeBel, P.J., B.J. Huebert, H.I. Schiff, S.A. Vay, S.E. VanBramer, and D.R. Hastie (1990) Measurements of tropospheric nitric acid over the Western United States and Northeastern Pacific Ocean. *J. Geophys. Res.*, **94**, 10,199-10,204.

Ridley, B.A., J.D. Shetter, B.W. Gandrud, L.J. Salas, H.B. Singh, M.A. Carroll, G. Hübler, D.L. Albritton, D.R. Hastie, H.I. Schiff, G.I. MacKay, D.R. Karechi, D.D. Davis, J.D. Bradshaw, M.O. Rodgers, S.T. Sandholm, A.L. Torres, E.P. Condon, G.L. Gregory, and S. M. Beck (1990) Rations of peroxyacetyl nitrate to active nitrogen observed during aircraft flights over the Eastern Pacific Ocean and continental United States. *J. Geophys. Res.*, **95**, 10,179-10,192.

Spivakovsky, C.M., R. Yevich, J.A. Logan, S.C. Wofsy, M.B. McElroy, and M.J. Prather (1990) Tropospheric OH in a threee-dimensional chemical tracer model: An assessment based on observations of CH_3CCl_3. *J. Geophys. Res.*, **95**, 18,441-18,471.

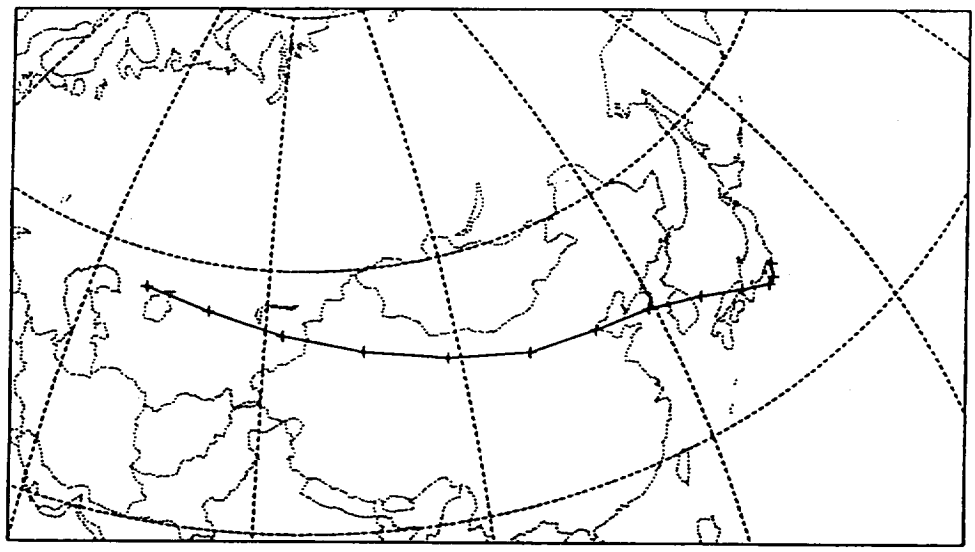

Figure 1: Trajectory of adopted air parcel. Tick marks are given every 6 hours. Trajectory starts over the continent and ends in the Tokyo area after 6 days, on September 23, 1990.

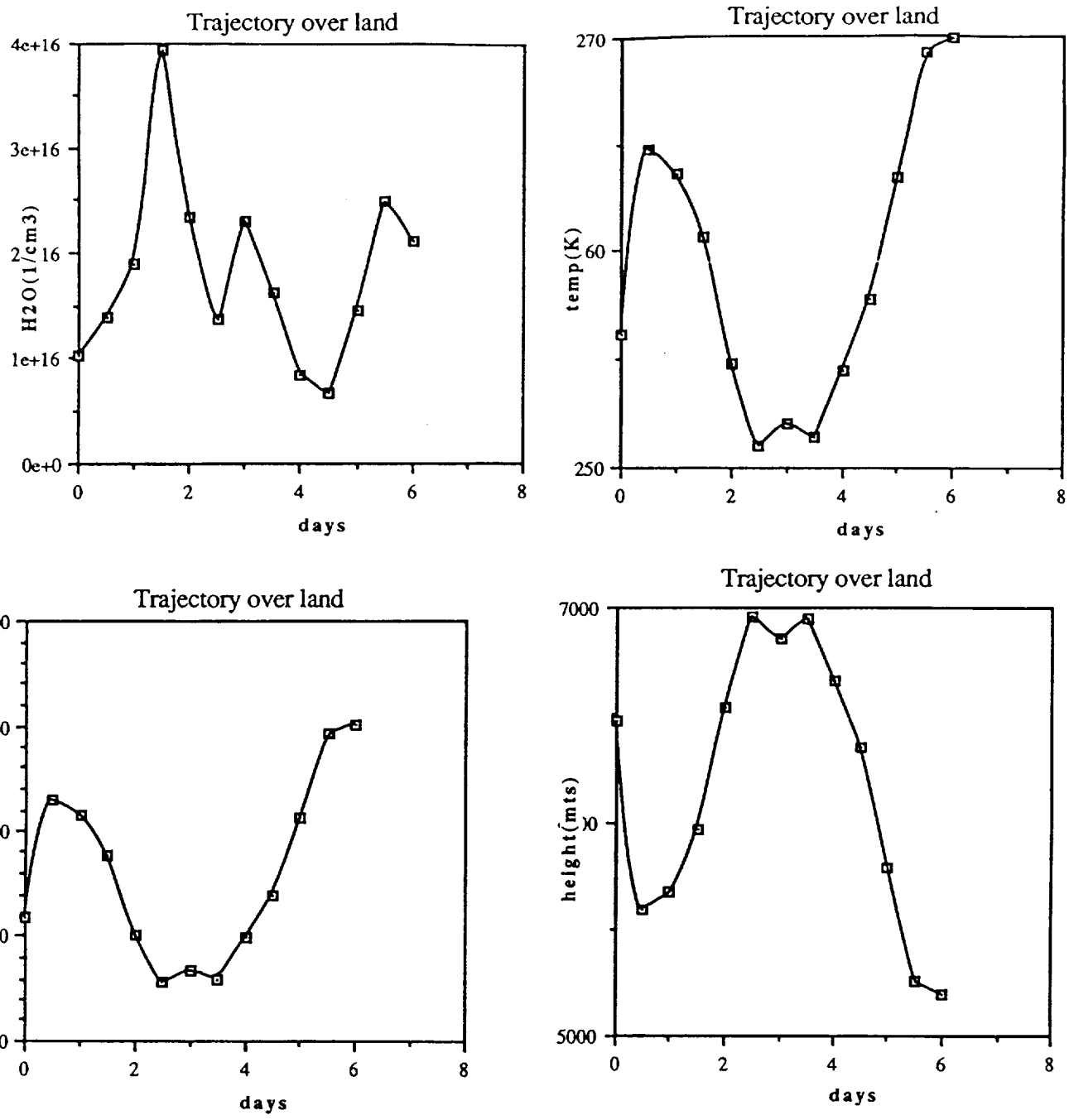

Figure 2: Changes in a) water vapor concentrations; b) temperature; c) pressure; and d) height (m) for the trajectory in Figure 1.

Figure 3. Sensitivity of results to adopted initial concentrations of NO_t ($NO + NO_2 + NO_3 + HO_2NO_2 + 2xN_2O_5 + ClNO_3$). High, average, and low values correspond to initial conditions of 100, 50, and 10 pptv, respectively. Other initial conditions are given in the "average" row of Table 1.

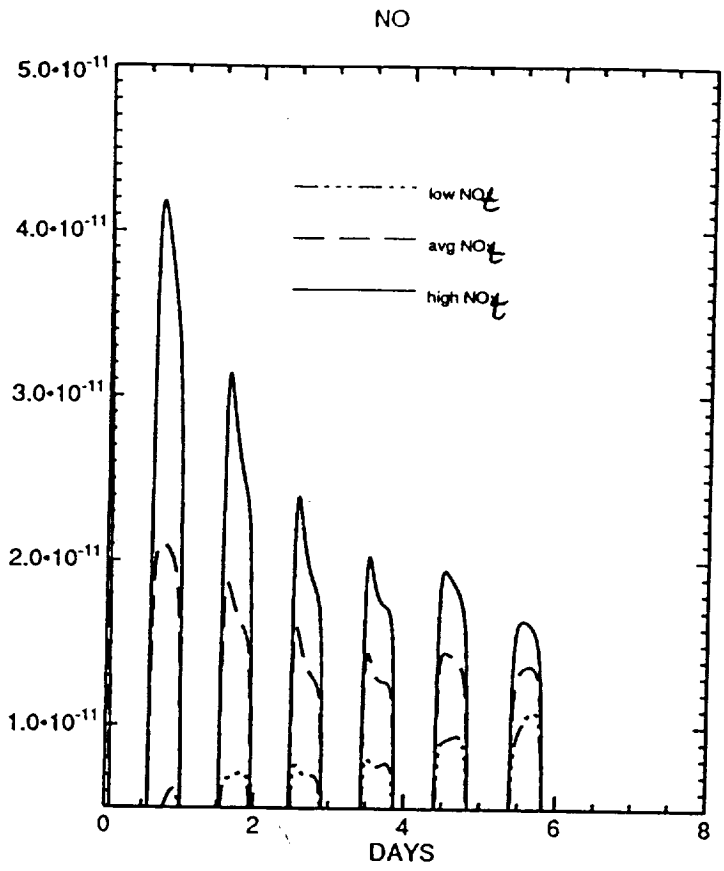
NO
low NOx
avg NOx
high NOx
5.0•10-11
4.0•10-11
3.0•10-11
2.0•10-11
1.0•10-11
0
2
4
6
8
DAYS

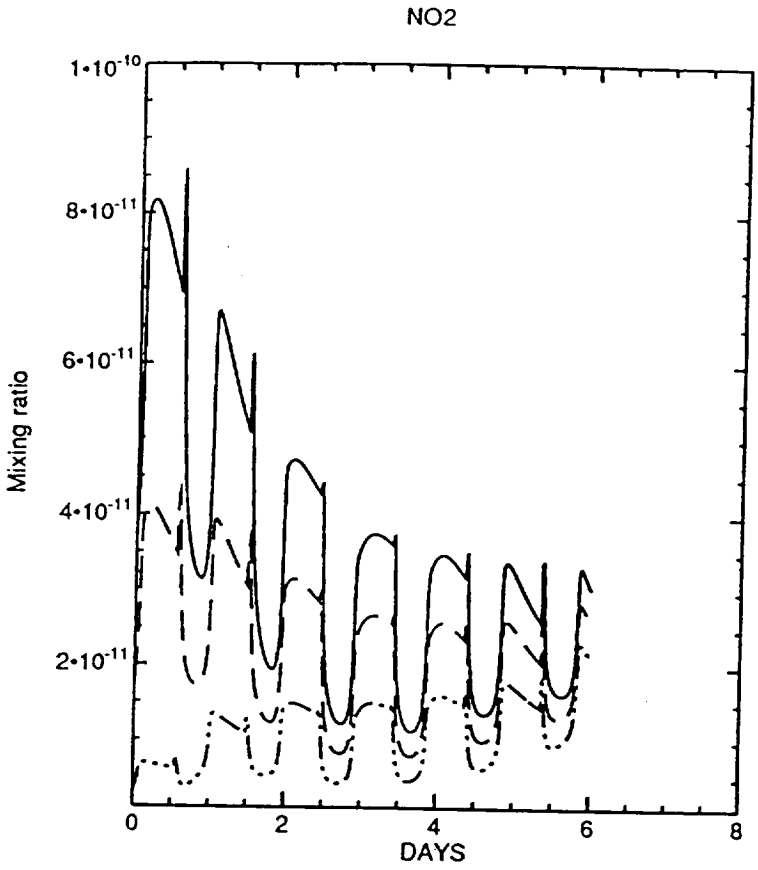
NO2
Mixing ratio
1•10-10
8•10-11
6•10-11
4•10-11
2•10-11
0
2
4
6
8
DAYS

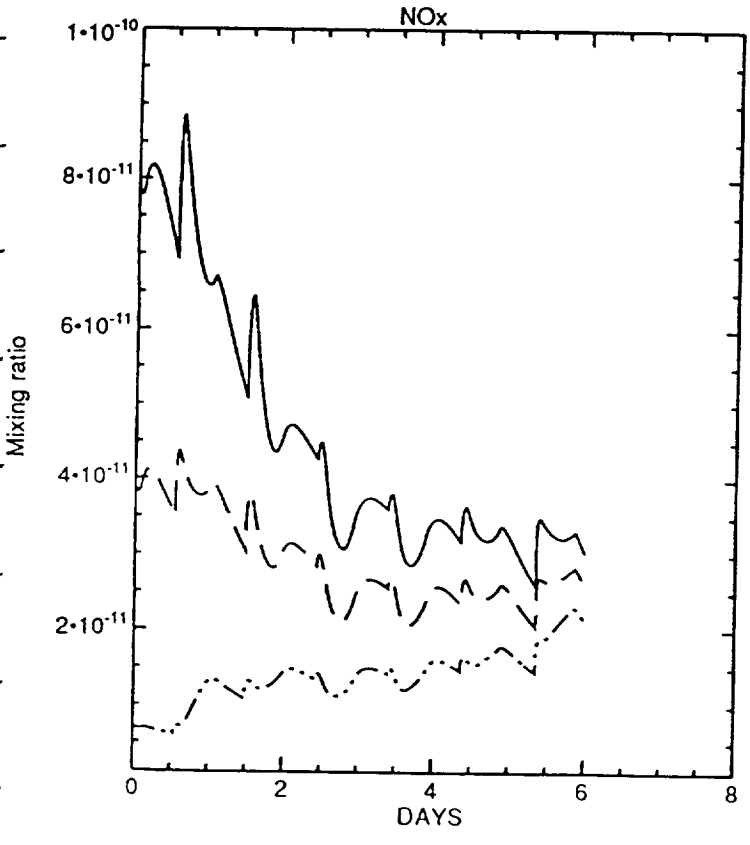
NOx
Mixing ratio
1•10-10
8•10-11
6•10-11
4•10-11
2•10-11
0
2
4
6
8
DAYS

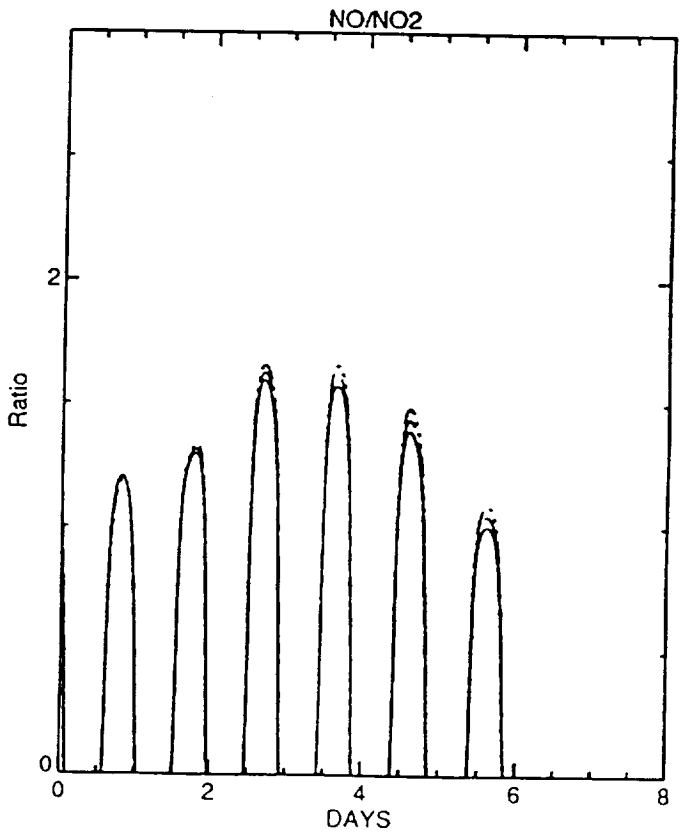
NO/NO2
Ratio
2
0
0
2
4
6
8
DAYS

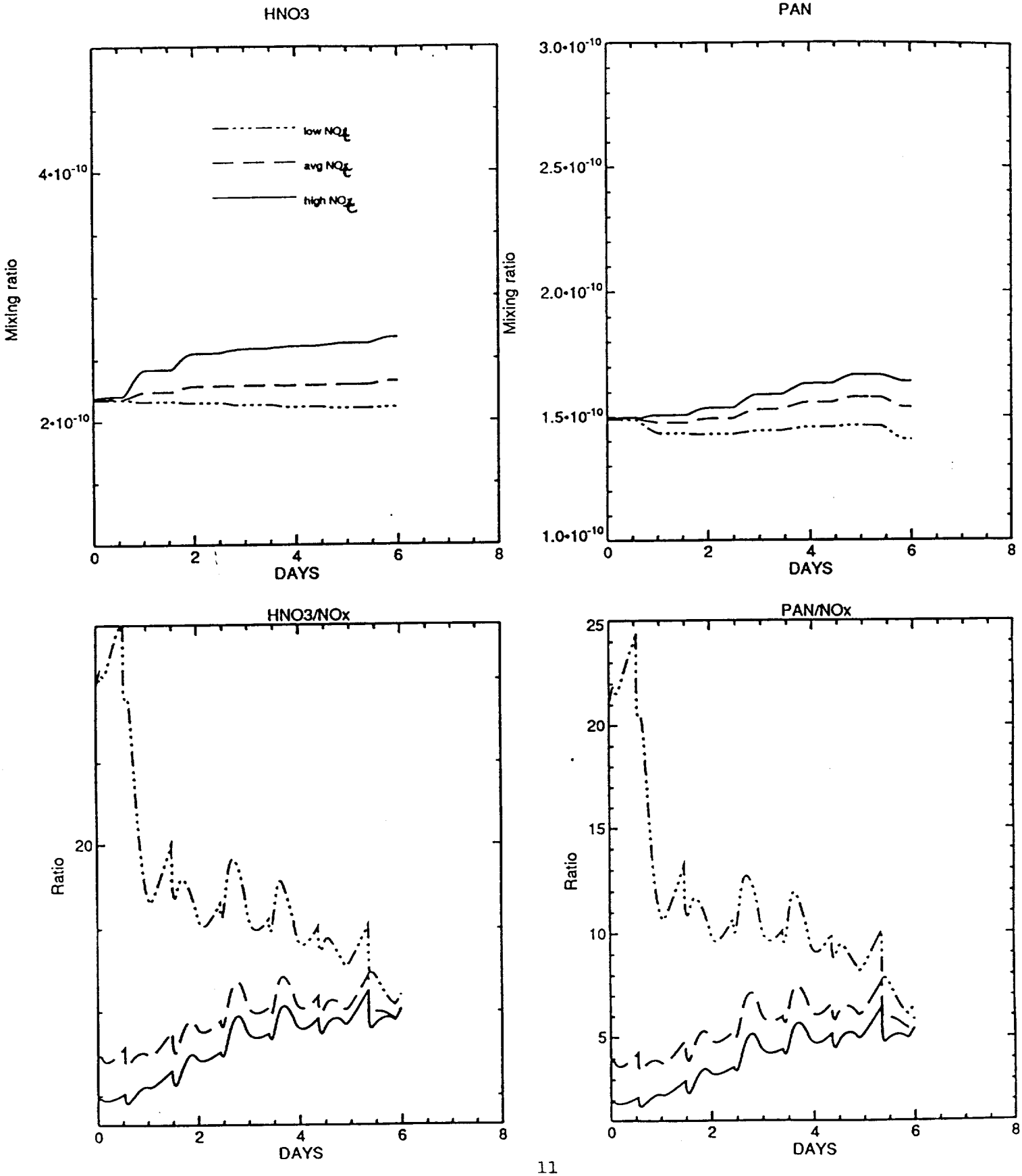
HNO3
low NOx
avg NOx
high NOx
4•10-10
2•10-10
Mixing ratio
0
2
4
6
8
DAYS
PAN
3.0•10-10
2.5•10-10
2.0•10-10
1.5•10-10
1.0•10-10
Mixing ratio
0
2
4
6
8
DAYS
HNO3/NOx
20
Ratio
1
0
2
4
6
8
DAYS
PAN/NOx
25
20
15
10
5
Ratio
1
0
2
4
6
8
DAYS

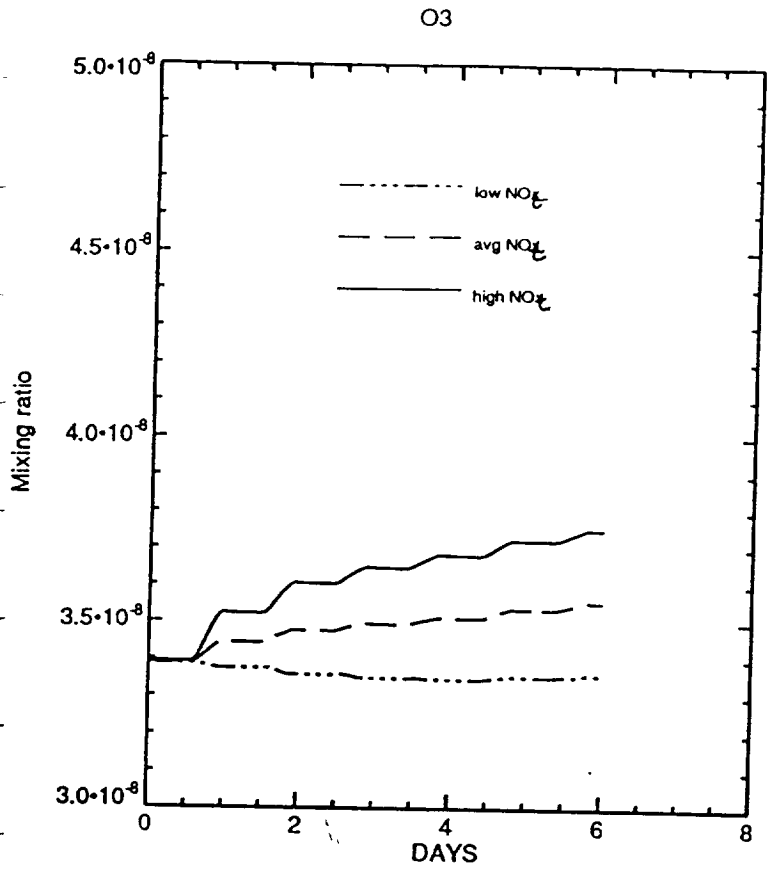
O3
Mixing ratio
5.0•10⁻⁸
4.5•10⁻⁸
4.0•10⁻⁸
3.5•10⁻⁸
3.0•10⁻⁸
low NOx
avg NOx
high NOx
0
2
4
6
8
DAYS

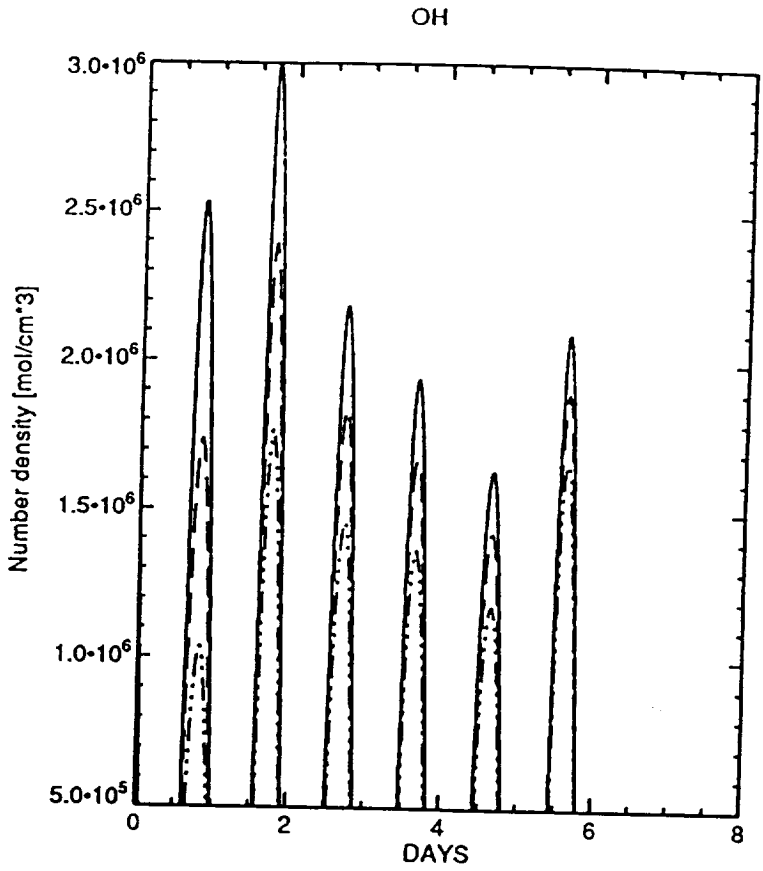
OH
Number density [mol/cm^3]
3.0•10⁶
2.5•10⁶
2.0•10⁶
1.5•10⁶
1.0•10⁶
5.0•10⁵
0
2
4
6
8
DAYS

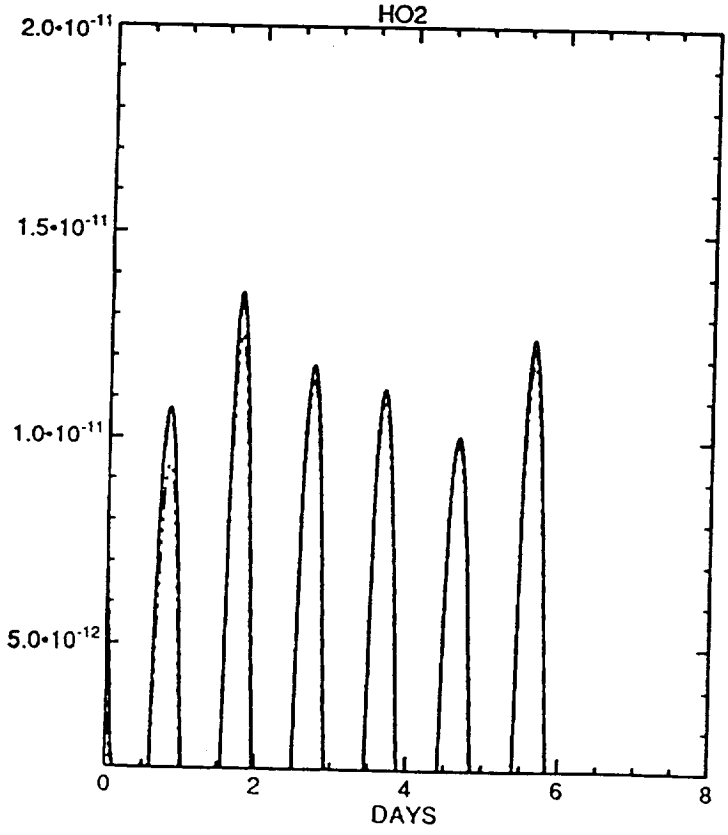
HO2
2.0•10⁻¹¹
1.5•10⁻¹¹
1.0•10⁻¹¹
5.0•10⁻¹²
0
2
4
6
8
DAYS

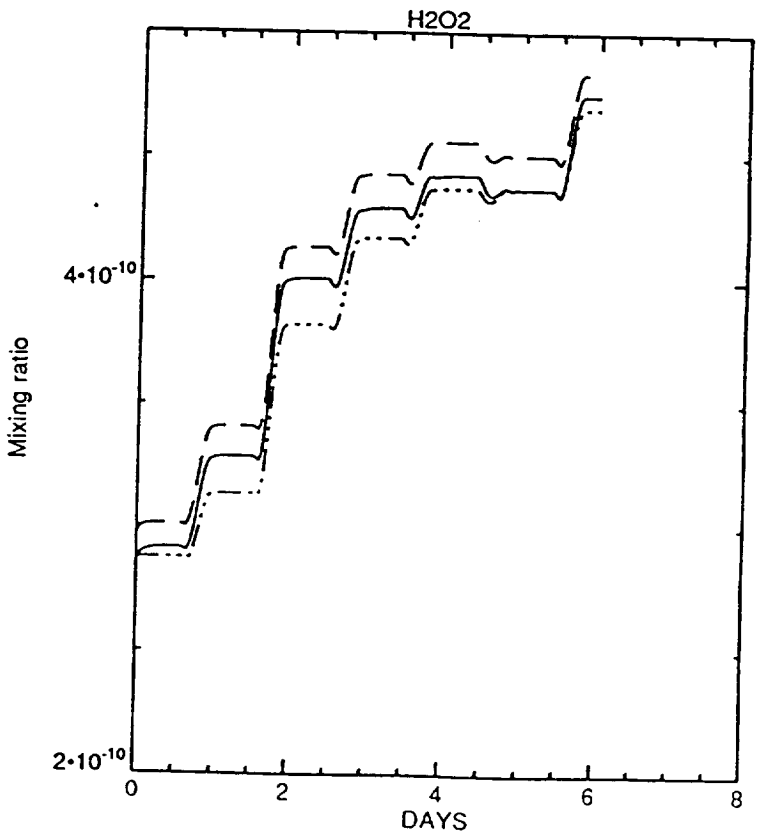
H2O2
Mixing ratio
4•10⁻¹⁰
2•10⁻¹⁰
0
2
4
6
8
DAYS

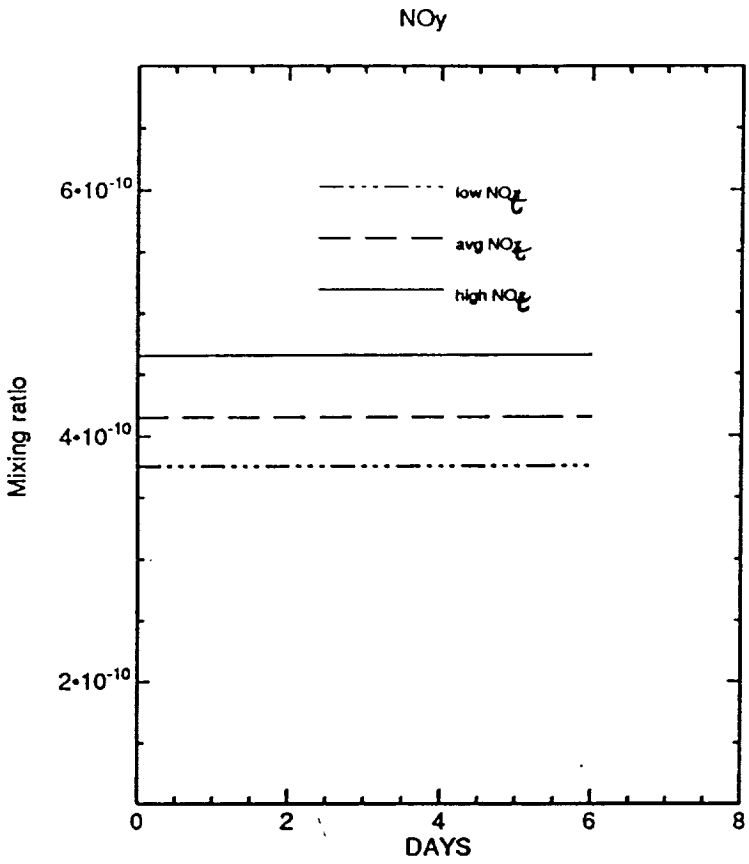
NOy
low NOz
avg NOz
high NOz
Mixing ratio
6•10-10
4•10-10
2•10-10
0
2
4
6
8
DAYS

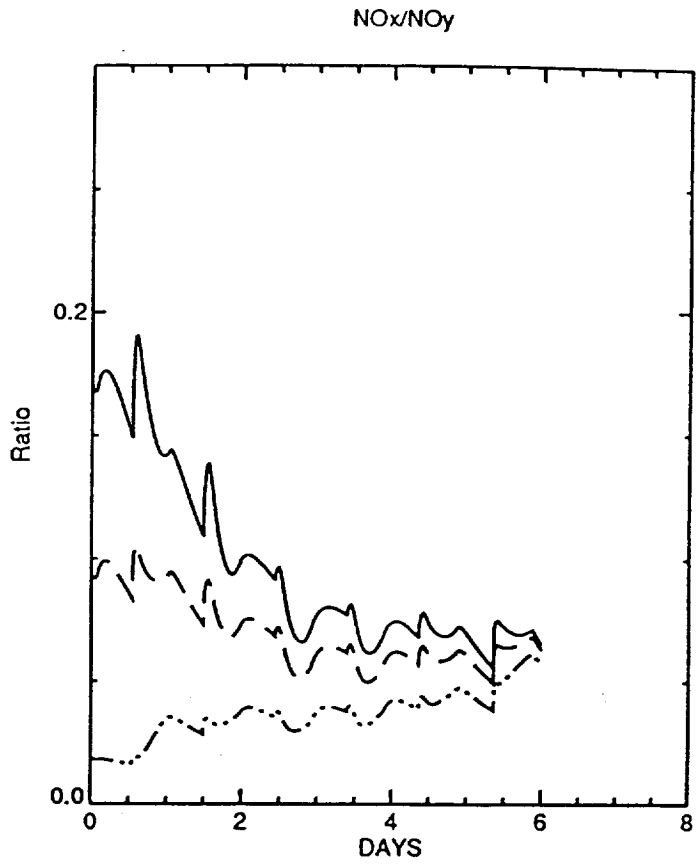
NOx/NOy
Ratio
0.2
0.0
0
2
4
6
8
DAYS

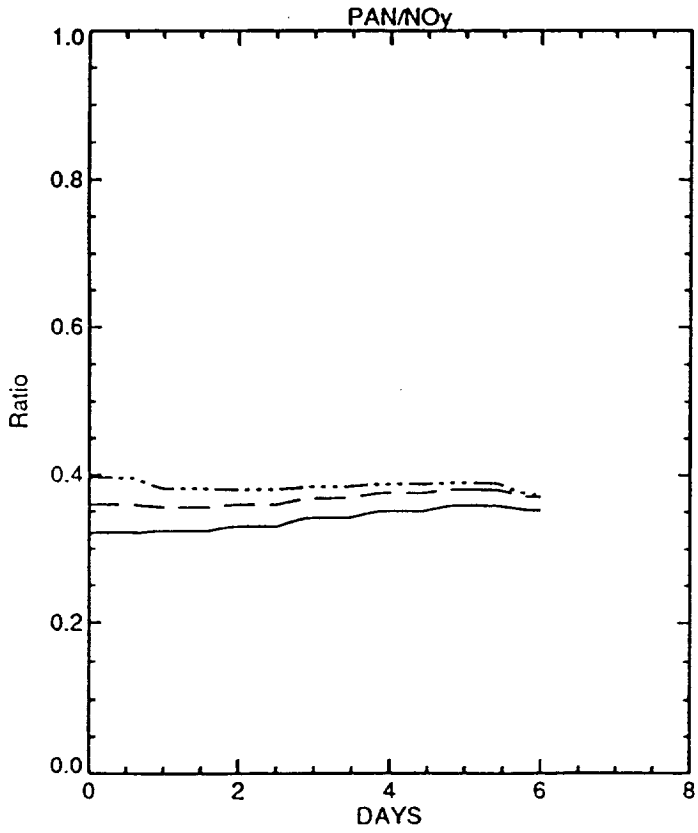
PAN/NOy
Ratio
1.0
0.8
0.6
0.4
0.2
0.0
0
2
4
6
8
DAYS

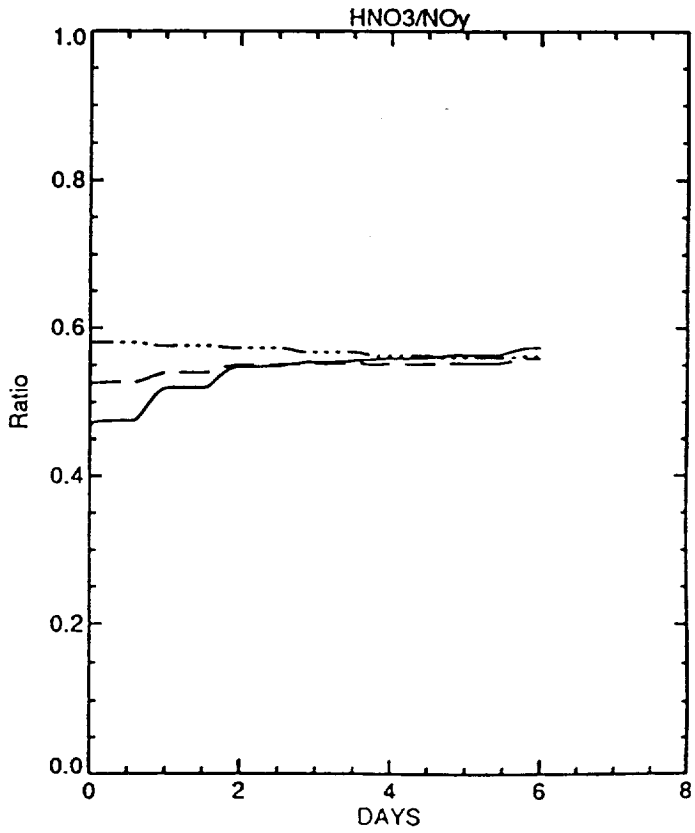
HNO3/NOy
Ratio
1.0
0.8
0.6
0.4
0.2
0.0
0
2
4
6
8
DAYS

Figure 4: Sensitivity of results to adopted initial concentrations of HNO_3. High, average, and low values correspond to initial conditions of 284, 218, and 150 pptv, respectively. Other initial conditions are given in the "average" row of Table 1.

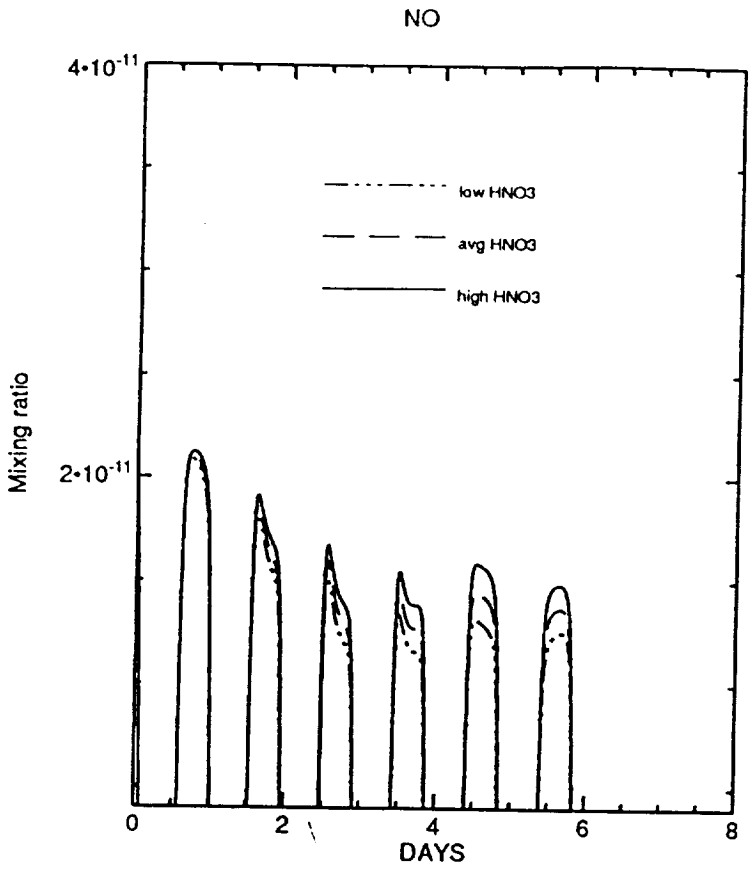
NO
low HNO3
avg HNO3
high HNO3
Mixing ratio
4•10-11
2•10-11
0
2
4
6
8
DAYS

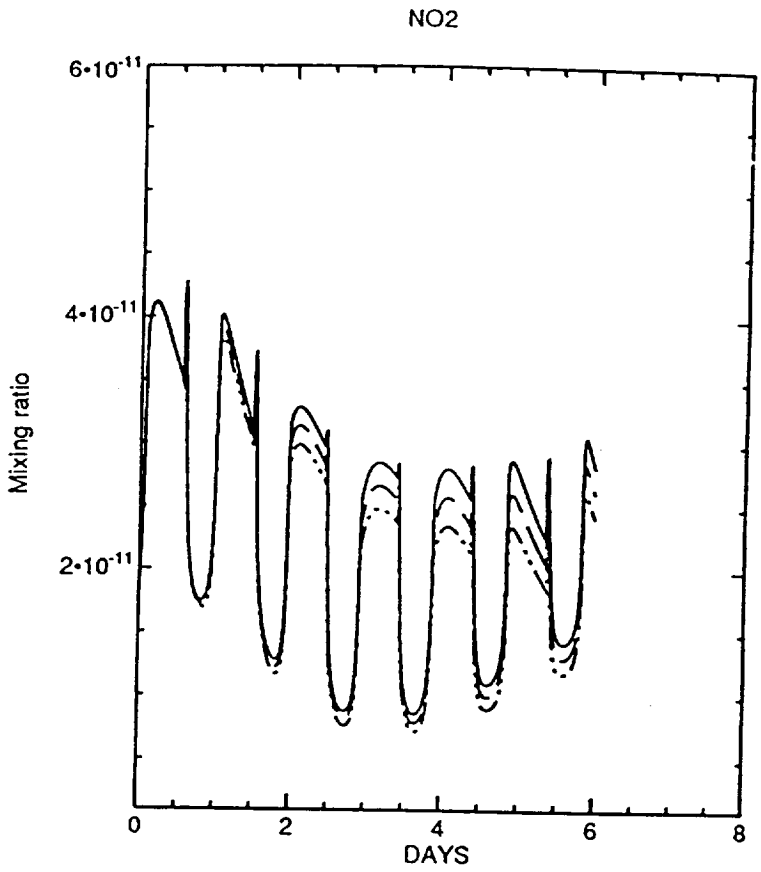
NO2
Mixing ratio
6•10-11
4•10-11
2•10-11
0
2
4
6
8
DAYS

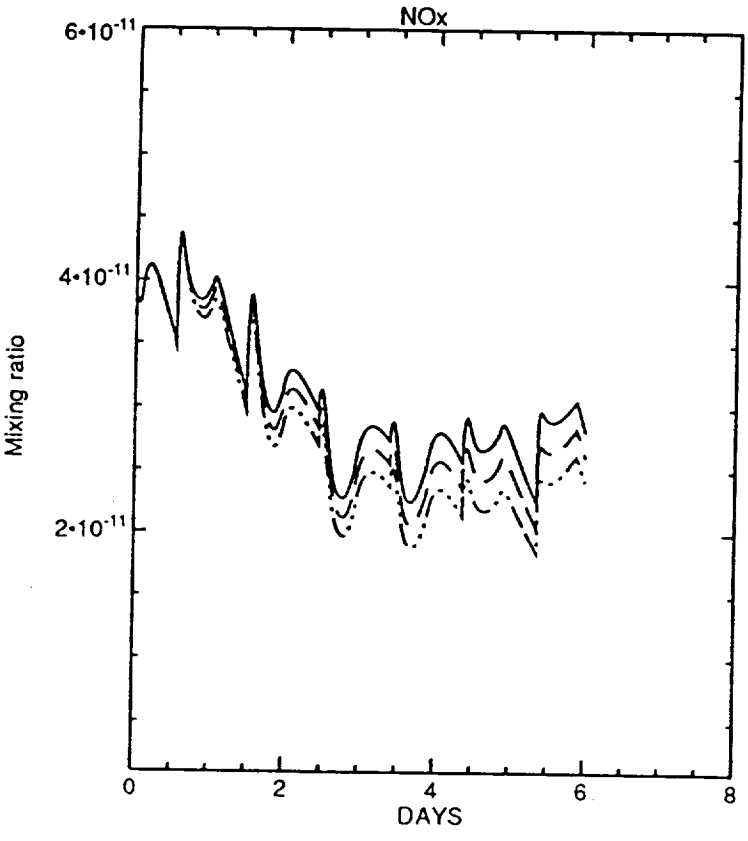
NOx
Mixing ratio
6•10-11
4•10-11
2•10-11
0
2
4
6
8
DAYS

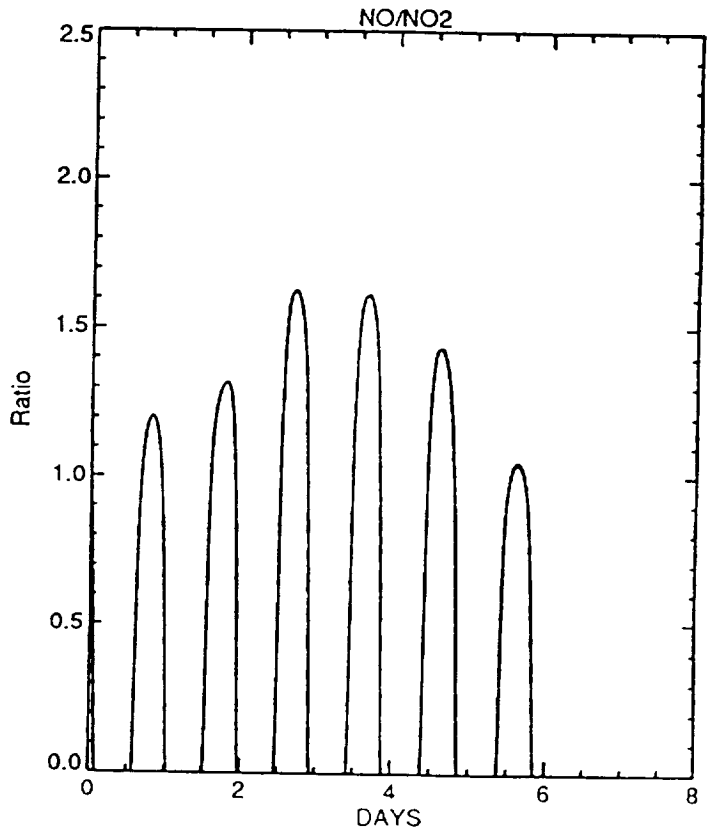
NO/NO2
Ratio
2.5
2.0
1.5
1.0
0.5
0.0
0
2
4
6
8
DAYS

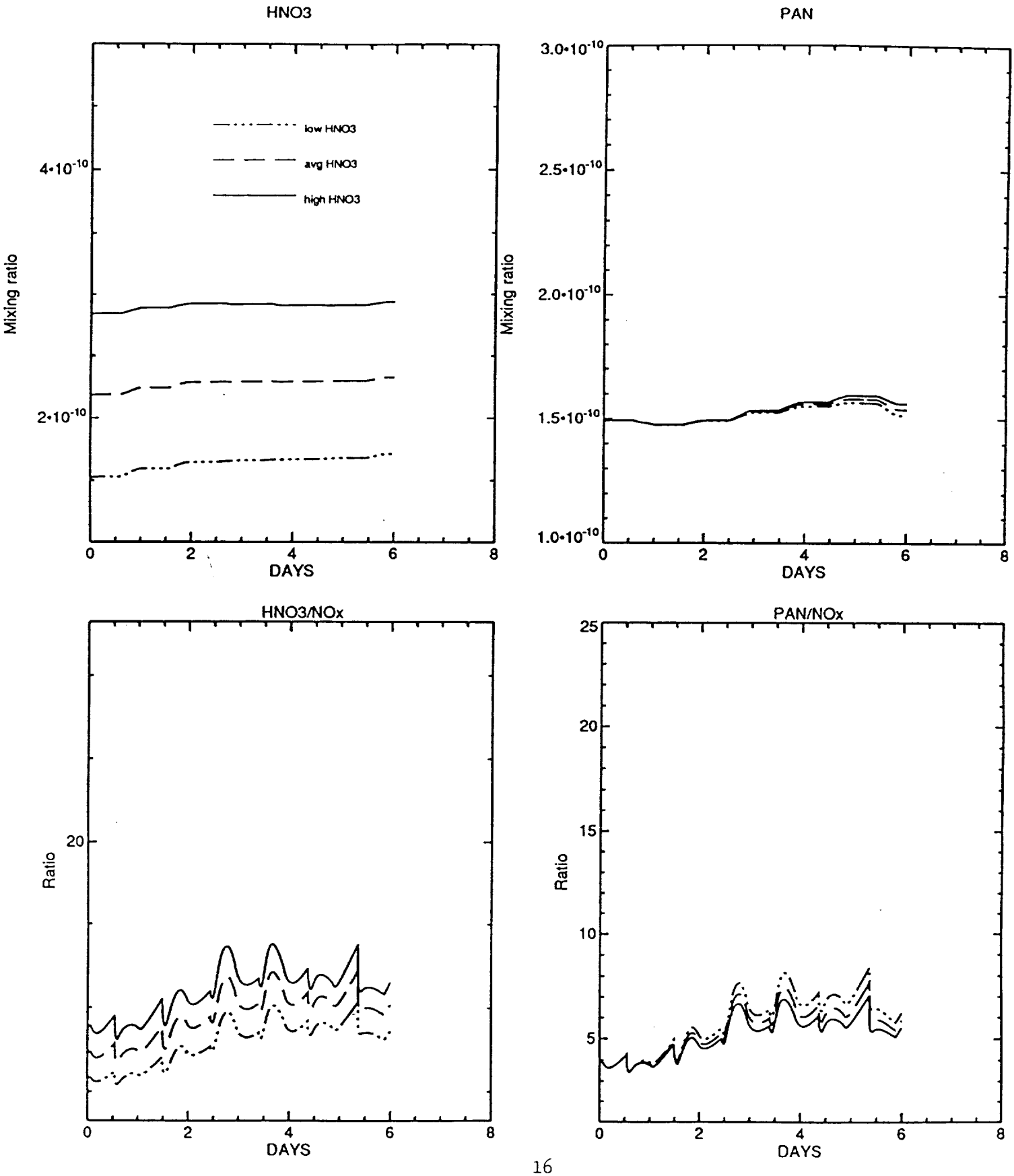
HNO3
low HNO3
avg HNO3
high HNO3
4•10-10
2•10-10
Mixing ratio
0
2
4
6
8
DAYS
PAN
3.0•10-10
2.5•10-10
2.0•10-10
1.5•10-10
1.0•10-10
Mixing ratio
DAYS
HNO3/NOx
20
Ratio
DAYS
PAN/NOx
25
20
15
10
5
Ratio
DAYS

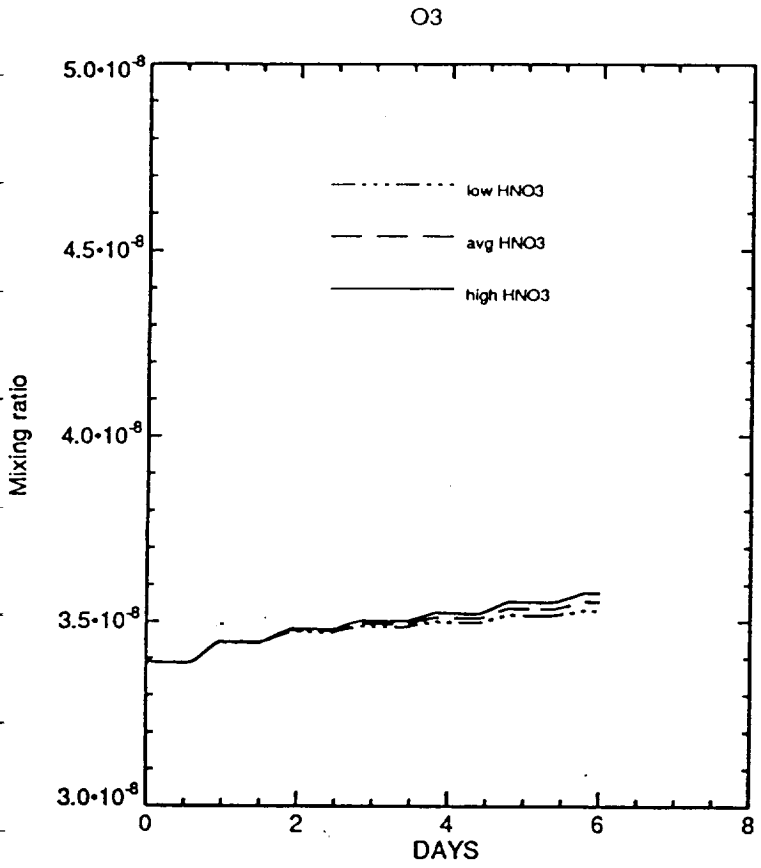
O3
low HNO3
avg HNO3
high HNO3
Mixing ratio
5.0•10-8
4.5•10-8
4.0•10-8
3.5•10-8
3.0•10-8
0
2
4
6
8
DAYS

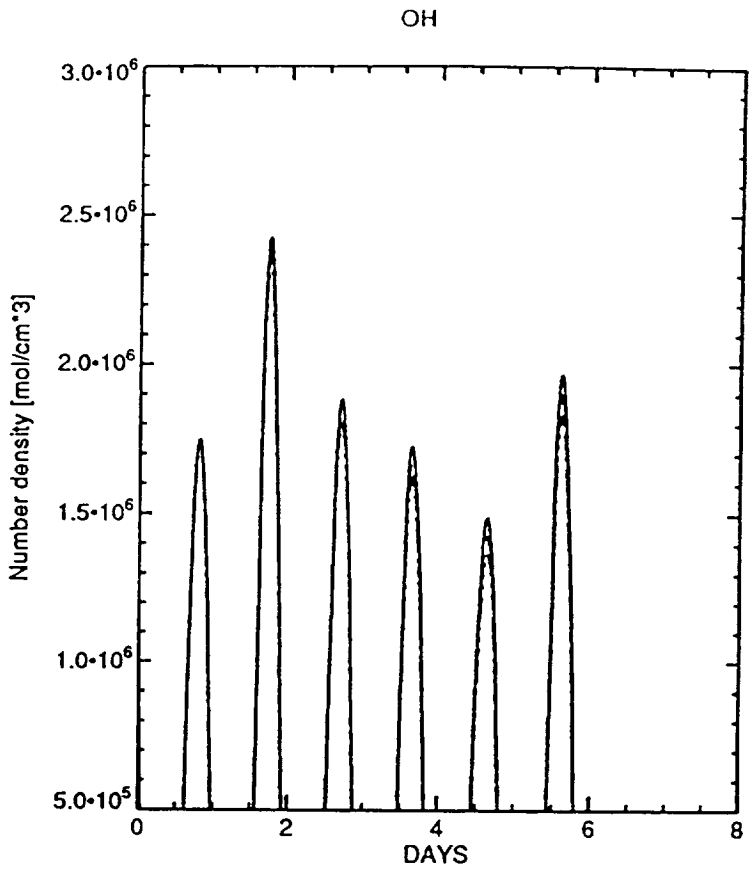
OH
Number density [mol/cm*3]
3.0•10^6
2.5•10^6
2.0•10^6
1.5•10^6
1.0•10^6
5.0•10^5
0
2
4
6
8
DAYS

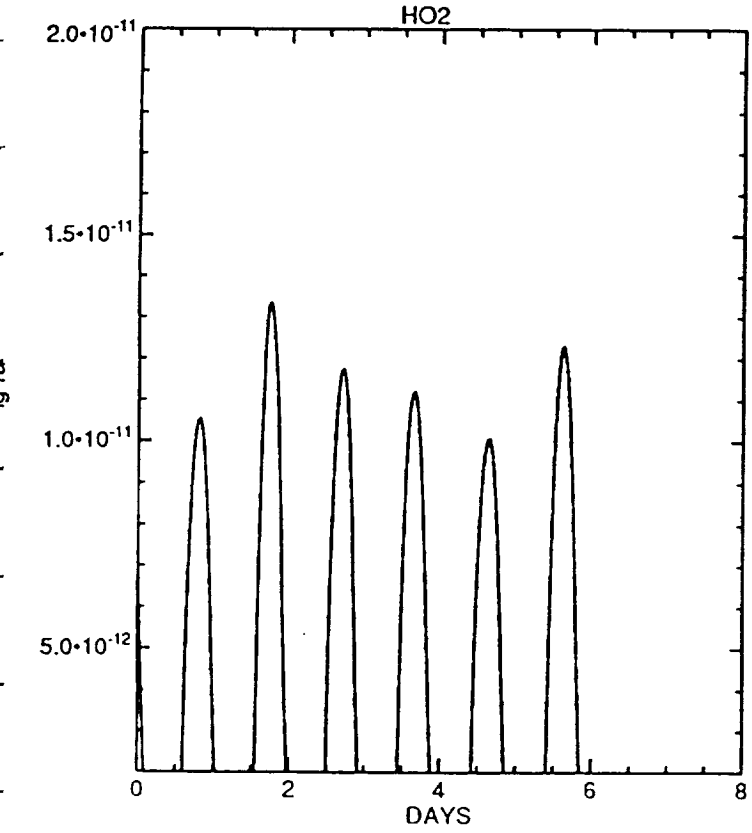
HO2
2.0•10-11
1.5•10-11
1.0•10-11
5.0•10-12
0
2
4
6
8
DAYS

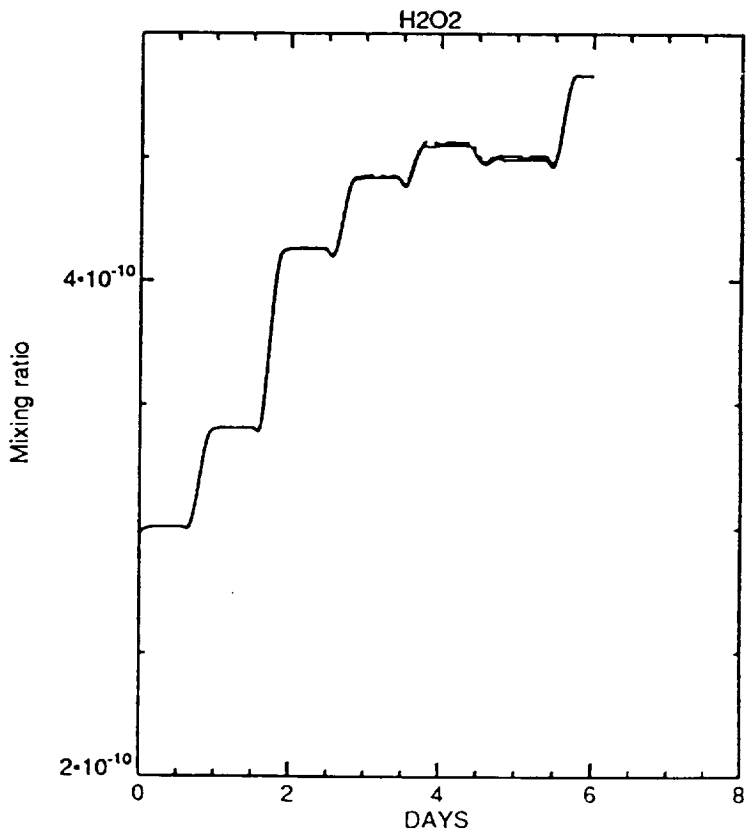
H2O2
Mixing ratio
4•10-10
2•10-10
0
2
4
6
8
DAYS

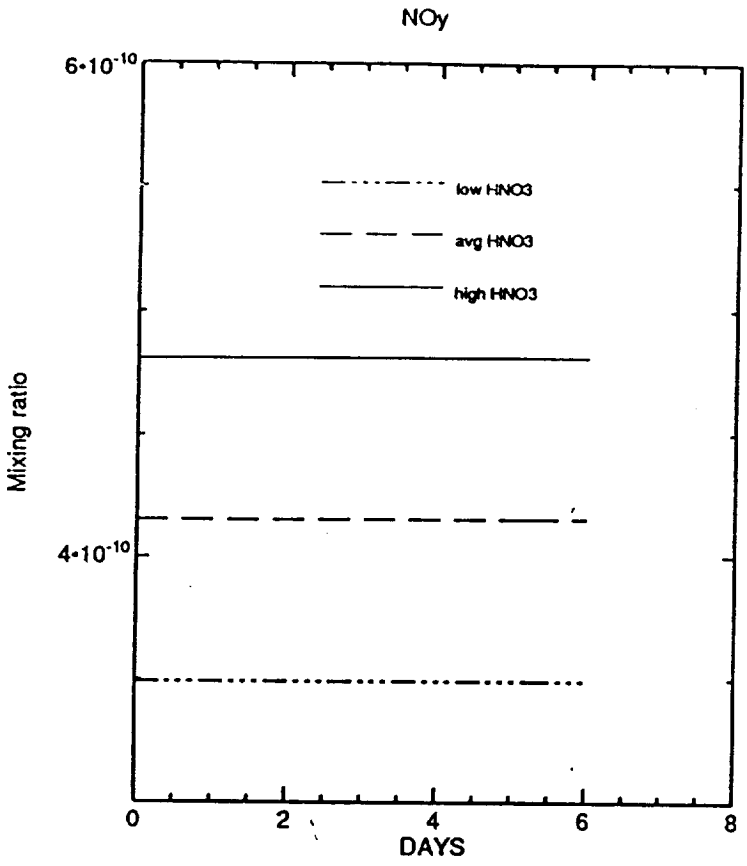
NOy
6•10-10
4•10-10
Mixing ratio
low HNO3
avg HNO3
high HNO3
0
2
4
6
8
DAYS

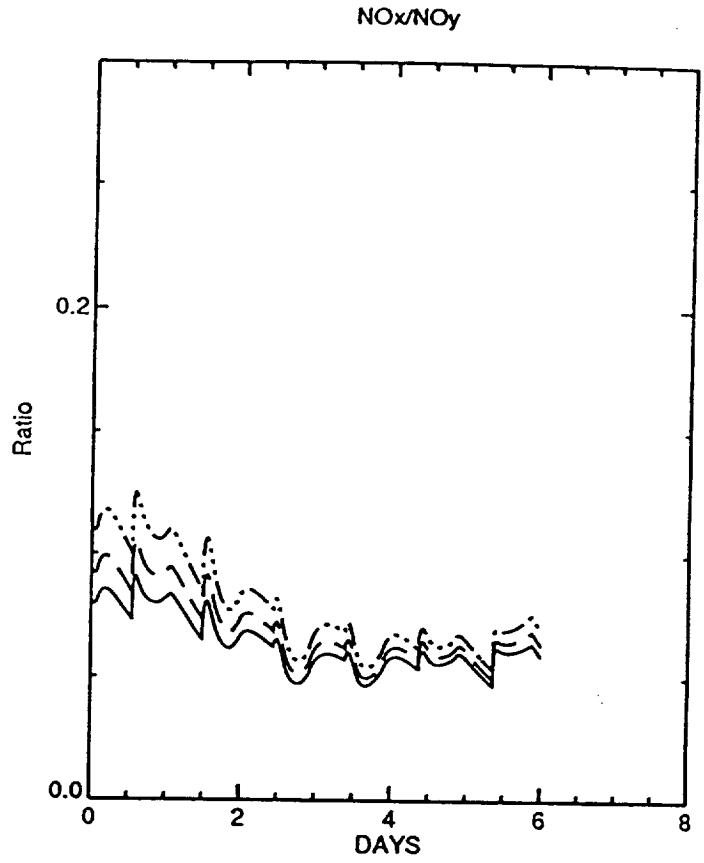
NOx/NOy
Ratio
0.2
0.0
0
2
4
6
8
DAYS

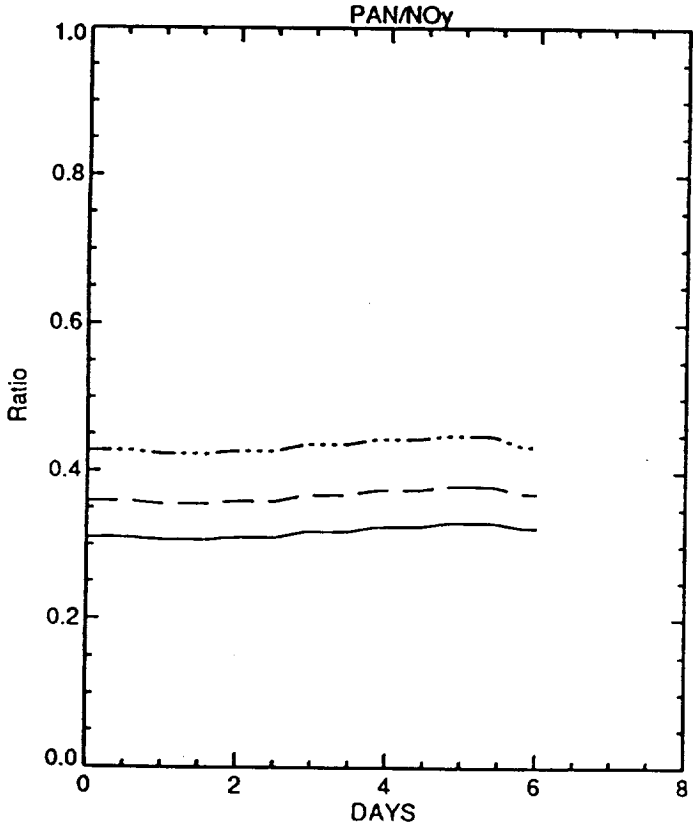
PAN/NOy
Ratio
1.0
0.8
0.6
0.4
0.2
0.0
0
2
4
6
8
DAYS

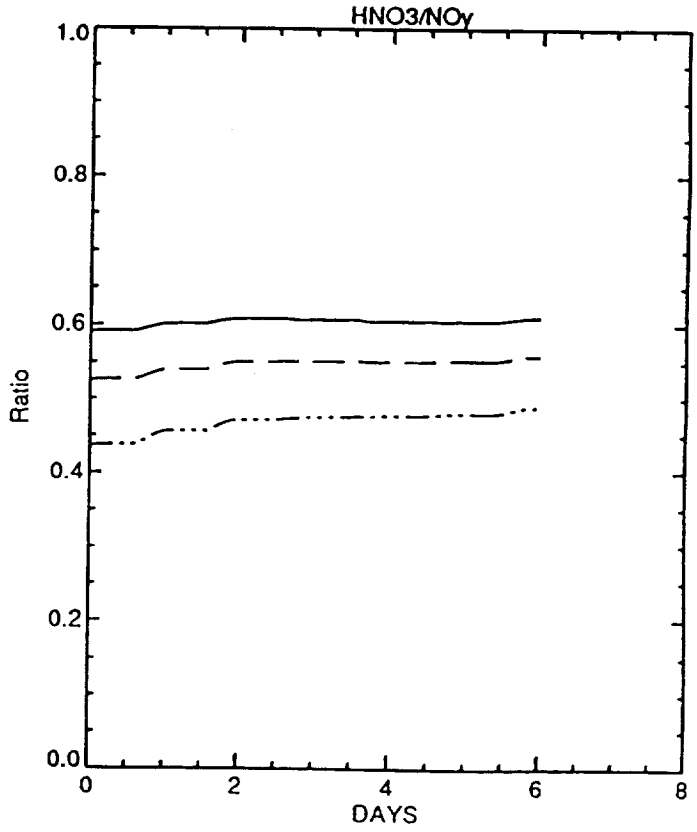
HNO3/NOy
Ratio
1.0
0.8
0.6
0.4
0.2
0.0
0
2
4
6
8
DAYS

Figure 5: Sensitivity of results to adopted initial concentrations of PAN. High, average, and low values correspond to initial conditions of 249, 149, and 49 pptv, respectively. Other initial conditions are given in the "average" row of Table 1.

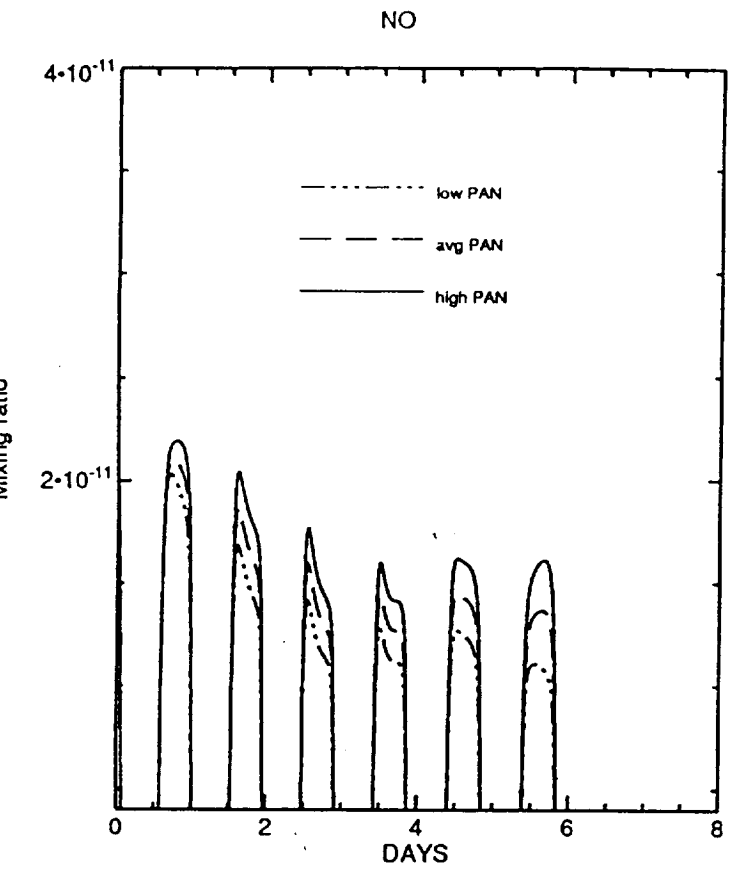
NO
low PAN
avg PAN
high PAN
Mixing ratio
4•10-11
2•10-11
0
2
4
6
8
DAYS

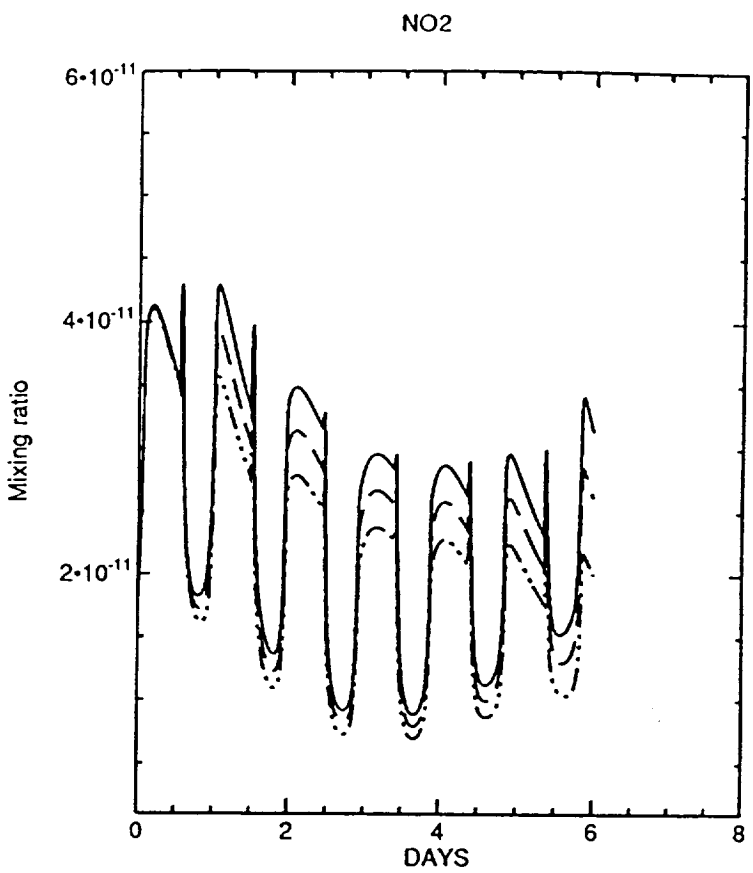
NO2
Mixing ratio
6•10-11
4•10-11
2•10-11
0
2
4
6
8
DAYS

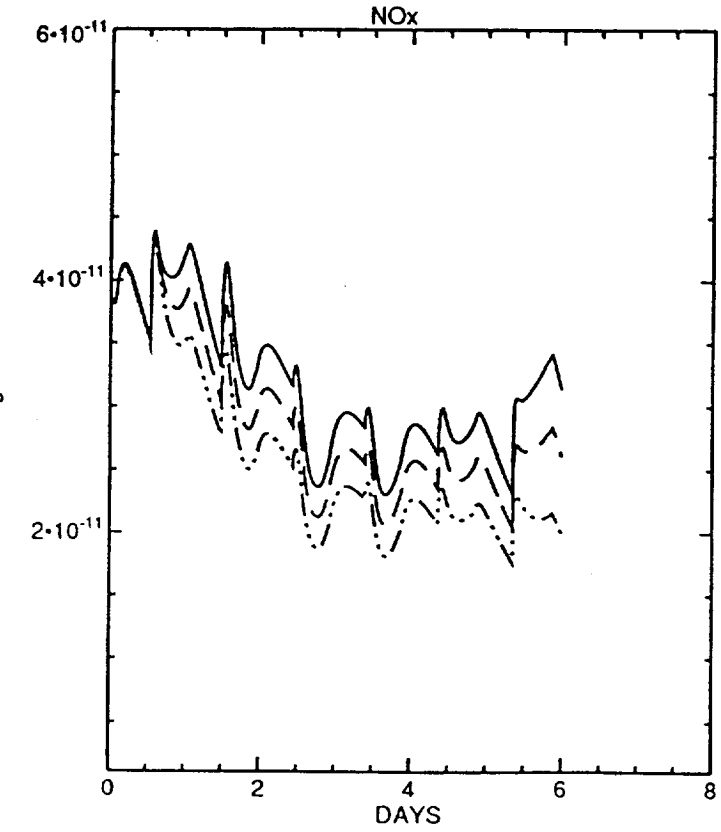
NOx
Mixing ratio
6•10-11
4•10-11
2•10-11
0
2
4
6
8
DAYS

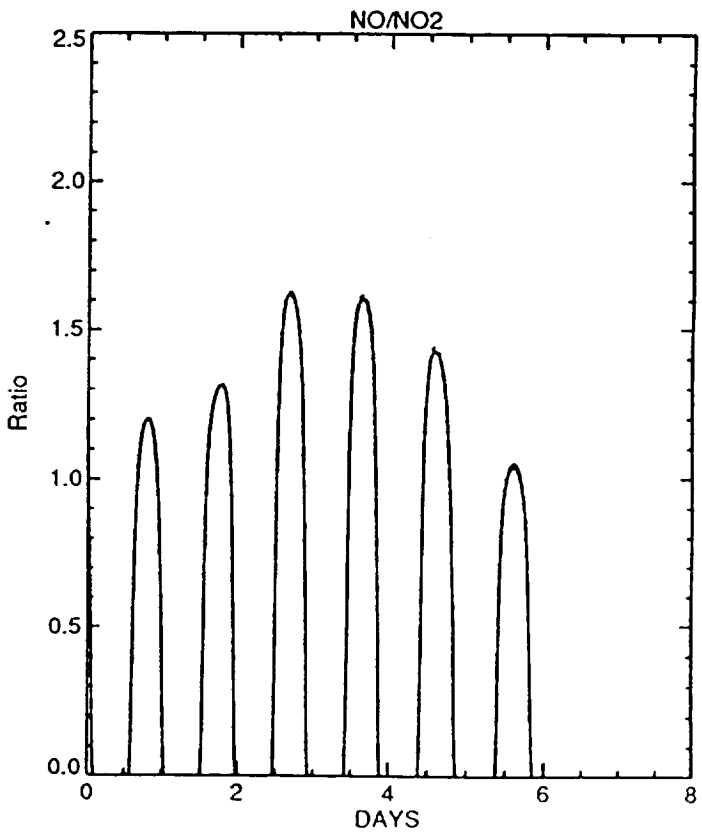
NO/NO2
Ratio
2.5
2.0
1.5
1.0
0.5
0.0
0
2
4
6
8
DAYS

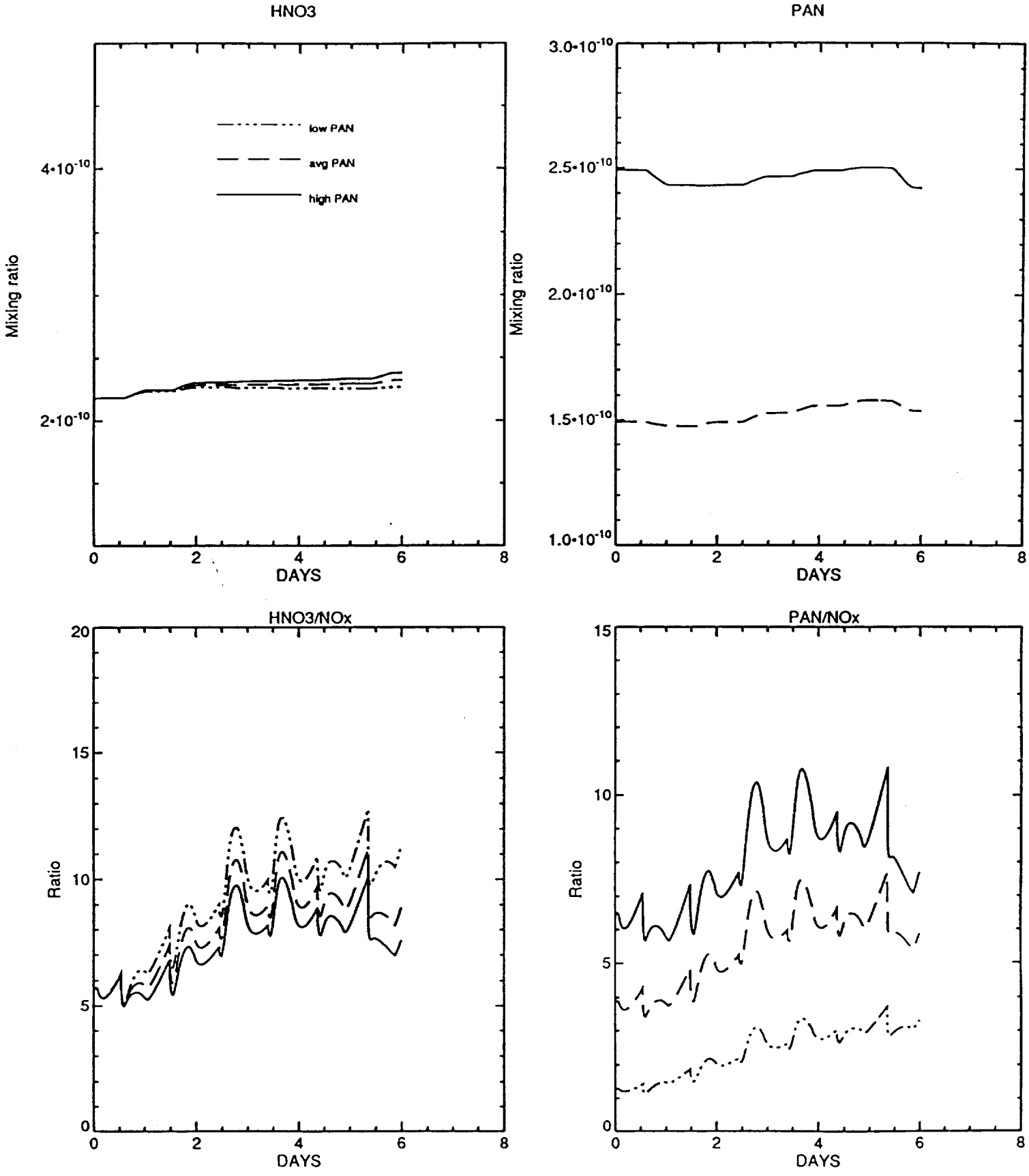
HNO3
low PAN
avg PAN
high PAN
4•10-10
2•10-10
Mixing ratio
0
2
4
6
8
DAYS
PAN
3.0•10-10
2.5•10-10
2.0•10-10
1.5•10-10
1.0•10-10
Mixing ratio
0
2
4
6
8
DAYS
HNO3/NOx
20
15
10
5
0
Ratio
0
2
4
6
8
DAYS
PAN/NOx
15
10
5
0
Ratio
0
2
4
6
8
DAYS

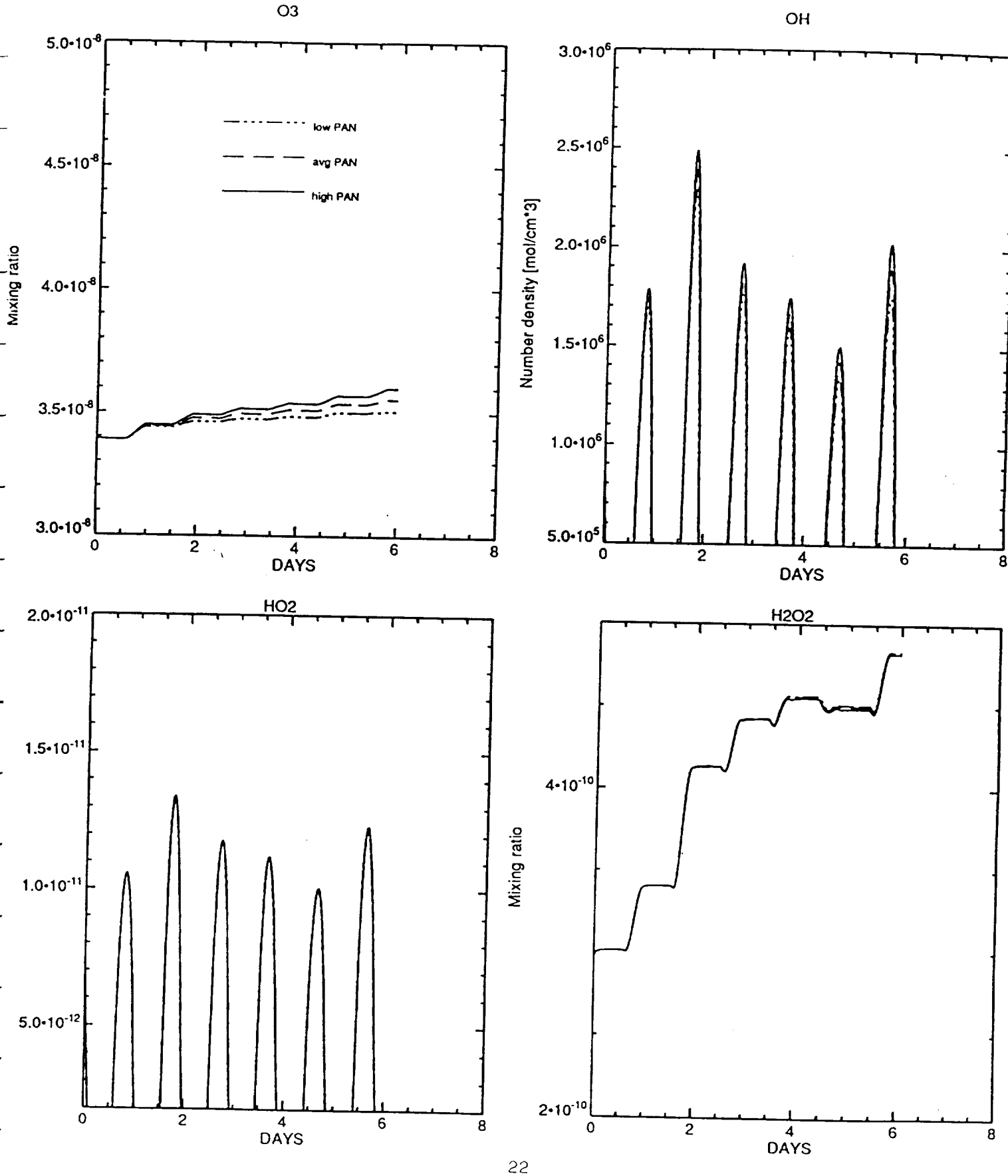
O3
5.0•10⁻⁸
4.5•10⁻⁸
4.0•10⁻⁸
3.5•10⁻⁸
3.0•10⁻⁸
Mixing ratio
low PAN
avg PAN
high PAN
0
2
4
6
8
DAYS
OH
3.0•10⁶
2.5•10⁶
2.0•10⁶
1.5•10⁶
1.0•10⁶
5.0•10⁵
Number density [mol/cm*3]
0
2
4
6
8
DAYS
HO2
2.0•10⁻¹¹
1.5•10⁻¹¹
1.0•10⁻¹¹
5.0•10⁻¹²
0
2
4
6
8
DAYS
H2O2
4•10⁻¹⁰
2•10⁻¹⁰
Mixing ratio
0
2
4
6
8
DAYS

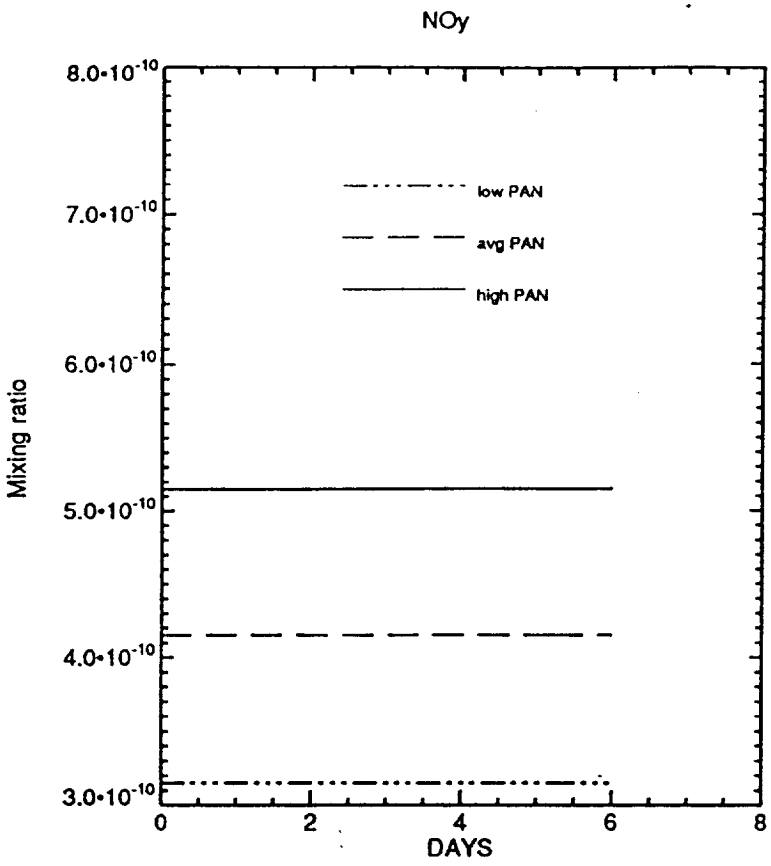
NOy
Mixing ratio
8.0•10-10
7.0•10-10
6.0•10-10
5.0•10-10
4.0•10-10
3.0•10-10
low PAN
avg PAN
high PAN
0
2
4
6
8
DAYS

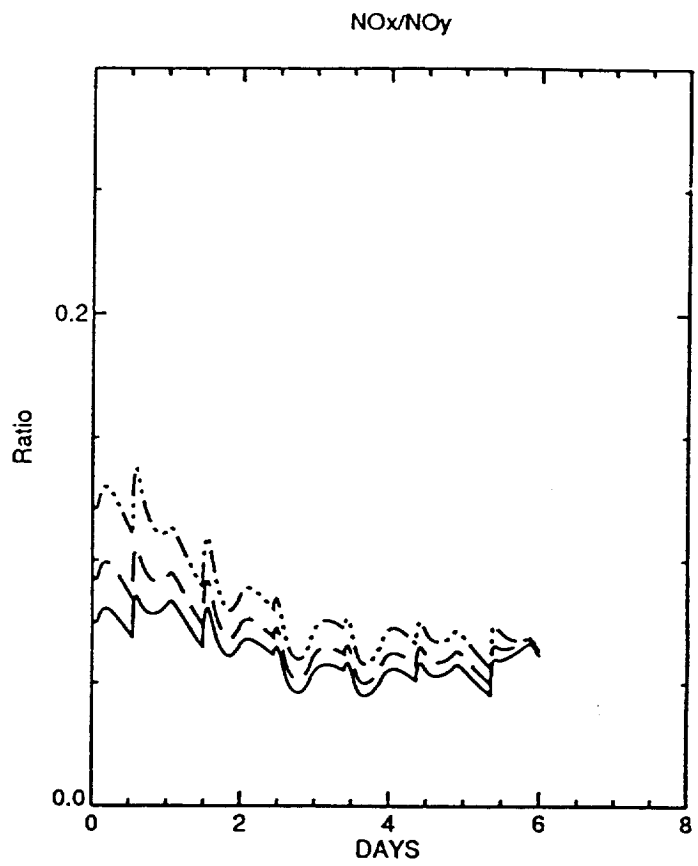
NOx/NOy
Ratio
0.2
0.0
0
2
4
6
8
DAYS

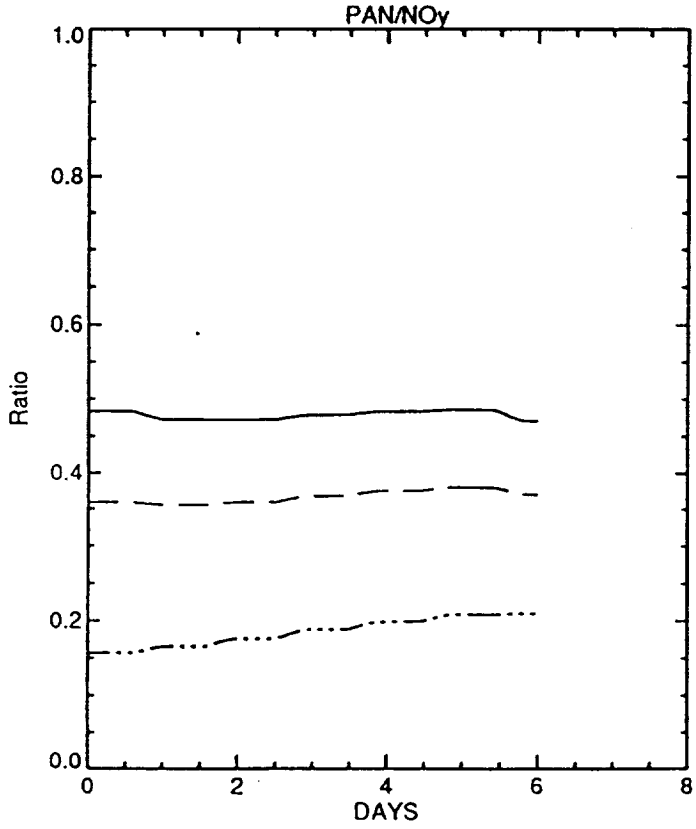
PAN/NOy
Ratio
1.0
0.8
0.6
0.4
0.2
0.0
0
2
4
6
8
DAYS

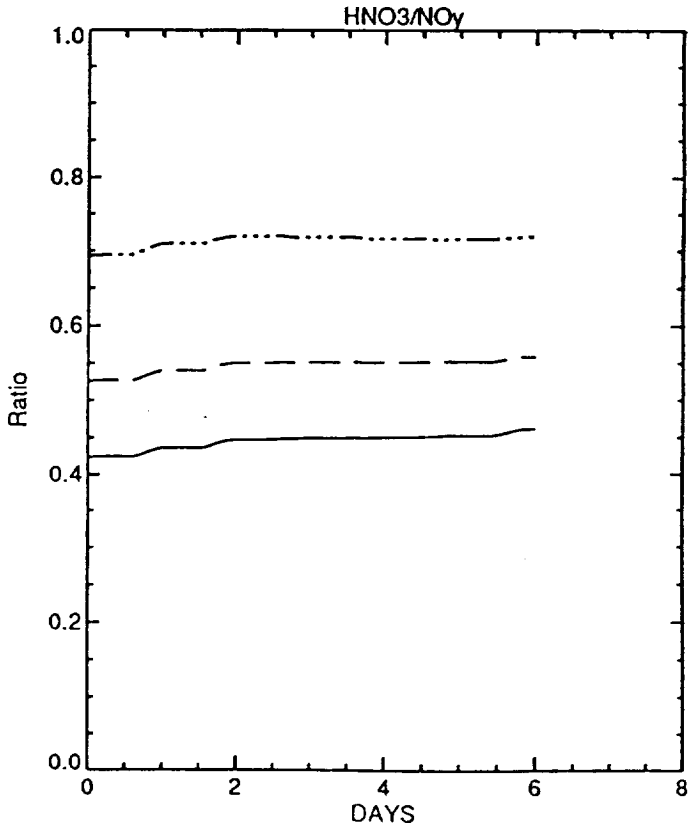
HNO3/NOy
Ratio
1.0
0.8
0.6
0.4
0.2
0.0
0
2
4
6
8
DAYS

Figure 6: Sensitivity of results to adopted initial concentrations of O_3. High, average, and low values correspond to initial conditions of 60, 34, and 20 ppbv, respectively. Other initial conditions are given in the "average" row of Table 1.

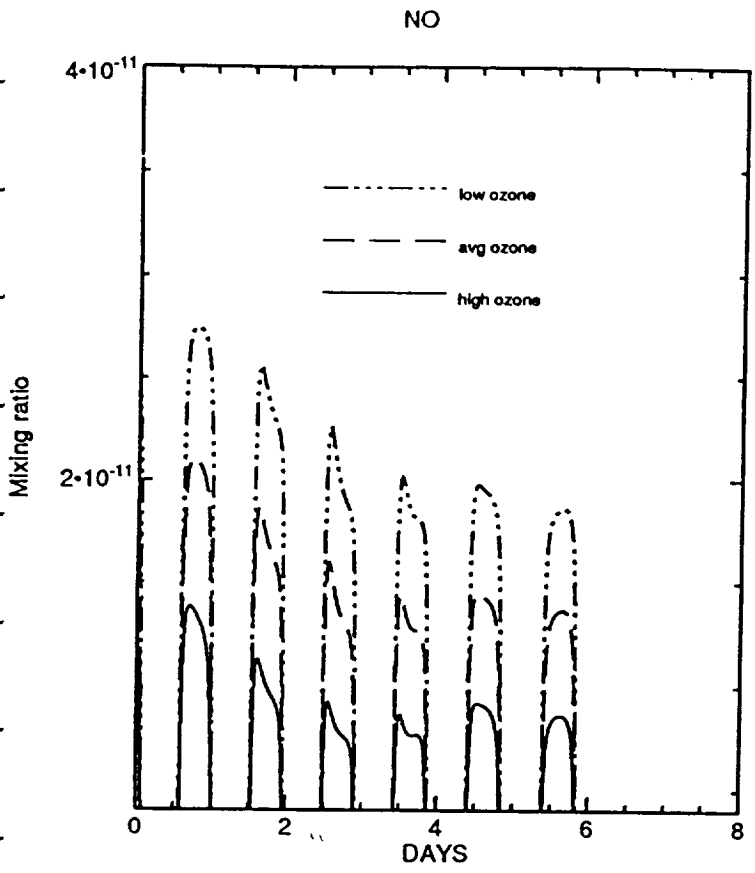
NO
low ozone
avg ozone
high ozone
Mixing ratio
4•10-11
2•10-11
0
2
4
6
8
DAYS

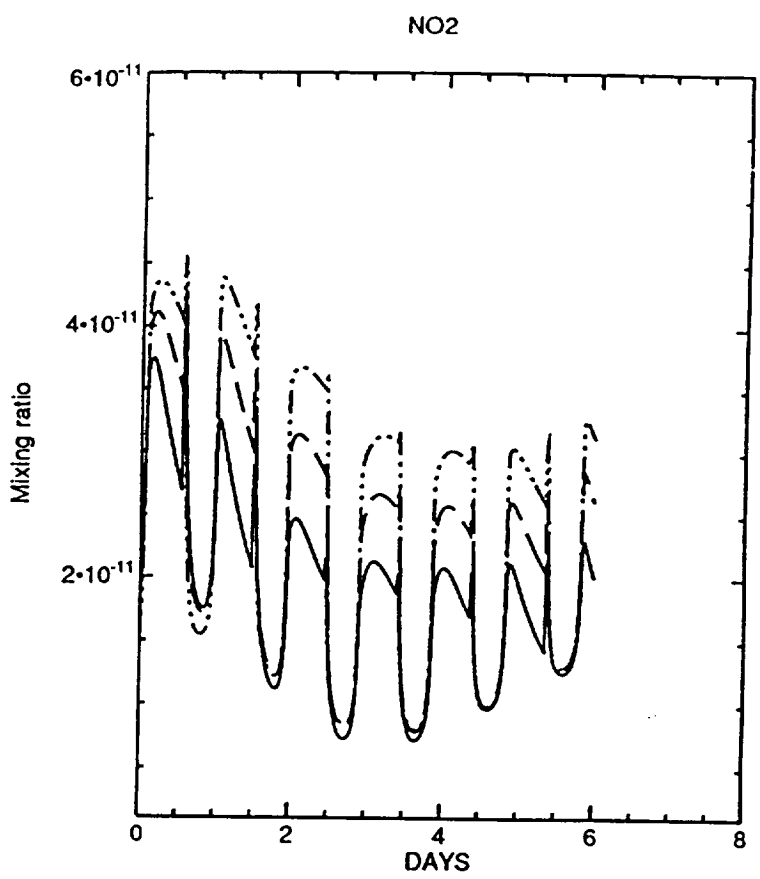
NO2
Mixing ratio
6•10-11
4•10-11
2•10-11
0
2
4
6
8
DAYS

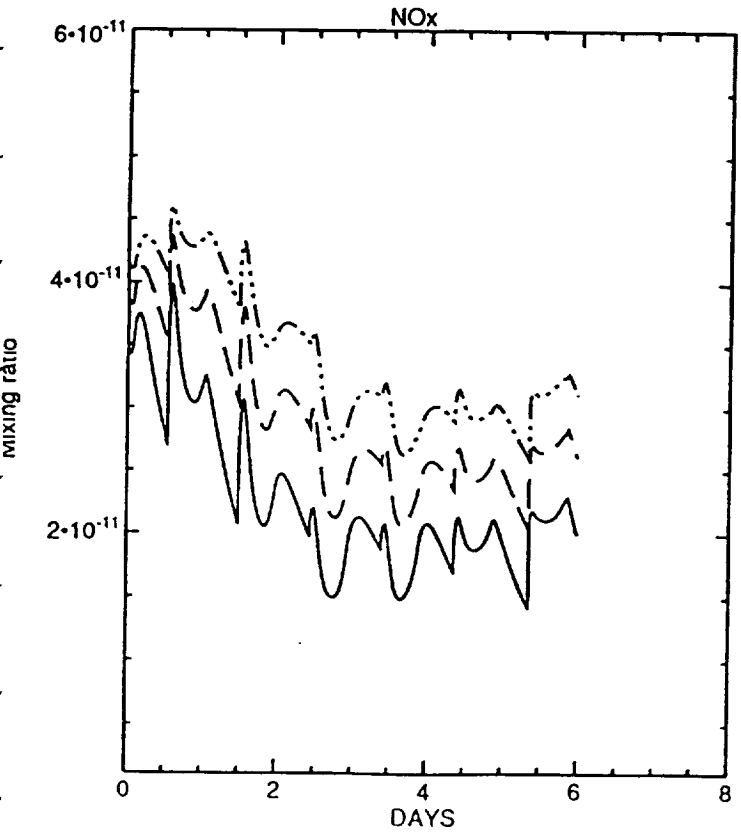
NOx
Mixing ratio
6•10-11
4•10-11
2•10-11
0
2
4
6
8
DAYS

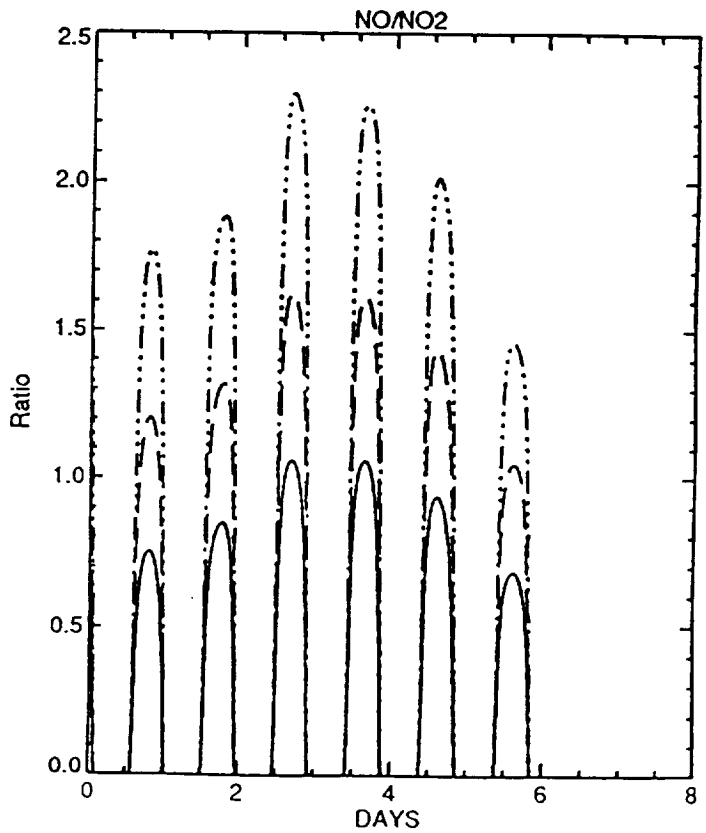
NO/NO2
Ratio
2.5
2.0
1.5
1.0
0.5
0.0
0
2
4
6
8
DAYS

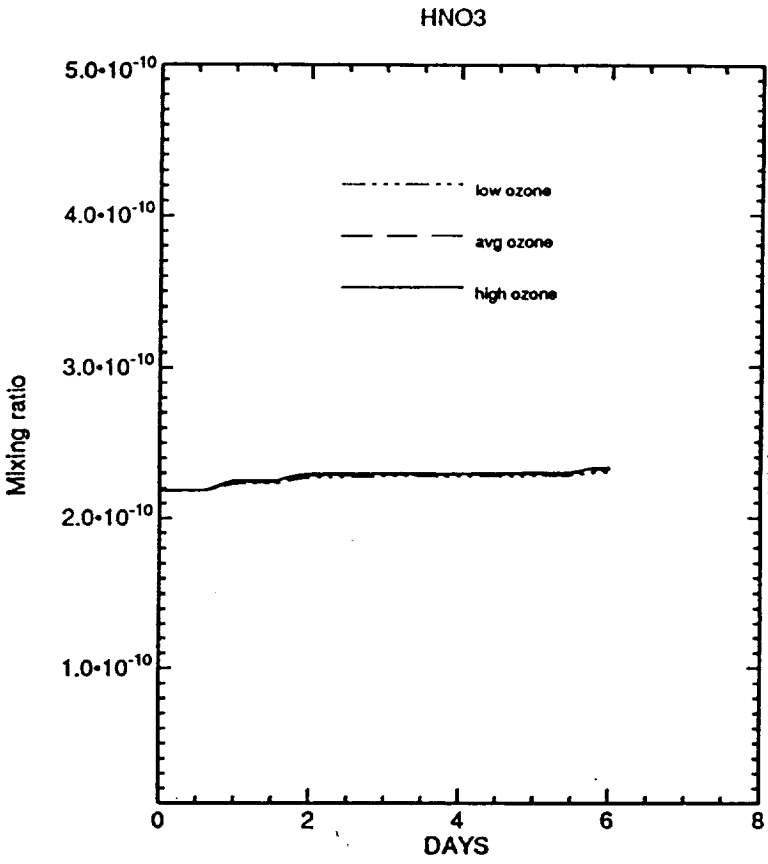
HNO3
low ozone
avg ozone
high ozone
Mixing ratio
5.0•10-10
4.0•10-10
3.0•10-10
2.0•10-10
1.0•10-10
0
2
4
6
8
DAYS

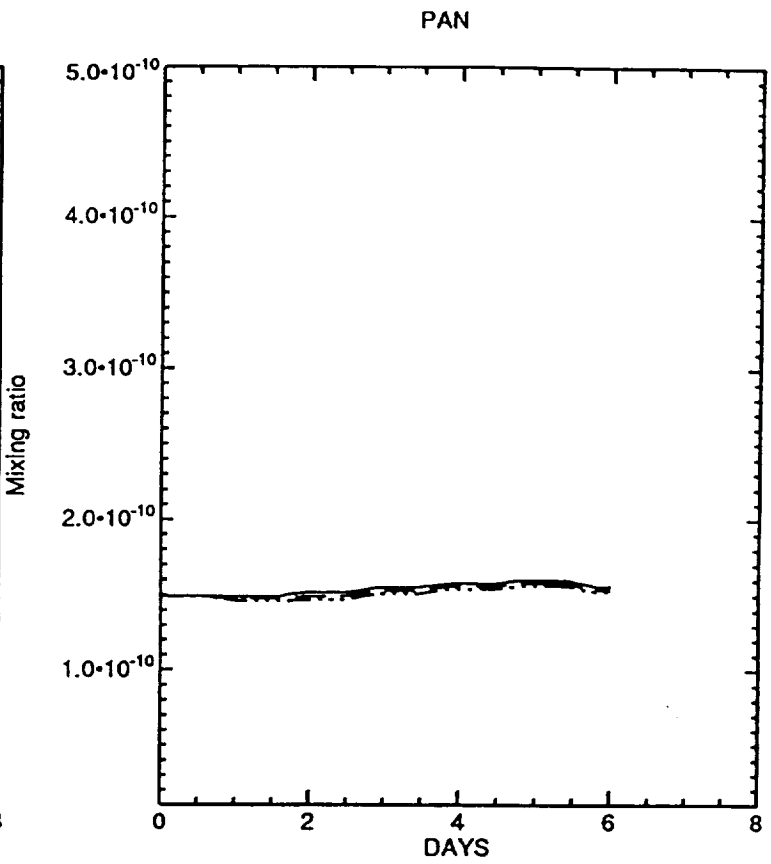
PAN
Mixing ratio
5.0•10-10
4.0•10-10
3.0•10-10
2.0•10-10
1.0•10-10
0
2
4
6
8
DAYS

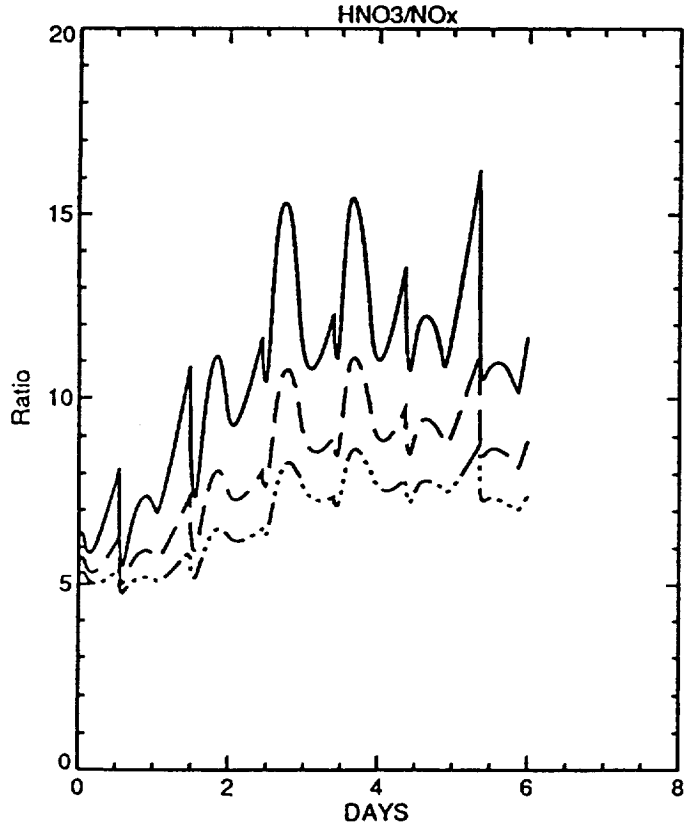
HNO3/NOx
Ratio
20
15
10
5
0
0
2
4
6
8
DAYS

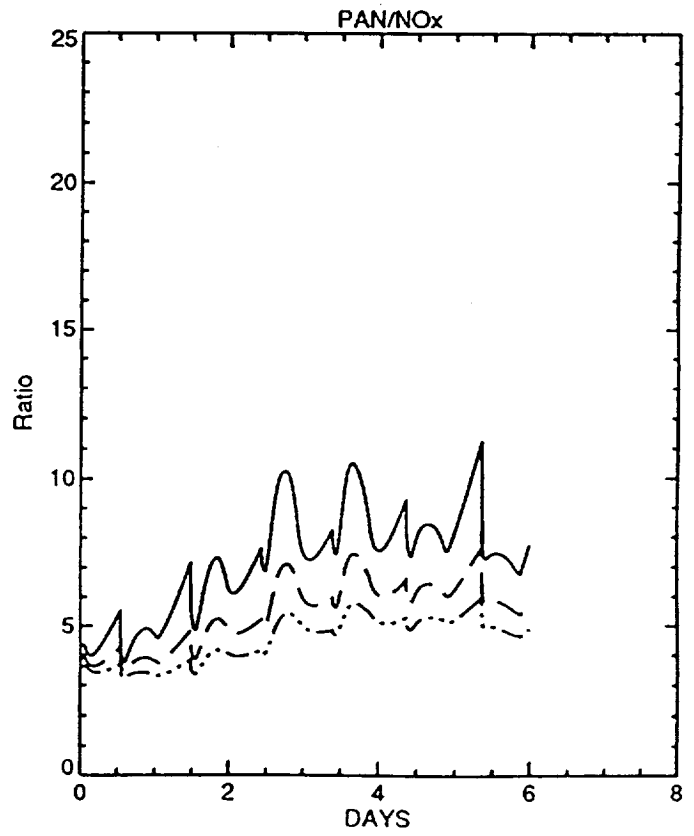
PAN/NOx
Ratio
25
20
15
10
5
0
0
2
4
6
8
DAYS

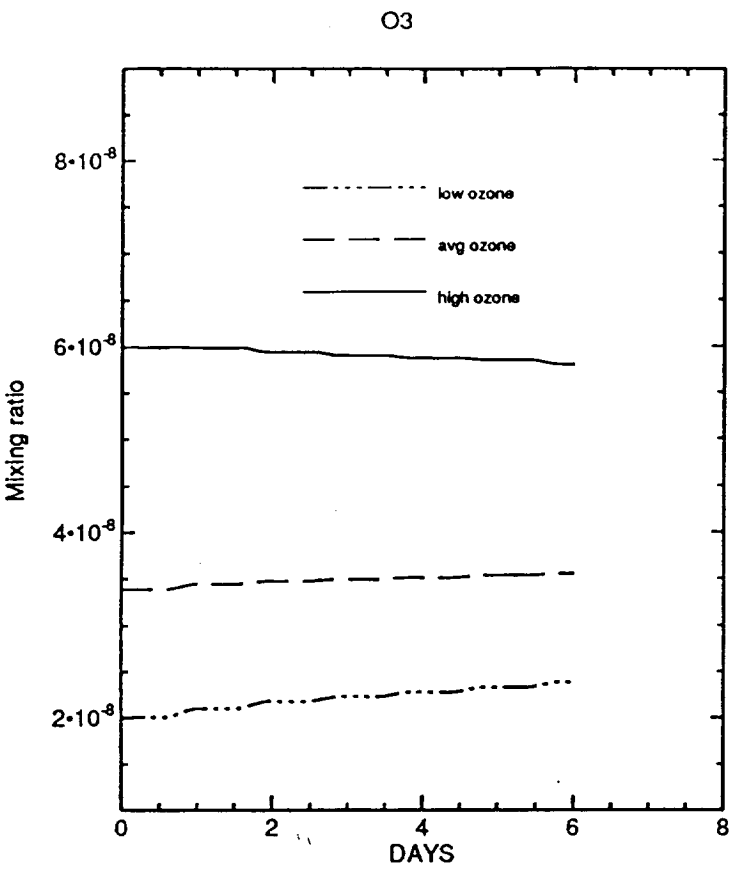
O3
low ozone
avg ozone
high ozone
Mixing ratio
8•10-8
6•10-8
4•10-8
2•10-8
0
2
4
6
8
DAYS

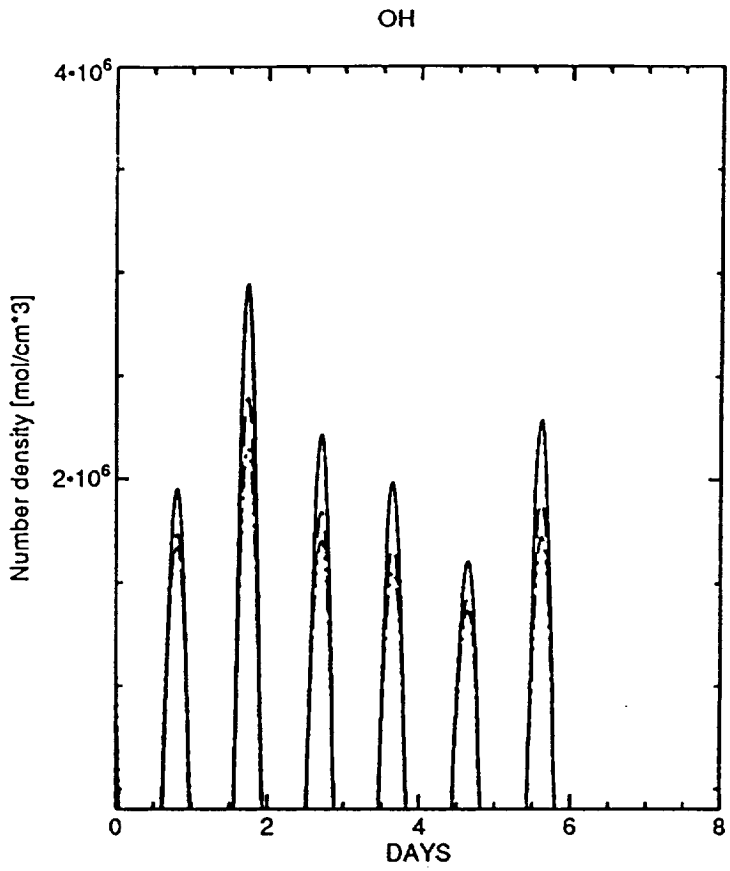
OH
Number density [mol/cm^3]
4•10^6
2•10^6
0
2
4
6
8
DAYS

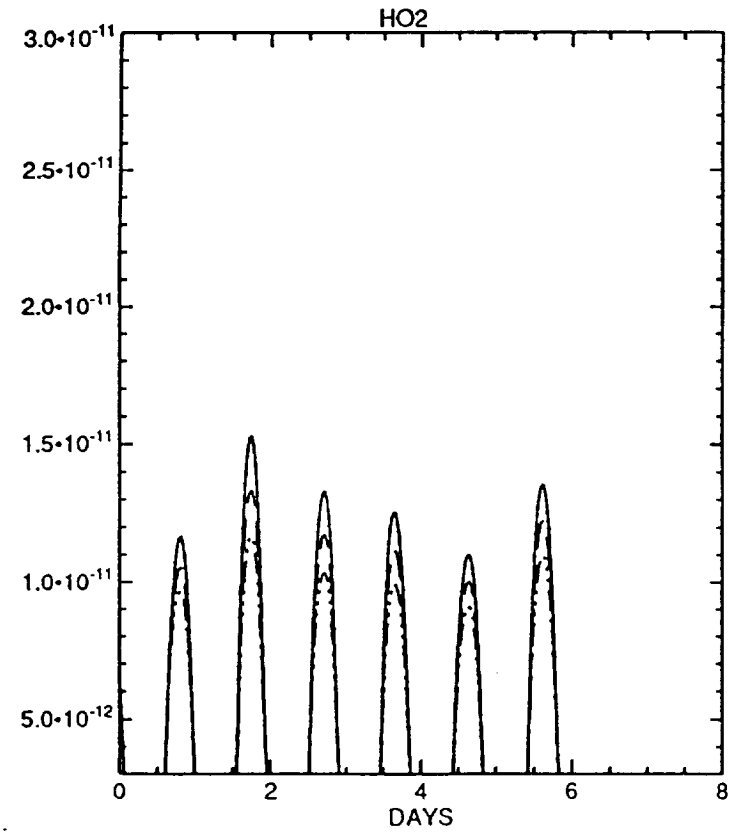
HO2
3.0•10-11
2.5•10-11
2.0•10-11
1.5•10-11
1.0•10-11
5.0•10-12
0
2
4
6
8
DAYS

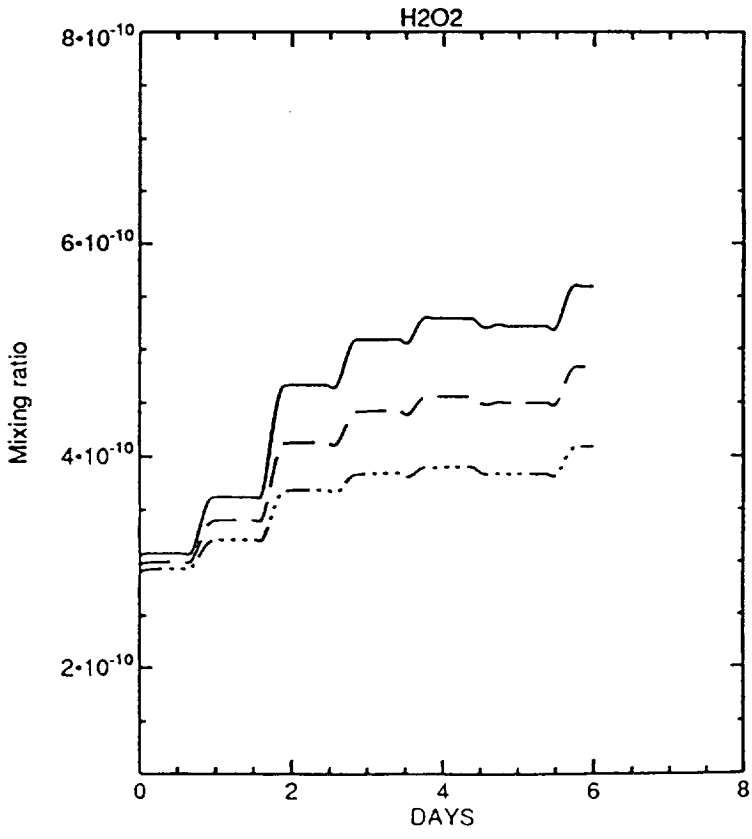
H2O2
Mixing ratio
8•10-10
6•10-10
4•10-10
2•10-10
0
2
4
6
8
DAYS

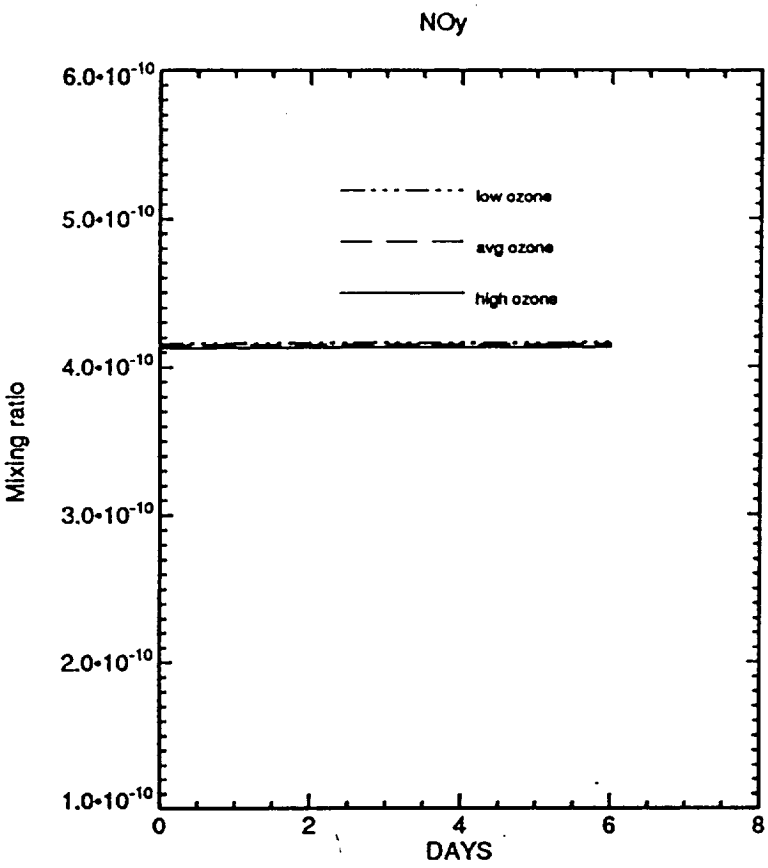
NOy
Mixing ratio
6.0•10^-10
5.0•10^-10
4.0•10^-10
3.0•10^-10
2.0•10^-10
1.0•10^-10
low ozone
avg ozone
high ozone
0
2
4
6
8
DAYS

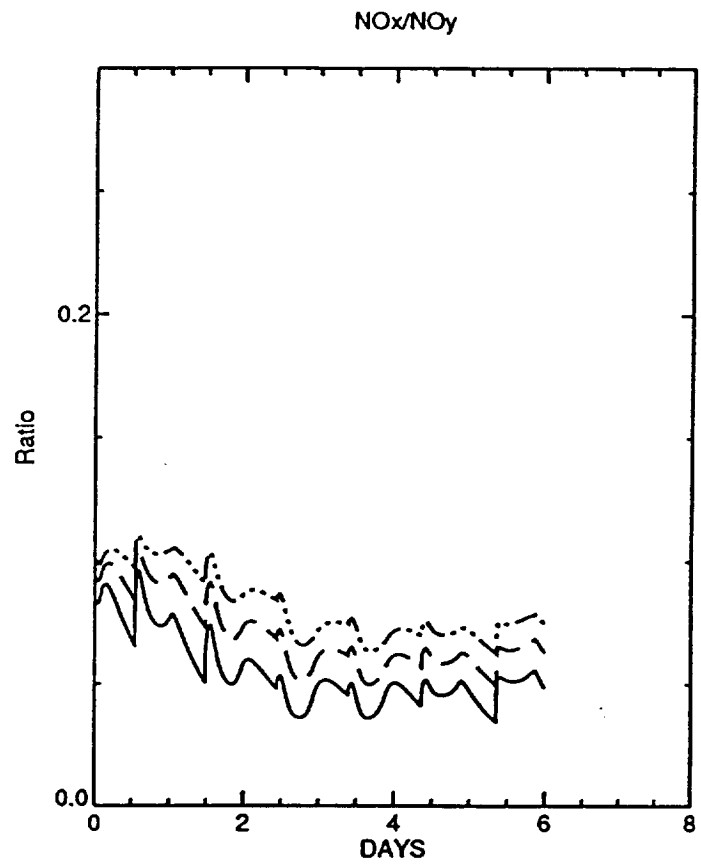
NOx/NOy
Ratio
0.2
0.0
0
2
4
6
8
DAYS

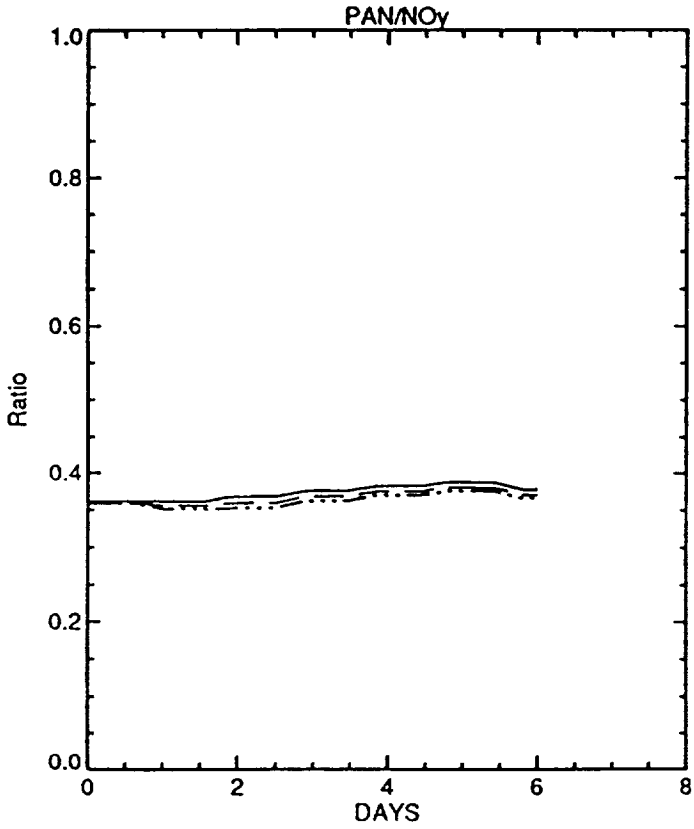
PAN/NOy
Ratio
1.0
0.8
0.6
0.4
0.2
0.0
0
2
4
6
8
DAYS

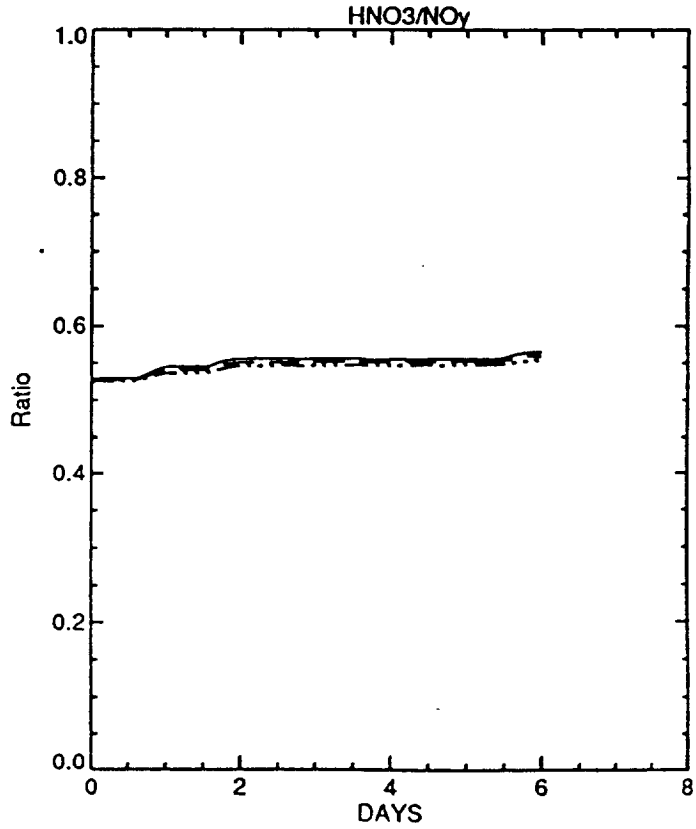
HNO3/NOy
Ratio
1.0
0.8
0.6
0.4
0.2
0.0
0
2
4
6
8
DAYS

Figure 7: Sensitivity of results to washout of HNO_3, H_2O_2, CH_2O, and aldehydes and hydroperoxides. An average removal time constant of 3 days is assumed for the washout case. Initial conditions for NO_t, HNO_3, PAN and O_3 are given in the "average" row of Table 1.

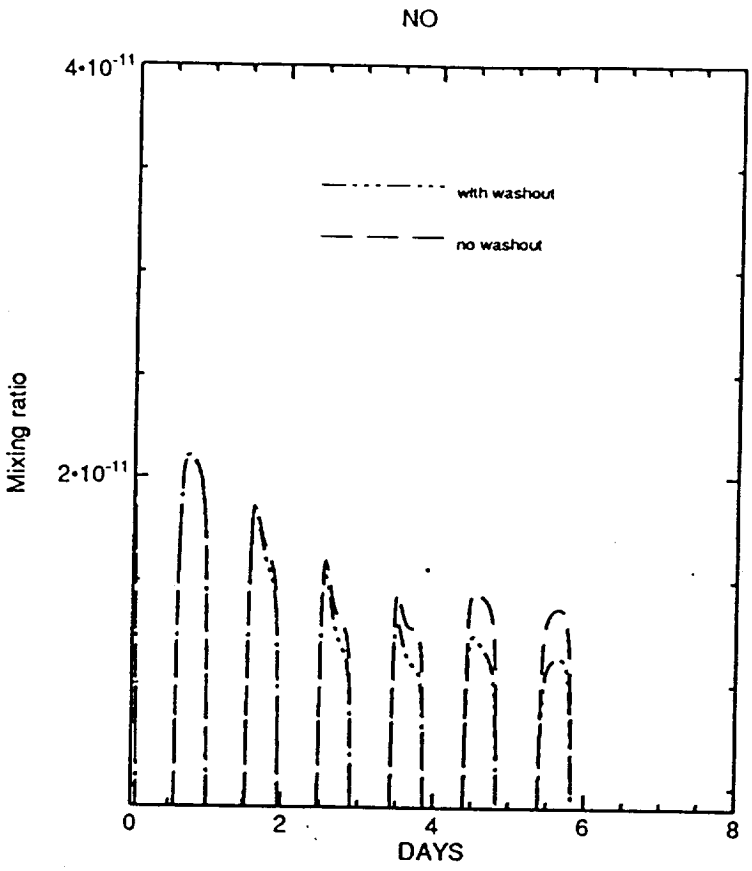
NO
4•10-11
2•10-11
Mixing ratio
with washout
no washout
0
2
4
6
8
DAYS

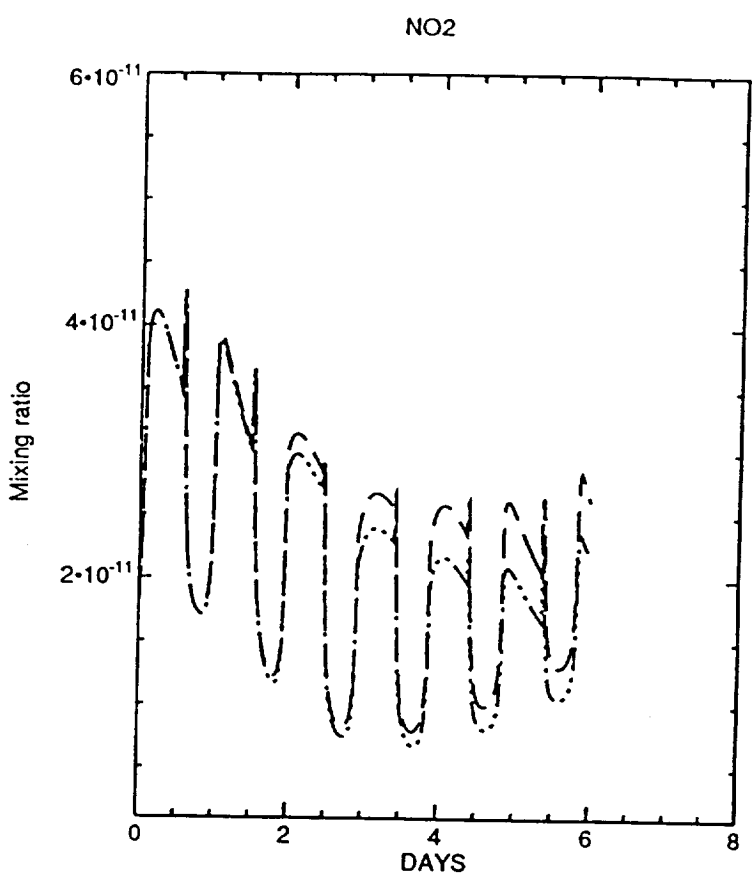
NO2
6•10-11
4•10-11
2•10-11
Mixing ratio
0
2
4
6
8
DAYS

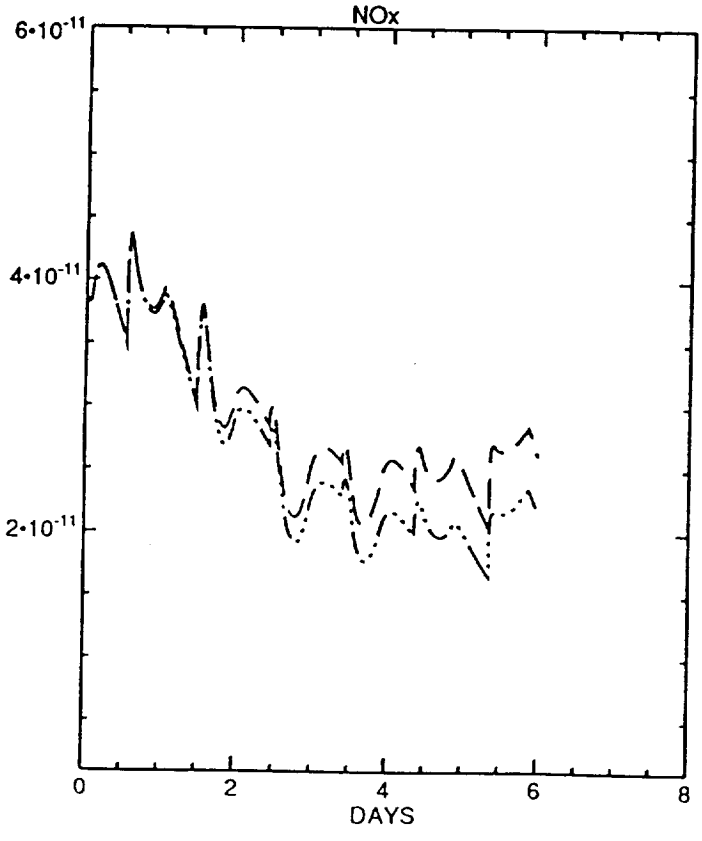
NOx
6•10-11
4•10-11
2•10-11
Mixing ratio
0
2
4
6
8
DAYS

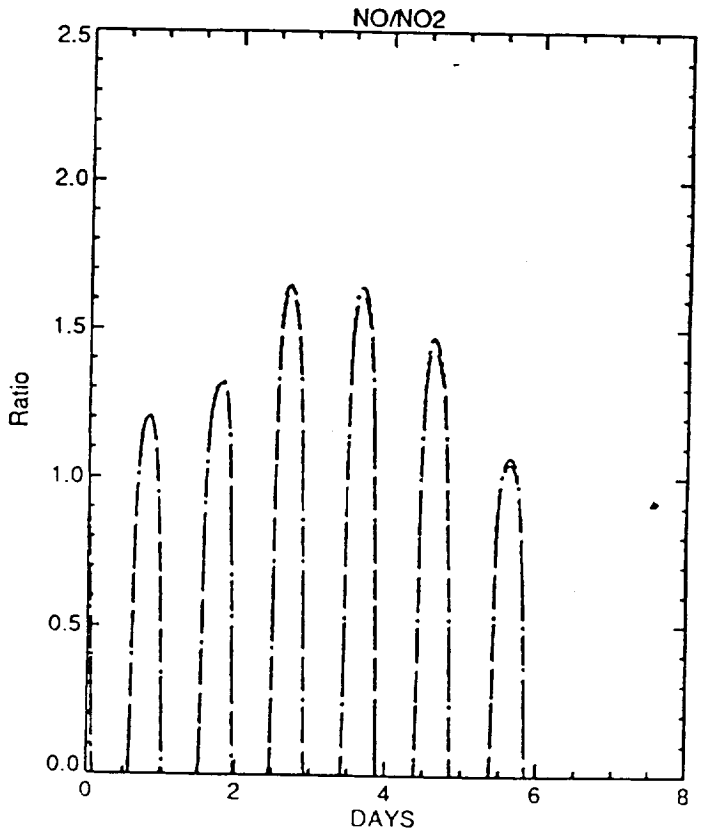
NO/NO2
2.5
2.0
1.5
1.0
0.5
0.0
Ratio
0
2
4
6
8
DAYS

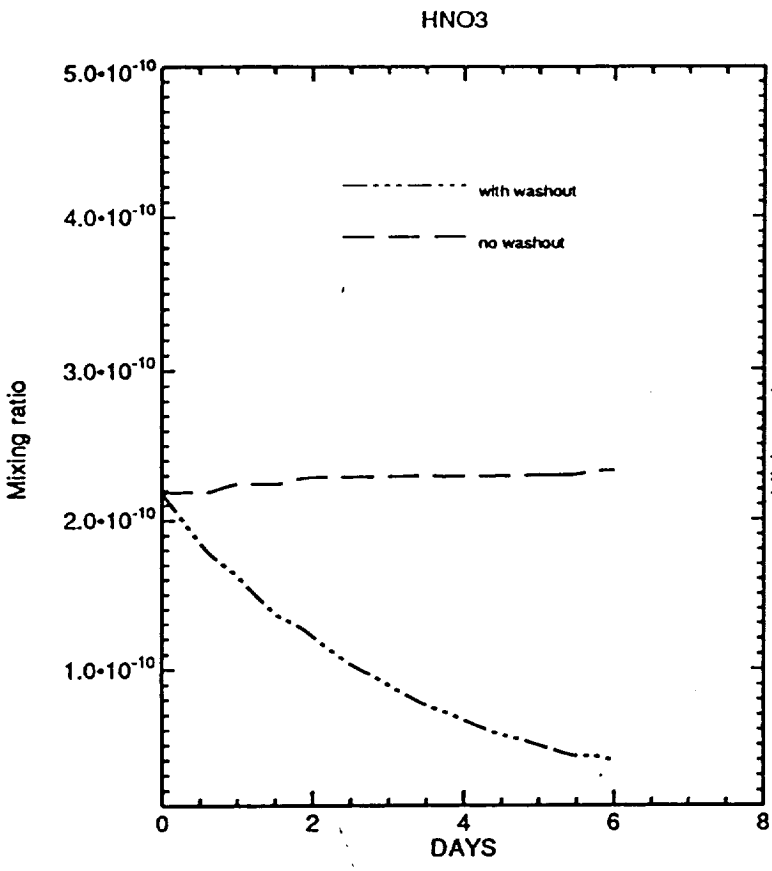
HNO3
with washout
no washout
Mixing ratio
5.0•10-10
4.0•10-10
3.0•10-10
2.0•10-10
1.0•10-10
0
2
4
6
8
DAYS

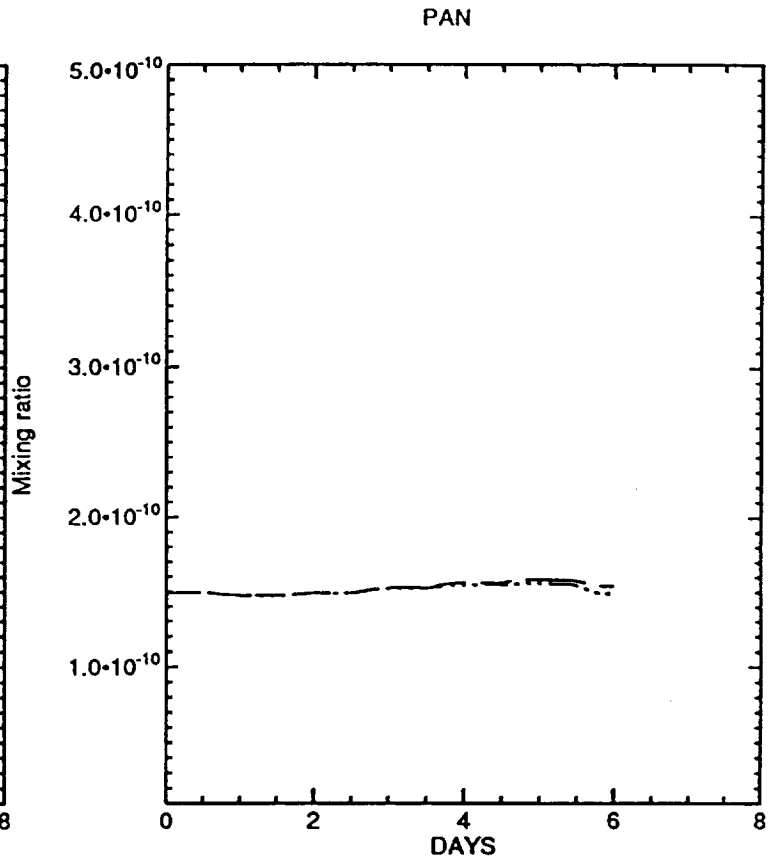
PAN
Mixing ratio
5.0•10-10
4.0•10-10
3.0•10-10
2.0•10-10
1.0•10-10
0
2
4
6
8
DAYS

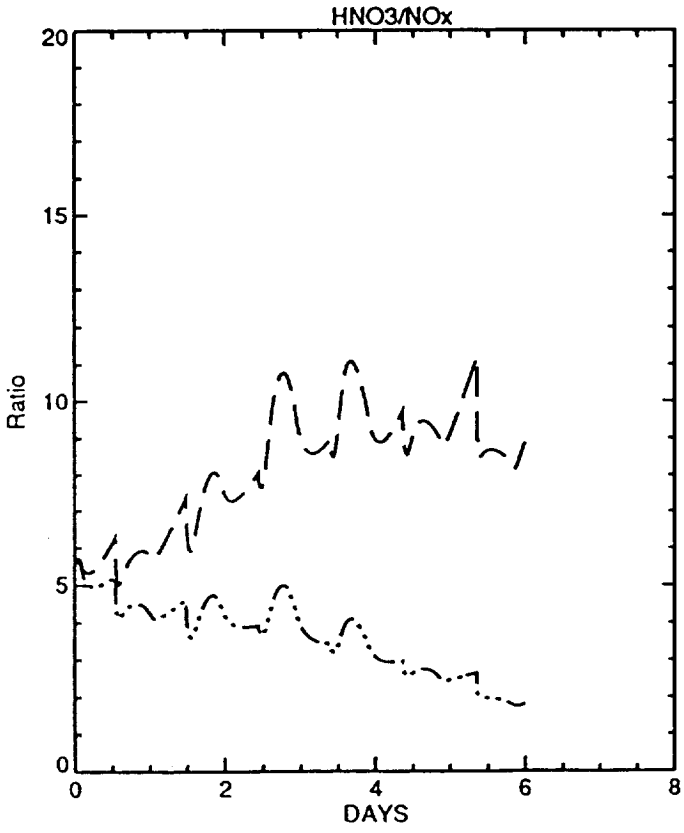
HNO3/NOx
Ratio
20
15
10
5
0
0
2
4
6
8
DAYS

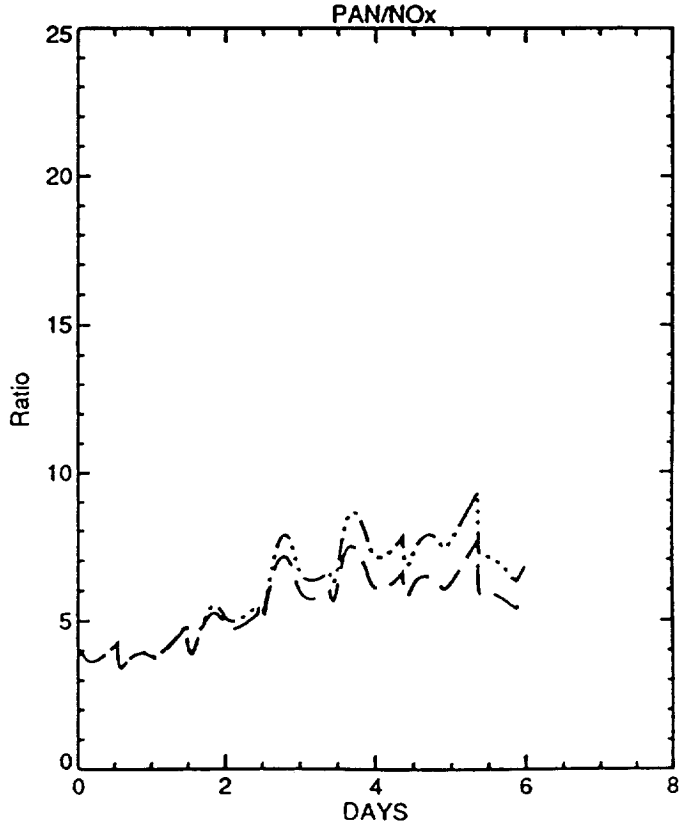
PAN/NOx
Ratio
25
20
15
10
5
0
0
2
4
6
8
DAYS

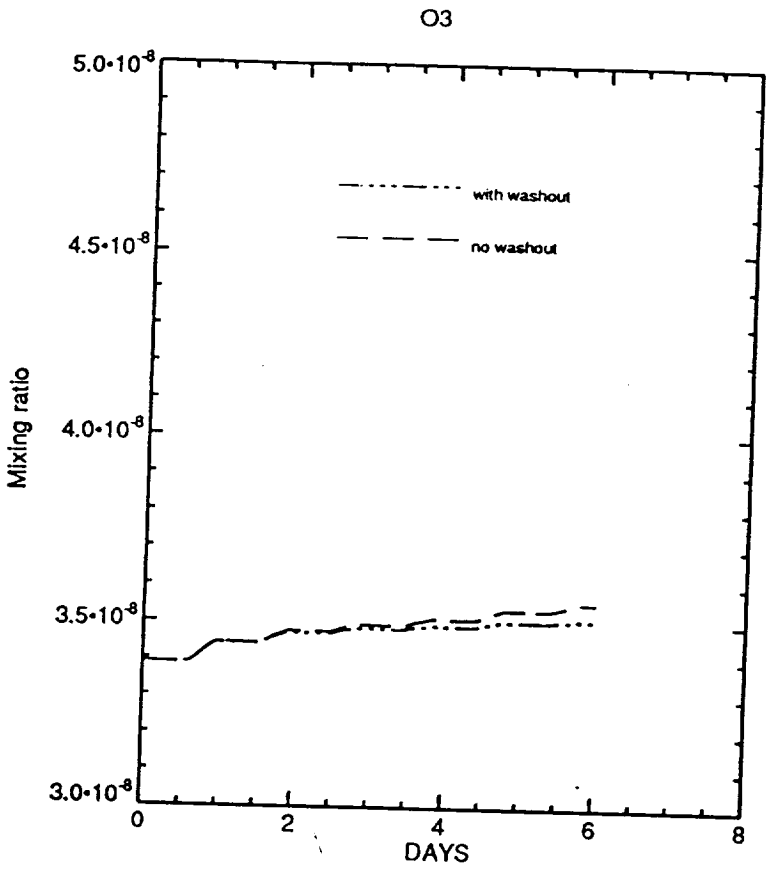
O3
5.0•10⁻⁸
4.5•10⁻⁸
4.0•10⁻⁸
3.5•10⁻⁸
3.0•10⁻⁸
Mixing ratio
with washout
no washout
0
2
4
6
8
DAYS

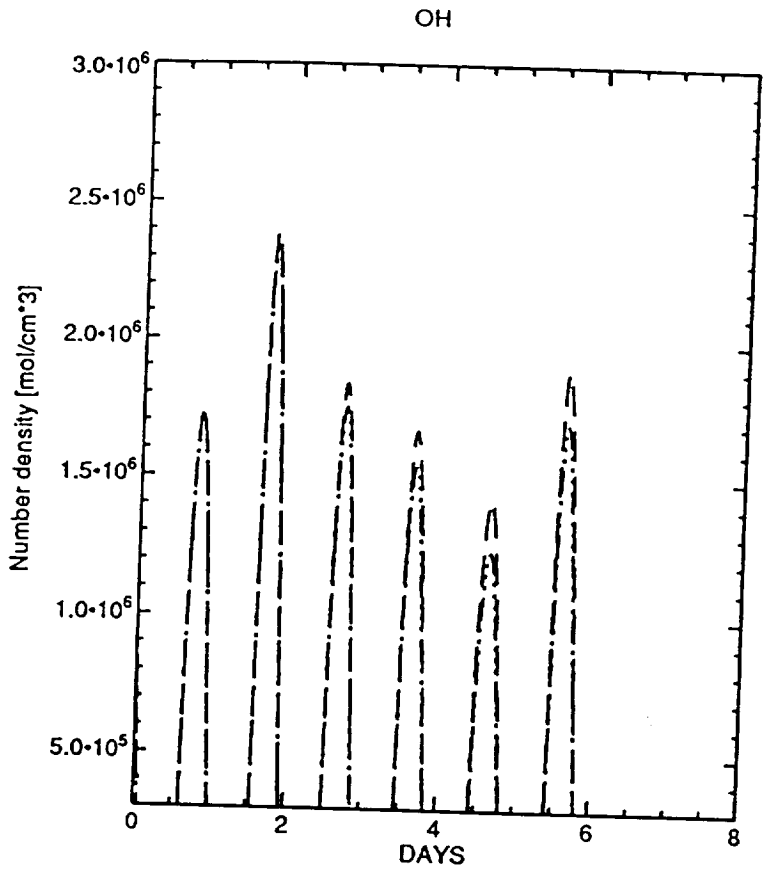
OH
3.0•10⁶
2.5•10⁶
2.0•10⁶
1.5•10⁶
1.0•10⁶
5.0•10⁵
Number density [mol/cm^3]
0
2
4
6
8
DAYS

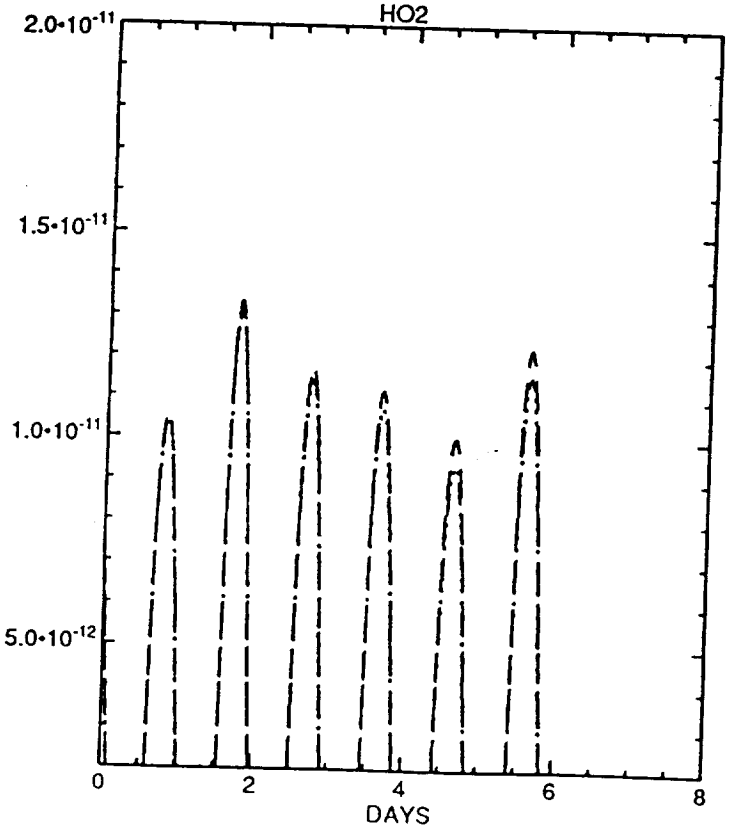
HO2
2.0•10⁻¹¹
1.5•10⁻¹¹
1.0•10⁻¹¹
5.0•10⁻¹²
0
2
4
6
8
DAYS

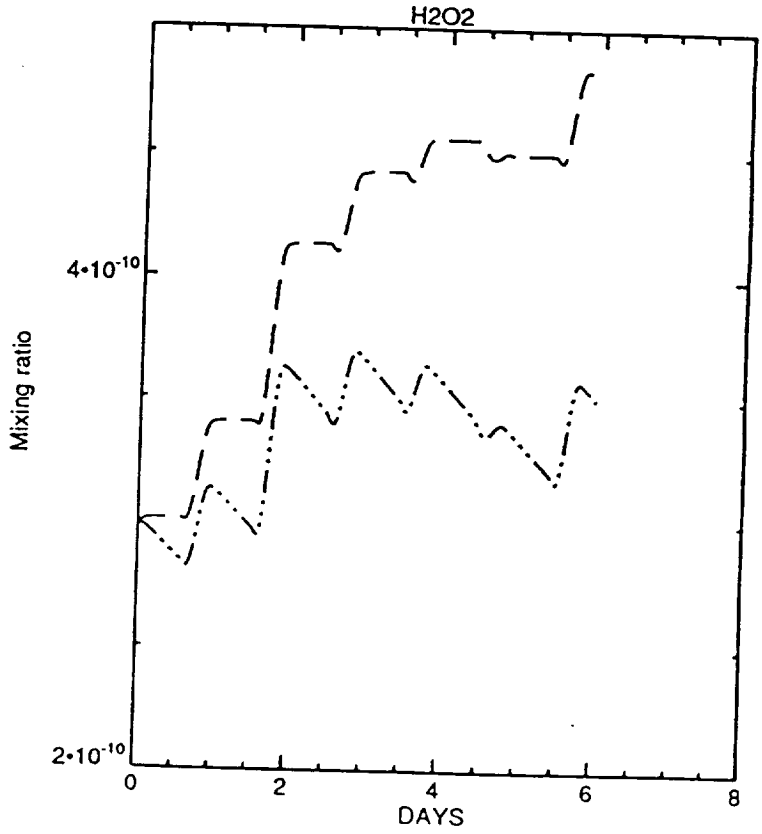
H2O2
4•10⁻¹⁰
2•10⁻¹⁰
Mixing ratio
0
2
4
6
8
DAYS

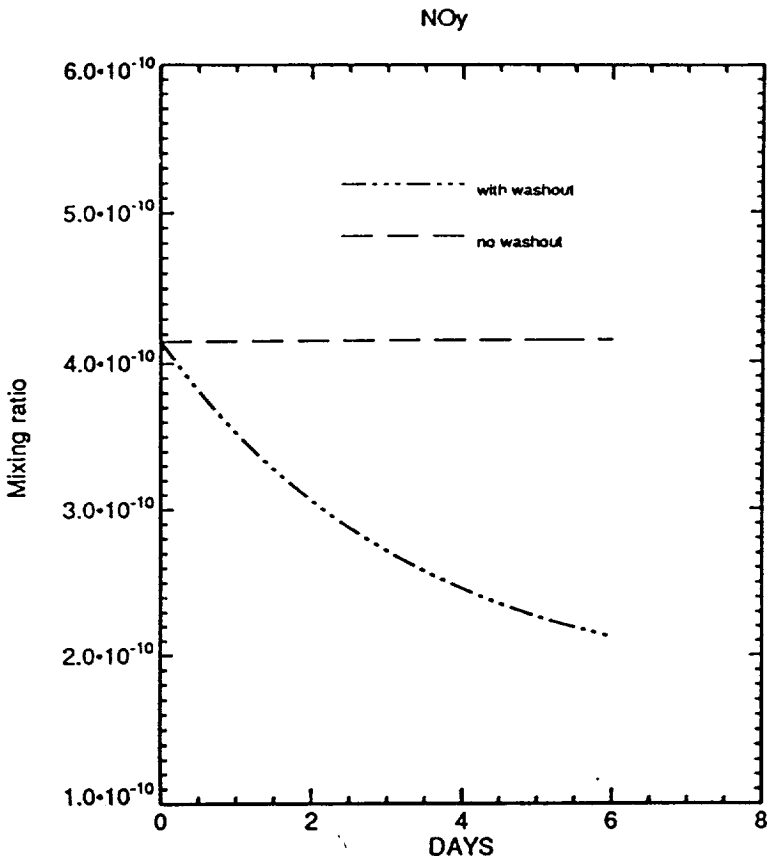
NOy
6.0•10^-10
5.0•10^-10
4.0•10^-10
3.0•10^-10
2.0•10^-10
1.0•10^-10
Mixing ratio
with washout
no washout
0
2
4
6
8
DAYS

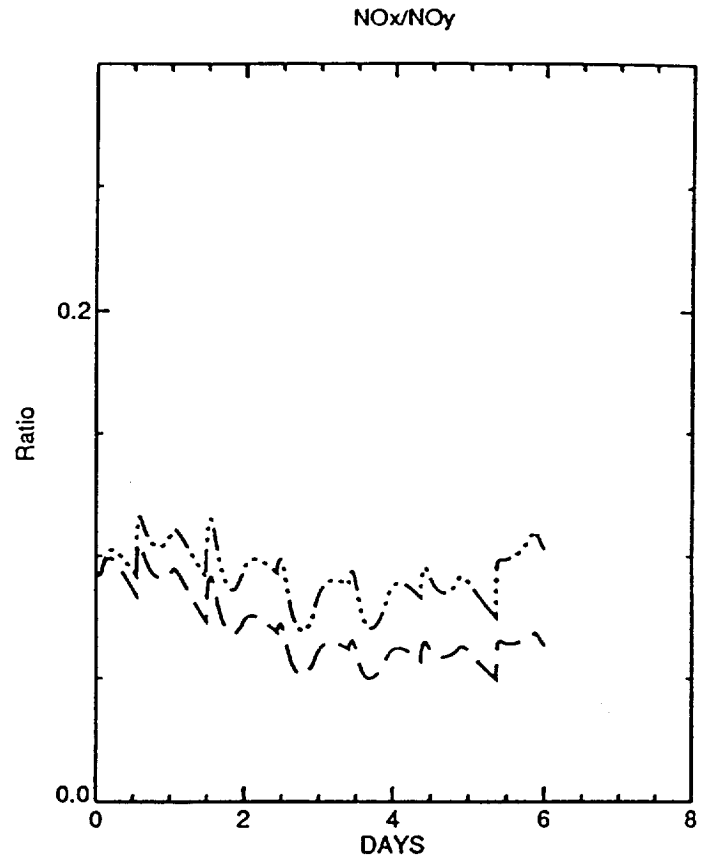
NOx/NOy
0.2
0.0
Ratio
0
2
4
6
8
DAYS

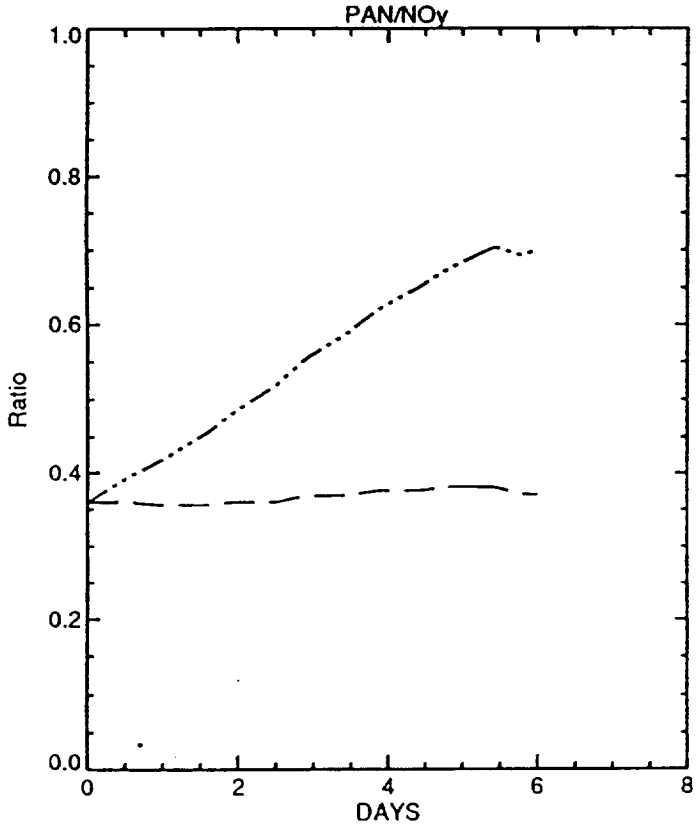
PAN/NOy
1.0
0.8
0.6
0.4
0.2
0.0
Ratio
0
2
4
6
8
DAYS

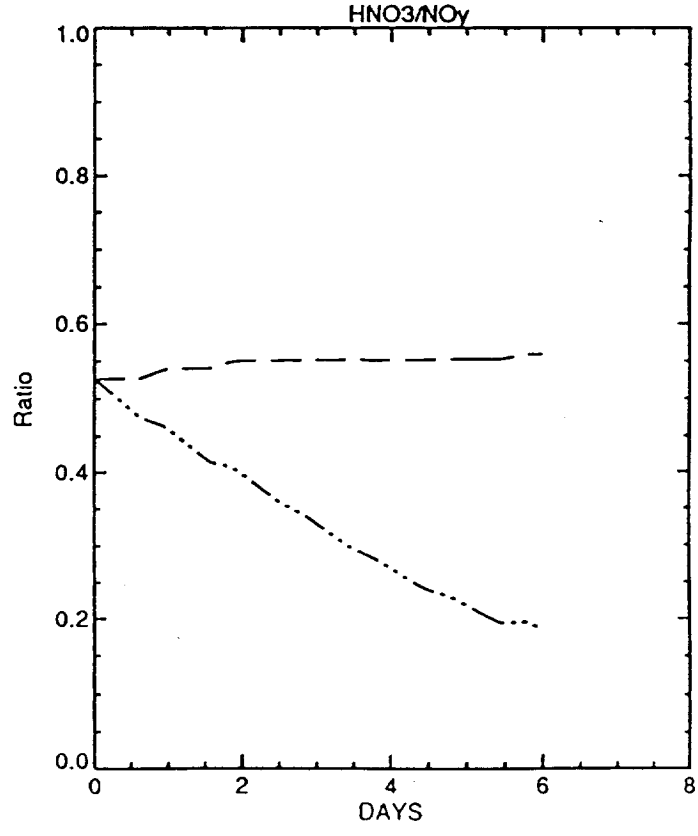
HNO3/NOy
1.0
0.8
0.6
0.4
0.2
0.0
Ratio
0
2
4
6
8
DAYS

Figure 8: Sensitivity of results to clear sky conditions, and 100% cloud coverage above and below the air parcel. Photolysis rates are modified according to the parameterization of Chang et al. (1987). An optical thickness of 12 is adopted for the clouds. Initial conditions for NO_t, HNO_3, PAN and O_3 are given in the "average" row of Table 1.

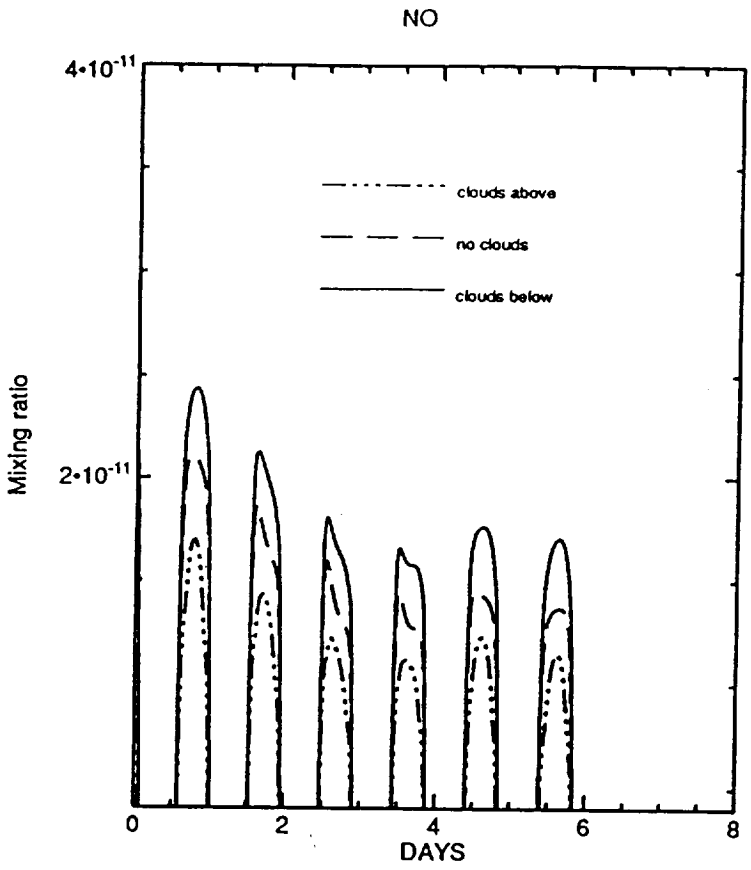
NO
clouds above
no clouds
clouds below
Mixing ratio
4•10-11
2•10-11
0
2
4
6
8
DAYS

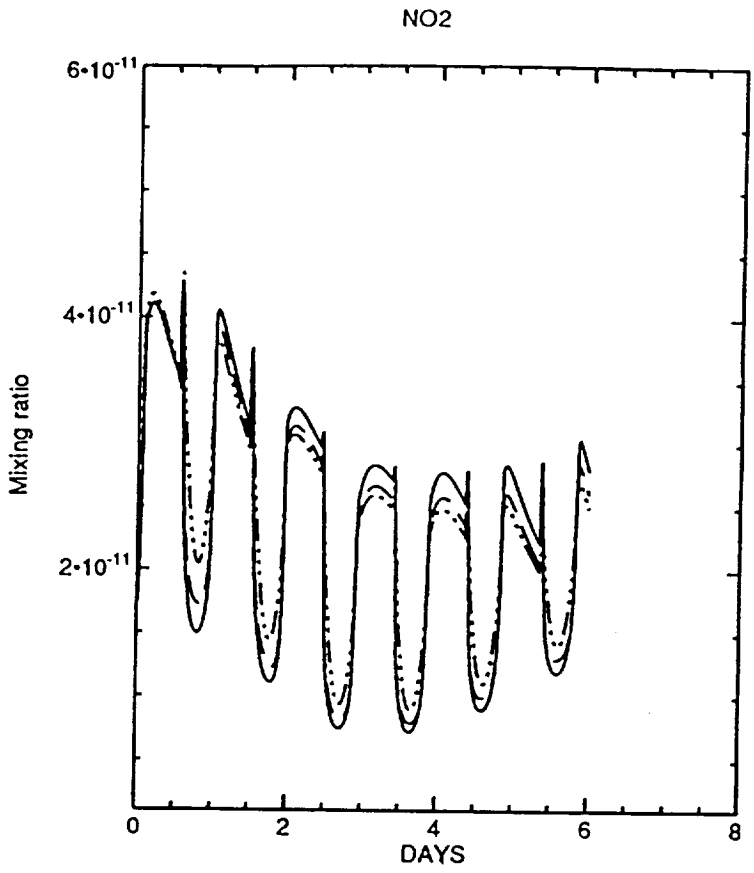
NO2
Mixing ratio
6•10-11
4•10-11
2•10-11
0
2
4
6
8
DAYS

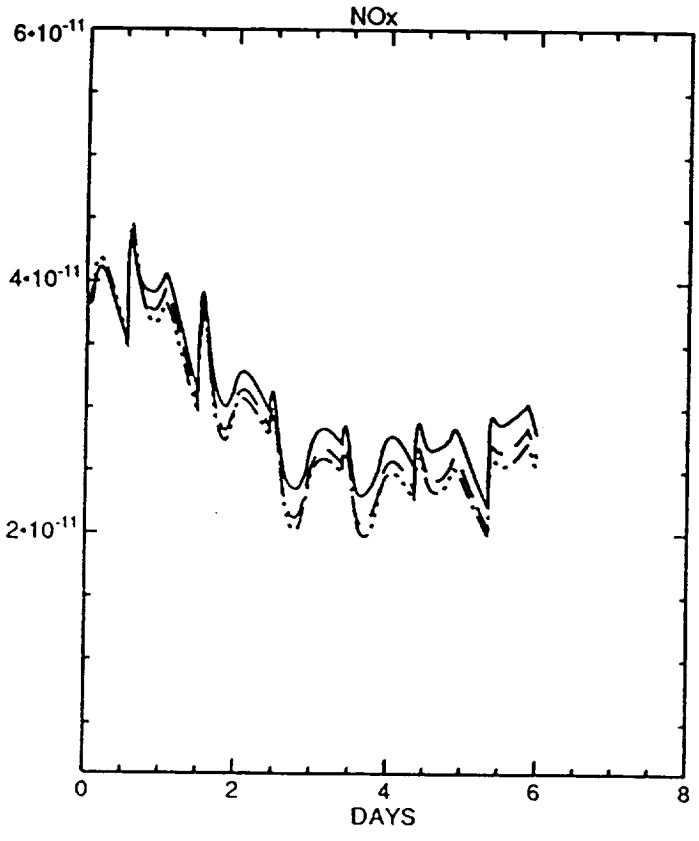
NOx
Mixing ratio
6•10-11
4•10-11
2•10-11
0
2
4
6
8
DAYS

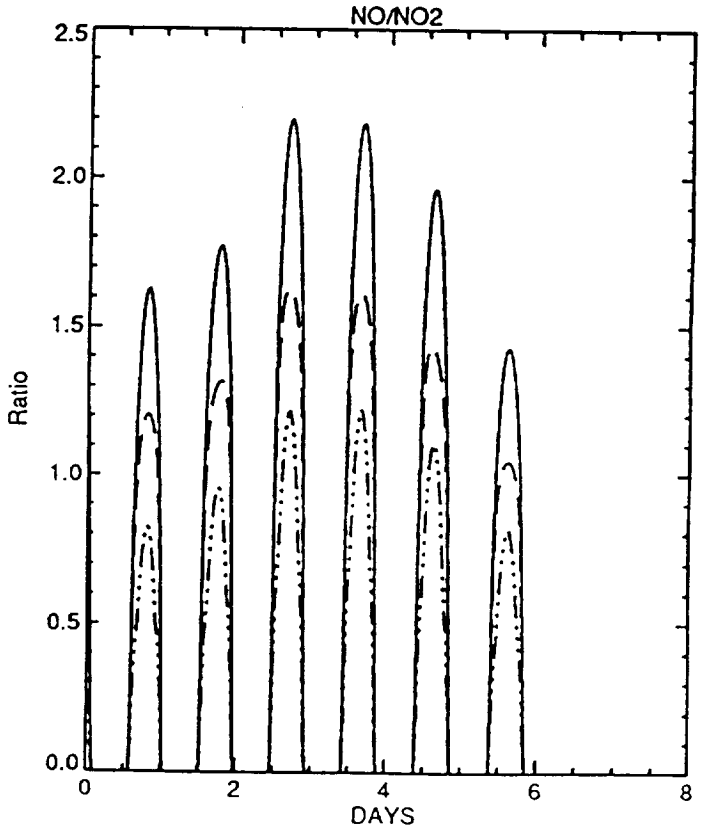
NO/NO2
Ratio
2.5
2.0
1.5
1.0
0.5
0.0
0
2
4
6
8
DAYS

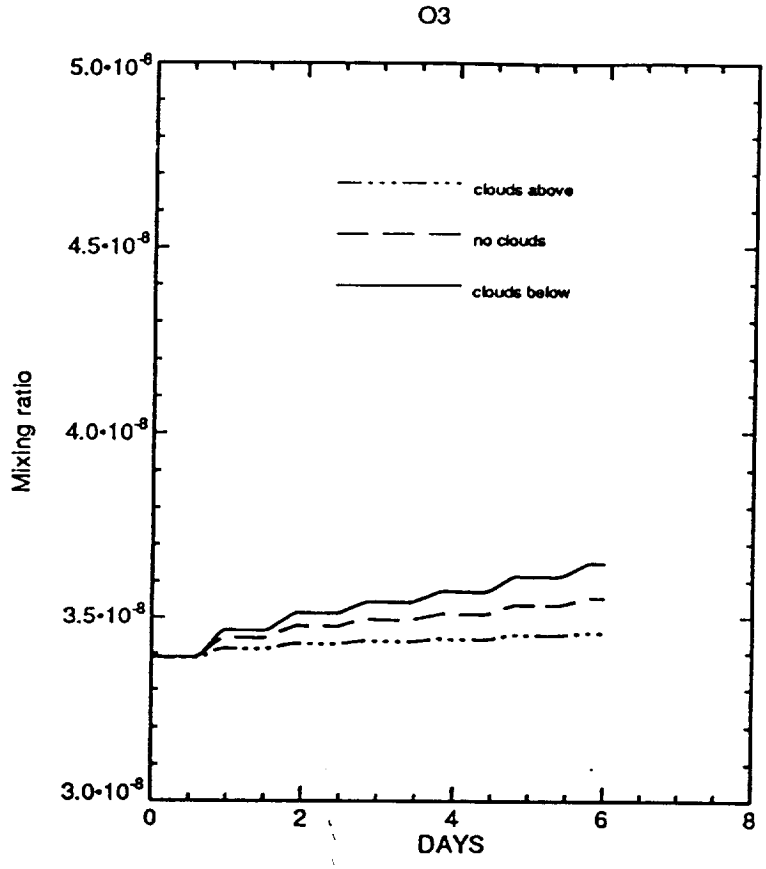
O3
clouds above
no clouds
clouds below
Mixing ratio
5.0•10⁻⁸
4.5•10⁻⁸
4.0•10⁻⁸
3.5•10⁻⁸
3.0•10⁻⁸
0
2
4
6
8
DAYS

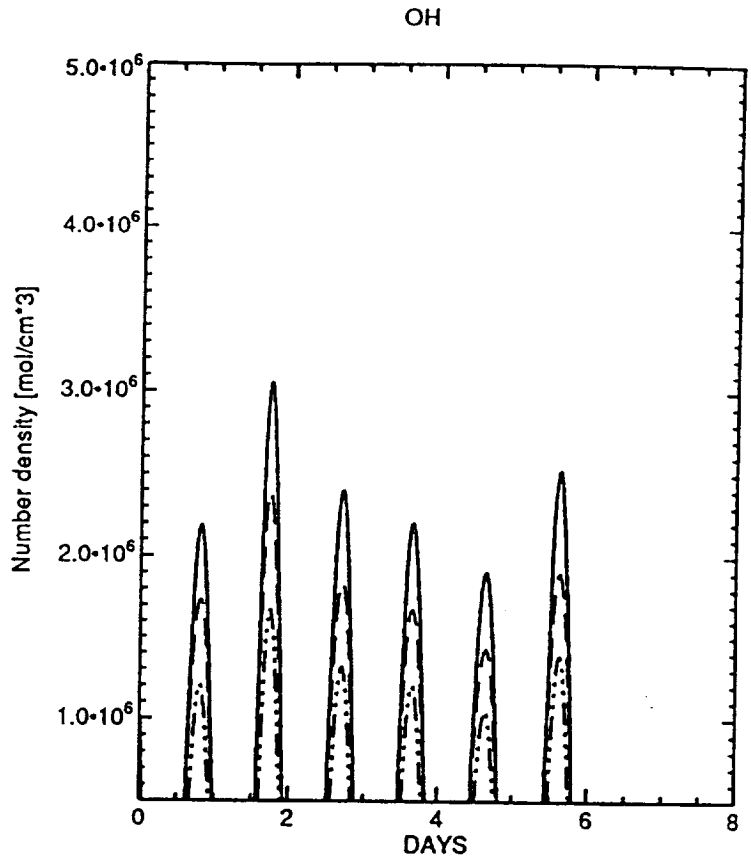
OH
Number density [mol/cm^3]
5.0•10⁶
4.0•10⁶
3.0•10⁶
2.0•10⁶
1.0•10⁶
0
2
4
6
8
DAYS

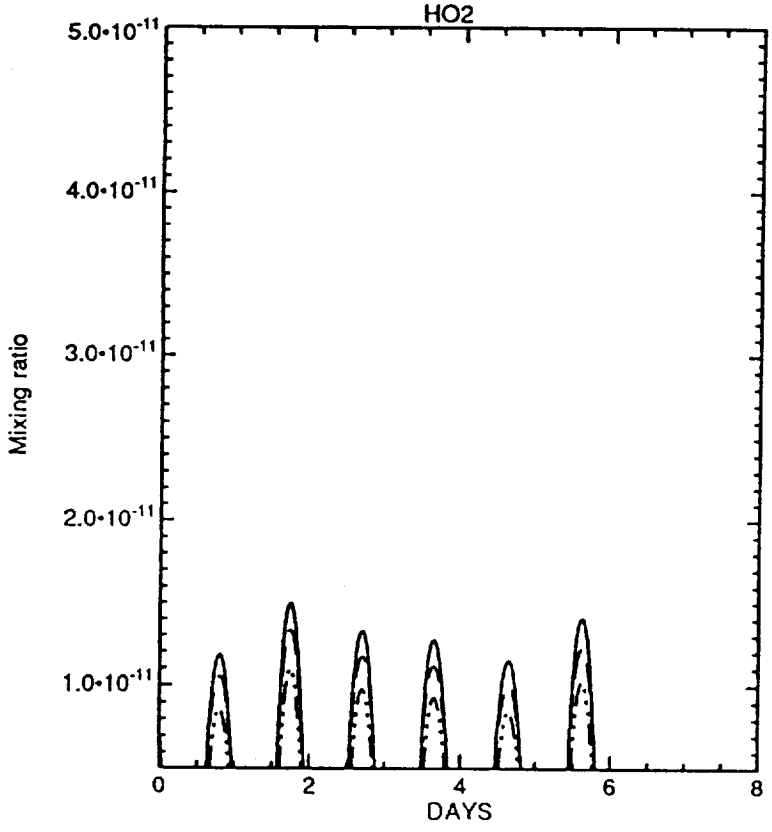
HO2
Mixing ratio
5.0•10⁻¹¹
4.0•10⁻¹¹
3.0•10⁻¹¹
2.0•10⁻¹¹
1.0•10⁻¹¹
0
2
4
6
8
DAYS

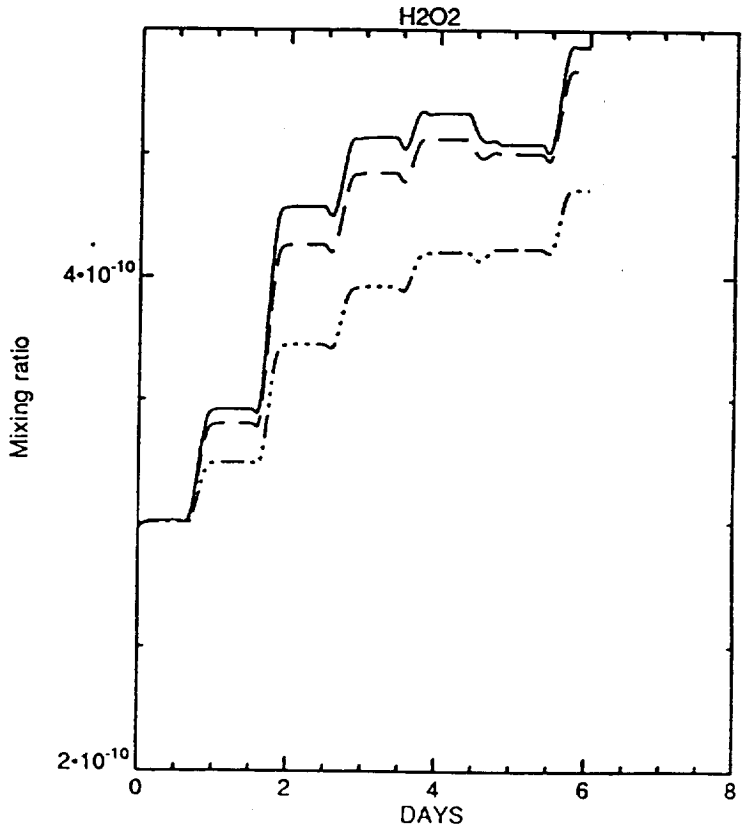
H2O2
Mixing ratio
4•10⁻¹⁰
2•10⁻¹⁰
0
2
4
6
8
DAYS

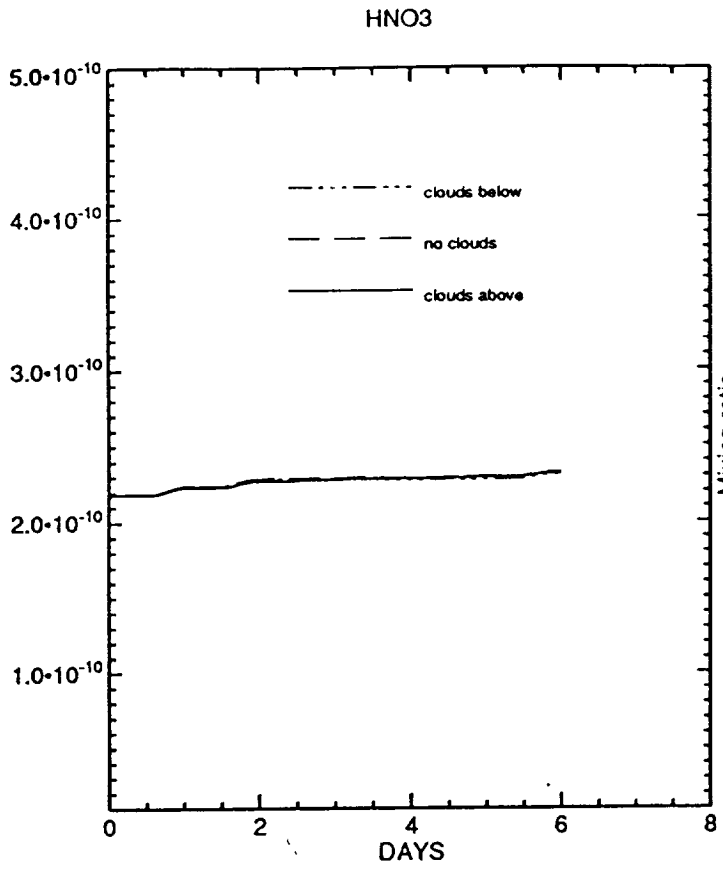
HNO3
clouds below
no clouds
clouds above
Mixing ratio
DAYS

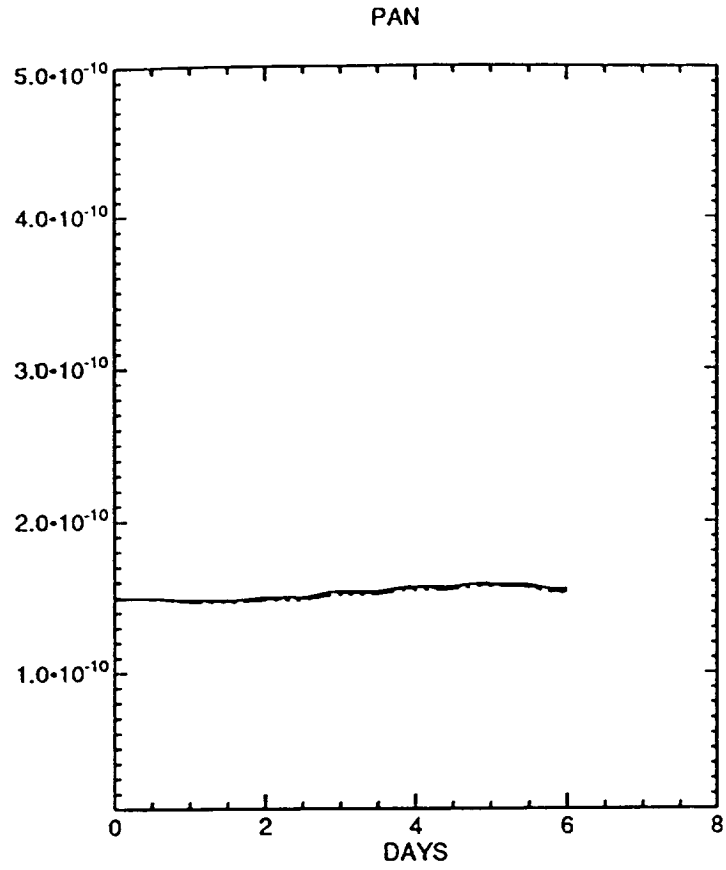
PAN
Mixing ratio
DAYS

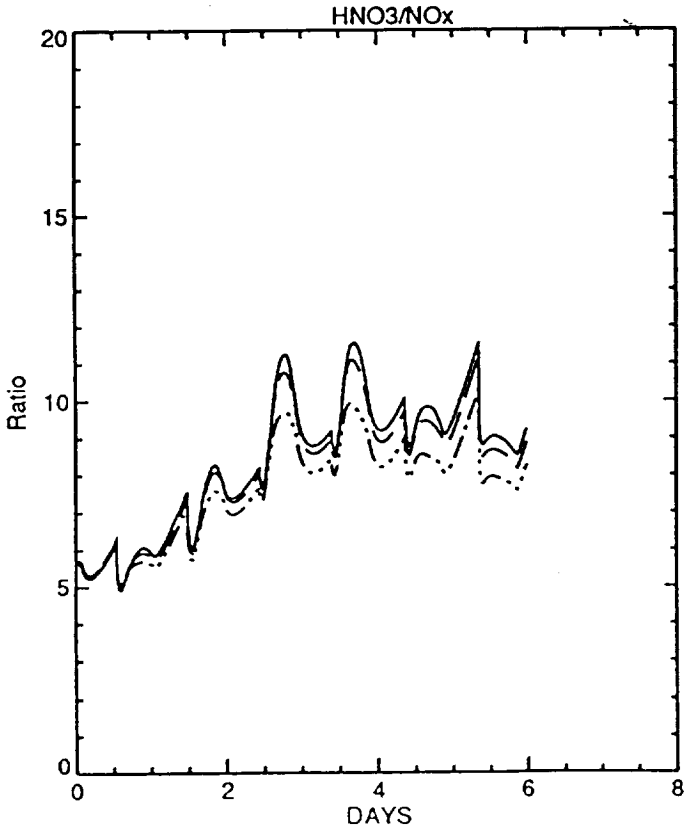
HNO3/NOx
Ratio
DAYS

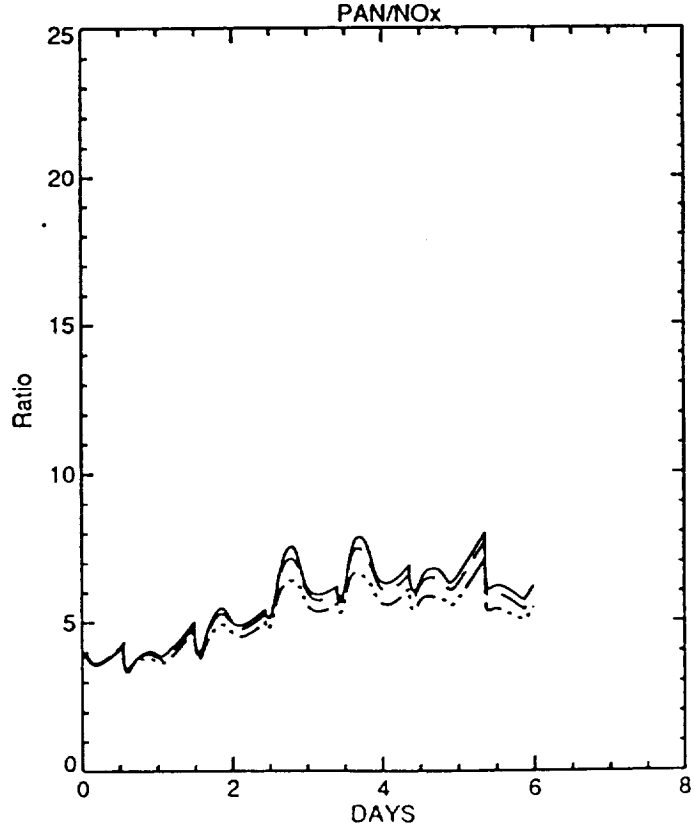
PAN/NOx
Ratio
DAYS